# NEW METHODS FOR IMMOBILIZATION OF ENZYMES AND WHOLE CELLS
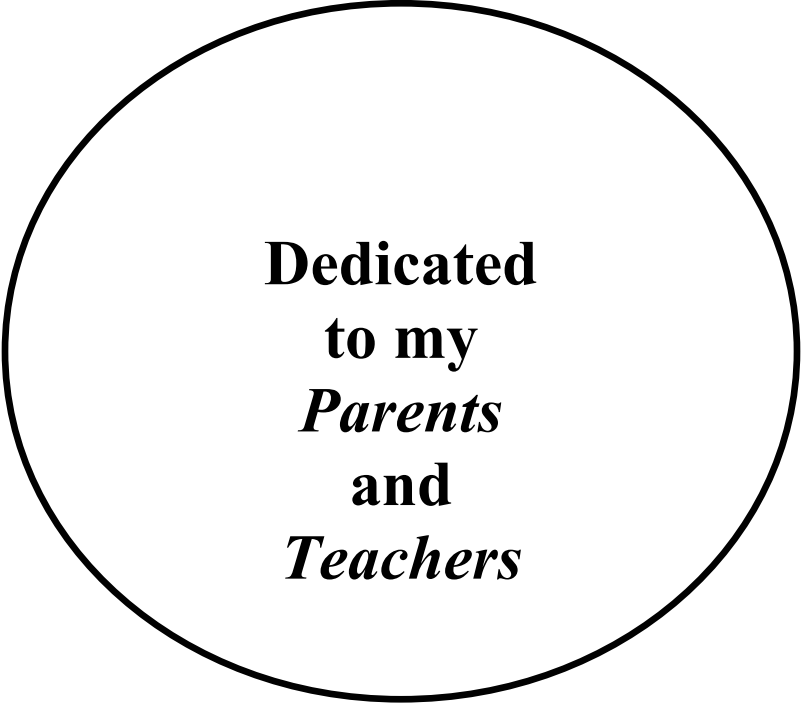
**THESIS SUBMITTED TO**

**UNIVERSITY OF PUNE**

**FOR THE DEGREE OF**

**DOCTOR OF PHILOSOPHY**

**IN**

**CHEMISTRY**

BY

## SUMANT B. PHADTARE

**PHYSICAL CHEMISTRY DIVISION**
**NATIONAL CHEMICAL LABORATORY**
**PUNE 411 008**
**INDIA**

## DECEMBER 2004

**Dedicated
to my
*Parents*
and
*Teachers***

# CERTIFICATE

This is to certify that the work discussed in the thesis entitled **"NEW METHODS FOR IMMOBILIZATION OF ENZYMES AND WHOLE CELLS"** by **SUMANT B. PHADTARE**, for the degree Doctor of Philosophy in Chemistry was carried out under my supervision at the Physical Chemistry Division of National Chemical Laboratory, Pune. Such material as has been obtained by other sources has been duly acknowledged in this thesis. To the best of my knowledge, the present work or any part thereof, has not been submitted to any other University for the award of any other degree or diploma.

Date:                                                                              Dr. Murali Sastry

Place: Pune                                                                (Research Guide)

# DECLARATION

I hereby declare that the thesis entitled **"NEW METHODS FOR IMMOBILIZATION OF ENZYMES AND WHOLE CELLS"** submitted for the degree Doctor of Philosophy in Chemistry to the University of Pune, has been carried out by me at the Physical Chemistry Division of National Chemical Laboratory, Pune under the supervision of Dr. Murali Sastry. Such material as has been obtained by other sources has been duly acknowledged in this thesis. The work is original and has not been submitted in part or full by me for any other degree or diploma to other University.


Date:                                                                        Sumant B. Phadtare

Place: Pune                                                          (Research Student)

# Acknowledgements

# Table of Contents

## CHAPTER 4: Assembly of gold nanoparticles on polyurethane and zeolite microspheres: Template for enzyme immobilization

## CHAPTER 5: Free-standing gold nanoparticle polymeric membrane: Scaffolds for enzyme and whole cell immobilization

## CHAPTER 6: Patterned thermally evaporated fatty lipid films for whole cell immobilization as enzyme sources in biotransformations

## CHAPTER 7: Conclusions

## List of Publications

# Chapter I

## Introduction

This chapter emphasizes the importance of studying protein-lipid interactions and need for immobilization of proteins/enzymes onto 2-D and 3-D supports. The different protocols used for the immobilization of biomolecules are discussed. This chapter also briefly describes the advantages of using self-organized multilayers (SOMs) for immobilization of enzymes in comparison with the as-deposited un-ordered lipid films. Gold nanoparticles assembled on different solid supports are used for the immobilization of enzymes is also described.

**1.1 Biological significance in Nanotechnology**

Biological self-assembly has stimulated biomimetic "bottom-up" approaches for the development of artificial nanometer-scaled materials which has potential commercially applications in microelectronics and micromechanical devices of increasingly small dimensions in the range of ~ 5 to 100 nm. In this regard, researchers had suggested some time ago that the synthetic nanometer-sized elements might be fabricated from biomolecular building blocks [1]. In biologically integrated devices multiple biomolecules are organized on surfaces with resolution from micron to nanometer scale. The fabrication of supramolecular structures and devices requires molecules that are capable of interlocking in a predictable, well-defined manner. Molecular self-assembly systems which exploit molecular-scale manufacturing precision of biological systems are prime candidates for supramolecular engineering.

Spatially controlled immobilization of biomolecules on solid surface of nanometer length scale is driven by the possibility of fabricating protein nano arrays with well-defined features in size, shape and spacing. Such structures are important for the fundamental study of interactions between cells and surfaces [2]. The miniaturized tools such as microarrays and microchips used in clinical applications carry great promise for the future. Protein chip consists of hundreds of proteins that are directly immobilized onto arrays on a solid support with control over density and orientation. Protein chips have emerged as an exciting technology for the broad characterization of the activities and interactions of proteins. Protein chips will prove to be essential to researchers in biology, drug discover and medical diagnosis. The limitation of such technology is that proteins are often immobilized in a range of orientations and usually undergo partial denaturation at the surface. Furthermore, the non-specific adsorption of proteins to a chip or by uncontrolled adsorption of soluble proteins in the course of an assay results in the obstruction of immobilized proteins.

In 2000, MacBeath and Schreiber showed that proteins could be printed and assayed in a microarray format [3a]. This enhanced prospects in protein chip technology. Synder and co-workers extended this concept to create protein chips comprising nearly 6000 yeast gene products and used this chip to identify new classes

of calmodulin and phospholipid binding proteins [3b]. The development of several new strategies will allow expressed proteins to be directly immobilized on substrates and avoid the need to purify or synthetically modify each protein. Several techniques have been examined for creating micron-level two-dimensional arrays of proteins on surfaces, including the use of conventional photoresist lithography, photochemistry and self assembled monolayers (SAMs) [4].

## 1.2 Building blocks in Nanotechnology

Manufactured products are made from atoms. The properties of those products depend on how these atoms are arranged. The idea of manipulating and positioning individual atoms and molecules is still new. In a classic talk Prof. Richard Feynman gave on December 29th 1959 at the annual meeting of the American Physical Society at Caltech entitled 'There's Plenty of Room at the Bottom' Prof. Feynman said, "The principles of physics, as far as I can see, do not speak against the possibility of maneuvering things atom by atom. It is not an attempt to violate any laws; it is something, in principle, that can be done; but in practice, it has not been done because we are too big." We need to apply at the molecular scale the concept that has demonstrated its effectiveness at the macroscopic scale: making parts go where we want by putting them where we want. What could we do with layered structures with just the right layers? What would the properties of materials be if we could really arrange the atoms the way we want them? In the future, nanotechnology will help to assemble these atoms or these building blocks to give new products. We'll be able to snap together the fundamental building blocks of nature easily, inexpensively and in most of the ways permitted by the laws of physics.

Nature has provided a limited number of basic building blocks such as amino acids, lipids and nucleic acids. The chemical diversity of these molecules and the different ways in which they can be polymerized or assembled provides an enormous range of possible structures. Furthermore, advances in chemical synthesis and biotechnology enable one to combine these building blocks to produce new materials and structures that have not been made by nature. These materials often have enhanced properties as well as unique applications. Moreover, one can understand nature and try

to mimic nature for the development of new materials. Biological molecules and systems have a number of attributes that make them highly suitable for nanotechnology applications. For example, proteins fold into precisely defined three-dimensional shape, and nucleic acids assemble according to well-understood rules. Antibodies are highly specific in recognizing and binding their ligands and biological assemblies such as molecular motors can perform transport operations.

Proteins/enzymes are macromolecules, which are extremely sensitive to environmental conditions. A number of interactions such as hydrophobic effect, hydrogen bonding, etc. are responsible for the stability of proteins. The primary, secondary and tertiary structures of proteins have been shown in Fig.1.1. All the atoms of the polypeptide chain interact with each other to guide the folding of the protein into its native state. In protein molecules, the amino acid residues are covalently linked to form very long, unbranched chains. They are united in a head-to-tail arrangement through substituted amide linkages called peptide bonds that arises by elimination of water from the carboxyl group of one amino acid and the $\alpha$-amino group of the next.
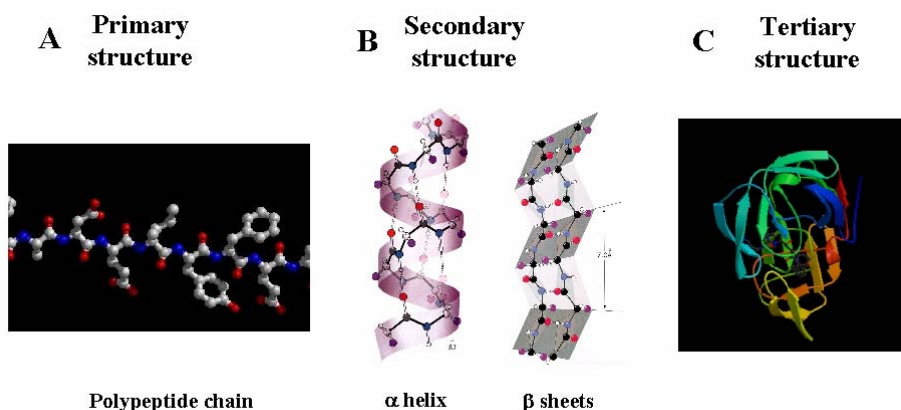


**Figure 1.1:** Schematic showing various structures of the protein. (A) Primary structure: simple polypeptide chains, (B) Secondary structure: $\alpha$-Helices, $\beta$-pleated sheets or random coils (C) Tertiary structure: weak interaction between $\alpha$-Helices, $\beta$-pleated sheets or random coils forming the overall structure of the protein.

These macromolecules are called polypeptides (Fig.1.1A). Polypeptides are found in periodic structures where each amino acid adopts the same backbone

confirmation. The periodic structures are known as secondary structures (Fig.1.1B). Covalent interactions in particular gives rigidity to the structure of a biomolecule, viz. the peptide bonds and S-S bond cross linking the cysteine residues which defines stable protein primary, secondary and tertiary structures respectively. These directional, short-range forces are of the order of inter-atomic separations (0.1 - 0.2 nm) with energy of the order 100-300 kT. Secondary interactions such as electrostatic, dipolar, van der Waals forces, hydrogen-bonding interactions, hydrophobic and hydrophilic interactions, and steric interactions play a key role in the various interactions associated with biomolecules and impart overall stability and structure to the biomolecule.

Biomolecules may easily denature or loose their biocatalytic activity after adsorbing on solid surfaces. This may be the primary reason for the design of a completely new class of materials, which can provide a biocompatible environment that can readily conserve the native structure of biomolecules. Hence, the area of interest of this thesis is to use electrostatic interactions and weak secondary interactions to form efficient biocomposite materials by immobilization of enzymes onto 2-dimentional (2-D) and 3-dimensional (3-D) supports. The 2-D supports used are the thin films of thermally evaporated fatty lipids, and hence protein-lipid interactions have also been studied. The nanoscale-curved surfaces of gold nanoparticles are used as 3-D template for the immobilization of enzymes.

## 1.3 Protein-lipid interactions

Studies on protein-lipid interactions have fundamental as well as technological importance [5]. Protein-lipid interactions are essential features of biological membranes, nevertheless many questions related to chemistry and physics of lipids and proteins are still not understood. The lack of proper understanding of molecular mechanism important for the functioning of the biological membranes also hinders practical applications in the industries. For instance, the application of drug encapsulation in lipid vesicles is hampered by short lifetime of the drug in the blood circulation caused by unstability of lipid bilayers. Lipid-protein interactions are probably the single most crucial factor that determines the action of protein molecules in biological membranes [6]. The basic structure of the biological membrane is

provided by a lipid bilayer. The lipid bilayer serves as a relatively impermeable barrier to the passage of most water-soluble molecules. The protein molecules, on the other hand, are dissolved in the lipid bilayer and mediate transport of specific molecules, function as enzymes, form structural links of plasma membrane to the cytoskeleton or other extracellular matrices, mediate energy conversion in the cell and are important receptors for receiving and transducing chemical signals. Furthermore, protein-lipid interactions are important in understanding the structure-function relationships in various diverse fields such as ion transport, photosynthesis, cell recognition, cell division etc. The protein-lipid interface has been extensively characterized, and it is well documented that the configuration of the lipid chains, interactions of the lipid head groups with protein residues, structure of the protein and overall conformation of the protein are important for a proper function of the membrane.

Surfactant-protein interactions have also been extensively investigated. In the simplest form, there is competition between surfactant self-association (micelle formation) and surfactant protein binding. The latter may lead to denaturation and/or conformational changes in the proteins. Investigations of the effects of surfactants on protein stability and conformational changes have provided insight into the structure of proteins [7a,b]. It is extremely difficult, if not impossible, to study the protein-lipid interactions *in-vivo* in membranes, hence micelles, microemulsions, monolayers, bilayers, vesicles, host-guest systems, and polyions have been used as membrane mimetic agents [7c]. Supported model membranes have been used extensively to study the structure and function of biomembranes. In particular, supported lipid bilayer membranes have been subjected to great attention because of their extraordinary ability to preserve many biological properties of cellular membranes [8a]. Sustained interest in these supported membranes is due to their relevance in designing synthetic biocompatible surfaces [8b]. Lateral fluidity of supported membranes is an important feature that distinguishes them from other surfaces. For supported membranes to maintain the structural and dynamic properties of free biomembranes, the interaction between the membrane and the substrate should be minimized.

Understanding protein-lipid interactions is also important in designing matrices for efficient immobilization of biomolecules, with enhanced temporal, temperature and pH stability, protection against degradation and intactness of natural confirmation of the immobilized biomolecule [9]. This is especially useful for enzymes, due to the tremendous applicability of immobilized biocatalysts for industries [9]. Immobilized proteins have potential use in biosensors, biomaterials, and the design of solid-phase catalysts [10a,b]. Enzyme electrodes and immunosensors are used in clinical diagnostics, food analysis and environmental monitoring applications [10c]. In biomaterials, immobilized biomolecules may be used for controlling cellular adhesion or increasing biocompatibility of the implants [11].

## 1.4 Biomolecule nanoparticle interactions

The unique electronic [12], optical [13] and catalytic [14] properties of metal and semiconductor nanoparticles in the range of 1-100 nm are used in the new generations of devices and materials that exhibit novel properties and functions [15]. The functionalized metal or semiconductor nanoparticles provide exciting building blocks for the emerging and rapidly progressing field of nanotechnology. The chemical functionalities associated with nanoparticles enable the assembly of two and three dimensional nanoparticle architecture on surfaces [16]. The assembly of nanoparticle architecture on surfaces has also led to the fabrication of nanoscale devices such as single electron transistor [17], nanoparticle based molecular switches [18], computing devices [19], capacitors [20], etc.

The conjugation of nanoparticles with biomolecules is a tempting research project as it may provide new dimensions into the area of nanobiotechnology [21]. The integration of nanotechnology with biology and medicine is expected to produce major advances in medical diagnostics, therapeutics, molecular biology and bioengineering [22]. Moreover, bioelectronics is also a rapidly progressing research field in modern science [22]. It involves the integration of biomaterials such as enzymes [23], antigen-antibodies [24], DNA [25] or cells [26] with electronic elements such as electrodes, field effect transistors and piezo-electric crystals with the aim to transduce biological events occurring on these elements by electronic signals. The discovery of

nanoparticles or nano-rods and the elucidation of their unique optical, photonic, and electronic properties suggest that the coupling of biomolecules and nanoparticles into hybrid systems could yield a new class of materials and add new perspectives to the field of bioelectronics. Semiconductor quantum dots (QDs) are used in biological labeling [27,28]. In comparison with organic dyes and fluorescent proteins, semiconductor quantum dots represent a new class of fluorescent labels with unique advantages and applications. Moreover, metal nanoparticles are also used for labeling biomolecules, since metal nanoparticles make detection possible, easier and more sensitive. Gold nanoparticles adsorbed to antibodies [29], other targeting agents such as proteins [30] or peptides [31] are widely used as labels for the detection or microscopic localization of molecular and macromolecular targets. In the early 1980's, Rembaum *et al.* [32] designed immunomicrospheres that are specially designed microscopic particles that had antibodies or similar molecules chemically bound to their surfaces and reacted in a highly specific way with target cells, viruses or other antigenic agents. The high surface-to-volume ratio offered by colloidal particles results in the concentration of the immobilized entity being considerably higher than that afforded by protocols based on immobilization on planar, 2-D surfaces, resulting in enhanced detection signals.

## 1.5 Various methods for protein immobilization

Surfaces play a vital role in biology and medicine with most biological reactions occurring at surfaces and interfaces. Protein adsorption to solid surfaces often induces structural changes that may affect the entire molecule [33,34]. For example, in some cases structural changes may be induced in the protein by the physicochemical nature of the solid surface, while other structural changes may occur due to intrinsic properties of the proteins essentially independent of the surface chemistry. In the study of immobilization of biomolecules, the principles of protein adsorption play a dominant role because the initial step of immobilization of a protein is always the adsorption process. Uncontrolled adsorption at the surface can adversely affect the activity and stability of biomolecules [35]. A number of different interactions prevail or can be utilized between the protein and the matrix for its immobilization. One of the two ways

to immobilize a biomolecule is either to modify it (so as to suit the matrix) or modify the matrix for ease of immobilization. The latter method is more effective as the immobilized biomolecule does not lose its biological activity. Immobilization of biomolecules can be generally defined as restricted mobility of biomolecules. The various methods for protein immobilization that currently exist in the literature are adsorption/attachment to prefabricated carriers, covalent binding, ionic binding, biospecific binding (use of specific interactions), crosslinking, encapsulation/inclusion in membranes, polymers, gels, microcapsules, liposomes/reversed micelles etc [36]. Some of the methods for immobilization of enzymes are discussed.

### 1.5.1 Langmuir-Blodgett films

The Langmuir-Blodgett (LB) technique has been used for the construction of monolayer and multilayer of protein films [37]. Most of the methods use the Langmuir-Schaefer method for the deposition of protein-lipid films instead of the conventional vertical lifting method. This is due to the bulkiness of the protein, which does not allow uniform multilayer deposition. Boussaad *et al.* showed by using the Langmuir-Blodgett technique that cytochrome c preoriented at the air/water interface forms a well-ordered monolayer and exhibits a reversible electron-transfer reaction after transferring onto a graphite surface [37b]. Nicolini *et al.* studied the temperature dependence of the secondary structure of photosynthetic reaction from *Rhodobacter sphaeroides* in Langmuir-Blodgett films using circular dichorism spectroscopy [37c]. Langmuir-Blodgett films is an example of self-assembly that involves attachment to the substance by weak physisorption forces that to film instability, for example with respect to removal by washing with water.

### 1.5.2 Self-assembled monolayers (SAMs)

Many of the useful properties of a solid object such as wetting and acceptance by biological systems are strongly dependent on the surface conditions. Appropriate modifications of the surface by a monolayer coating can dramatically alter these properties even though the changes induced in the corresponding bulk properties appear insignificant. Most often these monolayers are comprised of alkyl-chain compounds because of the inherent ability of alkyl chains to form very densely packed structures.

Langmuir-Blodgett films are weakly stable and for practical applications, it is necessary to prepare films that exhibit much higher degrees of stability. This can be accomplished in two ways: (1) chemical bonding between the substrate and the monolayer and (2) chemical bonding between the adsorbate molecules (crosslinking). Stenger *et al.* reported the formation of coplanar molecular patterns consisting of an alkylamine silane and perfluorinated alkylsilanes [38a]. This provides a positively charged, hydrophilic surface that has proved effective in promoting cell adhesion. SAMs of alhanethiolate terminated functional groups on gold were used for the adsorption of proteins [38b]. Monolayers that contained sufficiently large mole fraction of alkanethiolate groups terminated in oligo(ethylene oxide) chains resisted nonspecific adsorption of proteins. Moreover, resistance to the adsorption of protein increased with the length of the oligo (ethylene oxide) chains. Whitesides and co-workers have extensively investigated the role of SAMs terminating with different functional groups that resist protein/cells adsorption [38b-d]. By selecting specific functional groups with varying hydrophobicity, they achieved targeted assembly of various proteins/enzymes and biological cells. The main driving forces behind this work were applications in cell biology, biosensing, tissue engineering, and screening genomic libraries. They have used the technique of surface plasmon resonance (SPR) and contact angle titrations to investigate protein adsorption behaviour. They have extensively used the method of microcontact printing (μ-CP) for the formation of patterned SAMs for patterned and specific immobilization of biologicals [38c]. Crooks and co-workers have used this technique of μ-CP to study the patterned immobilization and growth of biological cells [38e].

### *1.5.3 Stacks of lipid bilayers*

In 1991, Kunitake and coworkers intercalated heme protein, myoglobin (Mb) in specific orientation into a multilayered cast film of phosphate/ammonium/zwitterionic bilayer membrane [39a-c]. The utility of lipid bilayers in enhancing the biological activity of the intercalated protein as compared to that of free protein has also been demonstrated [39c]. Rusling and co-workers have extensively studied the electrochemical applications of proteins/enzymes intercalated within lipid bilayers

[39d-e]. The enzymes can be incorporated into the self-assembled lipid bilayers with biotin-modified phospholipid on solid support and subsequently coupling using streptavidin modified glucose-oxidase [39f]. Due to both high specificity and affinity of the biotin-streptavidin interactions, this system represents a unique universal approach for making of different kinds of biosensors. Surface shielded porous silica beads can be non-covalently coated with a single lipid bilayer [39g]. The lipid retains their fluidity in this handy solid supported system, perfectly mimicking the soft-surface properties of cellular membrane and is used for the immobilization of membrane proteins.

*1.5.4 Adsorption on inorganic/polymer*

Adsorption of enzymes to water-insoluble supports, organic or inorganic, has been the simplest immobilization technique [40a]. This immobilization method typically involves mixing together the enzyme and support material under appropriate conditions and following a period of incubation, separating the insoluble material from the soluble material by centrifugation or filtration. The adsorption of proteins/enzymes at the interface is a complex phenomenon, which involves the following steps:

1) Transport to the interface by diffusion or convection. Mixing and shearing action would generally enhance this step.

2) Adsorption/desorption at the interface described by an interfacial chemical reaction and its related kinetic adsorption and desorption mechanism.

3) Structural alternations of molecules in contact with the interface and at higher occupancy, interactions with other adsorbed molecules.

4) Adsorption competition between molecules of different nature or molecular weight.

Adsorption of different proteins has been studied on polymers such as polystyrene, polyurethane etc. Zoungrana *et al.* studied thermal stability of α-chymotrypsin adsorbed onto different polystyrene surfaces [40b]. The adsorption on these hydrophobic sorbents leads to the reduction of the enzymatic activity. Moreover, pre-grafting of methoxy poly(ethylene oxide) methacrylate moieties on the sorbent surface reduces the loss in enzymatic activity and showed decrease in heat of denaturation. Polystyrene (PS) has shown to be the most suitable adsorption matrix for

antibodies. A number of researchers have demonstrated the adsorption of model proteins such as BSA onto PS as a function of pH, ionic strength, charge on the matrix, hydrophobicity of the protein etc [40c-h].

The support material used can be inorganic matrixes such as porous alumina, titania, zirconia, calcium carbonate, calcium phosphate gel, cellulose, clay, porous glass, ion-exchange resins, or silica gels [40a,41a]. Phosphorylated pepsin can be coupled to inorganic nanoparticles such as alumina through the interaction between phosphoserine on pepsin and the alumina surface in an orientation specific manner [41b]. Pepsin immobilized on alumina nanoparticles showed higher catalytic activity as compared to micron sized alumina particles. Adsorption of proteins from saliva on hydroxyapatite was compared with the adsorption of protein with different electric charges i.e. lysozyme, human serum albumin, β-lactoblobulin and ovalbumin [41c]. It was found that the saliva proteins have remarkable low adsorption affinity. The measured values for the electrophoretic mobilities indicate that positively charged proteins in the saliva mixture preferentially adsorb onto the negatively charged hydroxyapatite surface.

Lundqvist *et al.* studied the effect of adsorption of proteins on the surface of silica nanoparticle with diameters of 6, 9, 15 nm [41d]. This study shows that difference in particle curvature strongly influence the amount of the protein's secondary structure. Particles with longer diameter allow formation of larger particle-protein interaction surfaces and cause larger perturbations of the proteins secondary structure upon interactions. However, the effect on the tertiary structure seems to be independent of the particle curvature. Dordick and co-workers also studied the effect of chicken egg lysozyme on silica nanoparticles of various diameters [41e]. Monolayer adsorption of enzyme was observed on silica nanoparticles of 20 nm diameter whereas multilayer adsorption was observed on 100 nm. The decrease in the biocatalytic activity of the enzyme after adsorption on silica nanoparticles as compared to the free enzyme in solution was correlated to the decrease in change of α-helix content.

The purpose of a covalent binding method is to get more stable attachment of the proteins to the surface and long-term stability of the enzymes. Recently, $\gamma$-$Fe_2O_3$

magnetic nanoparticles have been used for the immobilization of *Candida rugosa* lipiase enzyme [42a]. The acylated nanoparticles were reacted directly with the enzyme, which was chemically bounded to the nanoparticle surface via C=N bond. Also the amine functionalized nanoparticles and enzyme were chemically bonded using glutaraldehyde. Proteins contain several lysine or cysteine residues, which can be used for binding onto noble metal surfaces. During such an immobilization, it is important that the amino acids essential for the catalytic activity of the enzyme are not involved in the covalent linkage to the support. Natan and co-workers have demonstrated the use of lysine rich pockets of cytochrome c for covalent immobilization onto colloidal gold/silver surfaces [42b]. Sasaki *et al.* demonstrated that the functional protein, myosin subfragment 1, binds to gold thin film surfaces through an Au-S bond involving cysteine residues in the protein [42c]. In this laboratory, we have also demonstrated the immobilization of enzymes such as pepsin, fungal protease (F-prot) and endoglucanase to colloidal gold particles. The immobilization is believed to occur via the thiols (cysteine) or amine groups (lysine) [42d-f]. Immunosensing is a major area where antibody/antibody- fragments are immobilized on the surfaces for efficient and early detection of disease. In these procedures glutaraldehyde, carboimide and other reagents such as succinimide esters, maleinimides and periodate are widely used. Proteins such as IgG, Fab' fragments of antigens, glycoproteins etc have been immobilized by a number of workers in this area for efficient and early detection of disease [42g-m].

*1.5.5 Strong interactions*

The affinity constant between avidin and biotin is $10^{15}$ L mol$^{-1}$, which is $10^5$ to $10^6$ times higher than that of regular antibody-antigen interactions. Therefore, the avidin-biotin linkage represents a practical conjugation approach to bind molecules onto nanoparticles. Usually biotin links easily to biomolecules to form recognition agents. As long as avidin molecules are immobilized on nanoparticle surface, upon avidin-biotin binding the enzymes are immobilized on the nanoparticle surfaces. Anzai *et al.* prepared protein multilayers on solid surface by using biotin-avidin interactions [43a]. Biotin labeled glucose oxidase was immobilized on avidin bound solid surface. Thereafter, by successive deposition of avidin and biotin labeled enzyme, multilayers

of enzymes were prepared. The use of the system has expanded gradually into medical diagnostics systems, particularly in DNA immobilization [43b]. Silica nanoparticles can also be surface-modified by activating them with sodium carbonate [43c]. A solution of cyanogens bromide in acetonitrile is then added to suspension to yield – OCN groups on the particle surface. The particles are then available for bioconjugation to the biomolecules containing free amino groups.

*1.5.6 Using microporous and mesoporous materials*

Inorganic templates such as layered zirconium phosphates, zeolites and mesoporous materials such as MCM-41 have been used for the immobilization of biomolecules. Kumar *et al.* [44a,b] have studied in detail the encapsulation of different proteins and enzymes in the galleries of α-zirconium phosphate [Zr (HPO$_4$)$_2$ x nH$_2$O; α-ZrP] and α-zirconium phosphonate [Zr(PO$_3$-CH$_2$COOH)$_2$ x nH$_2$O; α-ZrPAA). Kanzaki *et al.* have studied the intercalation of various enzymes with molecular weights ranging from 23,000 (papain) to 2,40,000 Da (catalase) into layered inorganic compounds γ-Titanium (IV) phosphate (Ti(HPO$_4$)$_2$) x 2H$_2$O [44c]. Mesoporous materials such as amine functionalized SBA-15 (pore size 59 Å) and mesocellular siliceous foam (MCF, pore size 160 Å) were used for the immobilization of conalbumin [44d]. Mesoporous inorganic materials such as MCM-41 and zeolites have also been used for the immobilization of various proteins and enzymes [44e].

*1.5.7 Polyelectrolytes and polyions*

A layer-by-layer (LBL) technique for the formation of layers of polyelectrolytes/polyions onto solid supports was proposed in 1991 by Decher, which works on the principle of charge overcompensation [45a,b]. This technique was successfully extended towards the realization of polyelectrolyte-nanoparticle/biomolecule multilayer films onto 2-D and 3-D supports by the groups of Caruso, Lvov, Kunitake, and Rusling [45c-i]. Different nanoparticles, proteins, enzymes and also DNA could be immobilized in polyelectrolyte multilayers using this method. Excellent biological activity of the immobilized enzyme was achieved. Multi-enzyme catalysis was also demonstrated using this technique. Crooks and co-workers

have shown the use of a hyperbranched polyelectrolyte film for the electrostatic entrapment of glucose oxidase [45j].

**1.6 Methods described in this thesis.**

In earlier studies carried out in this laboratory (1996), it has been established that thermally evaporated fatty acid lipid films can be spontaneously organized via selective ionic interactions of cations such as $Pb^{2+}$ by immersion of the lipid film in a lead chloride solution [46a]. Similarly, entrapment of $PtCl_6^{2-}$ ions organizes the amine matrix. The electrostatic entrapment of the $Pb^{2+}$ and $PtCl_6^{2-}$ ions in the acid and amine matrix thus the formation of metal salts of the fatty acid/amine leads to an organized lamellar film structure similar to $c$ - axis oriented Y-type LB films [46b]. Recognizing the principle of ion exchange is quite general, this approach has been extended to the reorganization of fatty amine films by using anions such as $AuCl_4^-$ and keggin anions $[PW_{12}O_{40}]^{3-}$ [46c-d]. The generality of this protocol was extended in 1997 to the incorporation of surface modified colloidal nanoparticles in thermally evaporated ionizable fatty lipid films [47]. It was demonstrated that both positively and negatively charged colloidal nanoparticles of silver, gold and cadmium sulfide (CdS) could be incorporated into fatty acid/amines via selective electrostatic interactions. It was found that the modulation of solution pH, film thickness and particle size, varied the amount of loading in the lipid films. The negatively charged carboxylic acid derivatized colloidal nanoparticles of silver, gold and CdS were incorporation into thermally evaporated fatty amine films [48]. The density of clusters incorporated into the organic matrix could be controlled by simple variation of colloidal solution pH, thereby leading to variation of charge on these particles as well as in the ionized lipid films. This approach has been recently extended to sequential entrapment of metal ions, formation of hetero-nanoparticle assemblies/core-shell nanoparticle structures and studied their low-temperature alloying behavior [49].

The charged nanoparticles of 3-5 nm in size were easily entrapped within the thermally evaporated stacks of lipid bilayers on solid support. Recognizing this biomolecules such as DNA, proteins, enzymes are looked as charged macromolecules and have the dimensions in the range 2-20 nm are entrapped in the thermally

evaporated lipid films. The negatively charged DNA was electrostatically entrapped within the cationic matrix [50]. The technique described in this thesis makes use of electrostatic interactions between oppositely charged proteins and the ionized stacks of lipid bilayers [51]. Other secondary interactions such as hydrophobic and hydrogen bonding also contribute to intercalation process.

Earlier immobilization of enzymes onto 3-D curved surfaces such as gold nanoparticles have been studied [42d-f]. The gold nanoparticle bioconjugate showed excellent stability and biological activity. An important feature of this work was that the enzyme retains significant biocatalytic activity after adsorption on the surface of the gold nanoparticles. However, a major drawback of this approach is that the gold nanoparticle bioconjugate material was not easily separated from the reaction mixture under ultrahigh centrifugation conditions and hence showed poor reuse characteristics. To overcome this problem, we have developed a protocol for the assembly of gold nanoparticle "shells" on massive polyurethane and zeolite submicron sphere "cores" [52]. In this manner gold nanoparticles assembled on the surface of these microspheres acts as the bulkier scaffolds for the immobilization of enzymes. These bulkier microspheres bound enzyme molecules are easily separated from the reaction mixture under mild centrifugation conditions and hence are subsequently reused. Moreover, gold nanoparticles embedded in the polymeric membranes are also used as scaffolds for the immobilization of enzymes [53]. Enzymes of cytochrome P450 monooxygenase family are present in the cell membranes of yeast cells are known to catalyze hydroxylation of arachidonic acid and are nicotinamide adenine dinucleotide phosphate (NADPH) dependent. These enzymes are difficult to extract and are unstable outside the cell membranes. Hence it was of paramount interest to used yeast cells for the hydroxylation of arachidonic acid. Since the yeast cells are used the cofactors such as NADPH are not required and are readily supplied by the cells along with the primary enzyme. Hence whole cells are immobilized on different biocompatible solid supports for the hydroxylation reactions [54].

## 1.7 Work described in this thesis

This thesis consists of seven chapters. Chapter 1 is an introduction to the thesis and gives a brief review about the types of interactions in nature, need for biomolecular

immobilization and various methods used for biomolecular immobilization. The chapter also briefly discusses the techniques developed in this thesis for immobilization of biolmolecules.

Chapter 2 describes the different experimental techniques that are extensively used for characterization of the biocomposite materials.

In chapter 3, the formation of penicillin G acylase (PGA), invertase and fungal protease (F-prot) fatty lipid biocomposite films is described. The immobilization of cationic proteins such as penicillin G acylase and fungal protease into an anionic lipid matrix such as stearic acid (StA) and anionic proteins such as invertase into cationic matrix octadecylamine (ODA) has been demonstrated. Analysis of the influence of parameters such as protein solution pH, role of buffers and thickness of the lipid films on the diffusion process has been discussed. It has been shown that the protein diffusion into the lipid films is governed to a large extent by electrostatic interactions. Secondary interactions such as hydrophobic and hydrogen bonding are also responsible for biocomposite formation. The kinetics of the protein diffusion process has been analyzed in terms of a one-dimensional (1-D) Fickian type diffusion model. Attempts at enhancing the diffusivity of the protein fungal protease in the lipid matrix (anionic StA) have been successfully demonstrated by pre-ordering the as-deposited unordered lipid films by entrapment of $Pb^{2+}$ ions within the stacks of lipid bilayers.

Chapter 4 deals with the immobilization of the enzyme pepsin on gold nanoparticles assembled on submicron polyurethane and amine functionalized zeolite particles. To overcome the *mass transport problem*, we have immobilized enzymes on the surface of gold nanoparticles assembled on massive polyurethane and zeolite particles 'core-shell' conjugate materials. The binding of the enzyme to the gold nanoparticles occurs through the amine groups and the cysteine residues present in the enzyme. The biocatalytic activity of the enzyme bound to the surface of the core-shell conjugate material is comparable to free enzyme in solution. Moreover, the substrates are easily accessible to the immobilized enzyme for the biocatalytic reactions. The bioconjugates are easily separated from the reaction medium by mild centrifugation

conditions and exhibit excellent reusability. The bioconjugates showed excellent temperature and pH stability.

In chapter 5, the immobilization of the enzyme pepsin and *Candida bombicola* whole cells as a source of cytochrome P450 enzyme on gold nanoparticles embedded in a polymeric membrane is described. A free-standing gold nanoparticle polymeric membrane is formed at the interface between chloroform containing bis(2-(4-aminophenoxy)ethyl)ether (DAEE) and aqueous chloroauric acid solution. Simple immersion of the gold nanoparticle polymeric membrane in pepsin solution results in binding of pepsin with the membrane resulting in a new biocatalyst with a number of advantages over previously used gold nanoparticle based immobilization protocols. The biocatalyst shows excellent specific activity, reusability and temperature/pH stability. The gold nanoparticle polymeric membranes are easily functionalized with various molecules such as amino acids, fatty amines etc. The amine groups in the octadecylamines (ODA) bind to the gold nanoparticles and the terminated alkyl chains provide the hydrophobic character to the gold nanoparticle polymeric membranes. This hydrophobic character can be successively used for the binding of the whole cells. The *Candida bombicola* yeast cells are then immobilized on the hydrophobic gold nanoparticle polymeric membrane and are used for the synthesis of sophorolipids from arachidonic acid. The acid hydrolysis of these sophorolipids yields 20-hydroxyeicosatetraenoic acid (20-HETE).

Chapter 6 describes the studies on the generation of patterned surfaces for the immobilization of whole cells. Thermally evaporated fatty acid/amine lipids (stacks of lipid bilayers prepared on solid support) are also used for the generation of patterned surfaces for the immobilization of protein and cells. The *Candida bombicola* yeast cells immobilized on lipid films are used for the synthesis of sophorolipids from arachidonic acid. The acid hydrolysis of these sophorolipids yields 20-hydroxyeicosatetraenoic acid (20-HETE). The cells bound to the octadecylamine (ODA) matrix is strong enough, hence reusability of the biocomposite films is possible.

Chapter 7 summarizes the work presented in the thesis. It also discusses the potential future developments for research in the area.

**References:**

1)   Drexler, K. E. *Proc. Natl. Acad. Sci. USA* **1981**, *78*, 5275-5278. (b) Haddon, R. C.; Lamola, A. A. *Proc. Natl. Acad. Sci. USA* **1985**, *82*, 1874-1878.

2)   Ziauddin, J.; Sabatini, D. M. *Nature* **2001**, *411*, 107-110.

3)   (a) MacBeath, G.; Schreiber, S. L. *Science* **2000**, *289*, 1760-1763. (b) Zhu, H.; Bilgin, M.; Bangham, R.; Hall, D.; Casamayor, A.; Bertone, P.; Lan, N.; Jansen, R.; Bidlingmaier, S.; Houfek, T.; Mitchell, T.; Miller, P.; Dean, R. A.; Gerstein, M.; Synder, M. *Science* **2001**, *293*, 2101-2105.

4)   Blawas, A. S.; Reichert, W. M. *Biomaterials* **1998**, *19*, 593-609.

5)   (a) Singer, S. J.; Nicolson, G. L. *Science* **1972**, *175*, 720-751. (b) Tamm, L. K.; McConnell H. M. *Biophys. J.* **1985**, *47*, 105-113. (c) Sackmann, E. *Science* **1996**, *271*, 43-48.

6)   Mouritesen, O. G.; Bloom, M. *Biophys. J.*, **1984**, *46*, 141-153.

7)   (a) Reynolds, J. A.; Gallagher, J. P.; Steinhardt, J. *Biochemistry* **1970**, *9*, 1232-1238. (b) Steinhardt, J.; Krijn, J.; Leidy, J. G. *Biochemistry* **1971**, *10*, 4005-4015. (c) Fendler, J. H. *Membrane mimetic chemistry* Wiley-Interscience, USA, **1982**.

8)   (a) Jost, P. C.; Griffith, O. H. *Lipid-Protein Interactions* Vol. 2, John Wiley & Sons, USA, **1982**. (b) Sackman, E.; Tanaka, M. *Trends Biotechnol.* **2000**, *18*, 58-64.

9)   (a) Avnir, D.; Braun, S. *Biochemical Aspects of Sol-Gel Science and Technology* Kluwer: Hingham, M A, **1996**. (b) Tischer, W.; Kasche, V. *Trends. Biotechnol.* **1999**, *17*, 326-335.

10)  (a) Mosbach, K. *Meth. Enzymol.* **1988**, 137. (b) Shabat, D.; Grynszpan, F.; Saphier, S.; Turniansky, A.; Avnir, D.; Keinan, E. *Chem. Mater.* **1997**, *9*, 2258-2260. (c) Turner, A. P. F.; Karube, I.; Wilson, G. S. *Biosensors: Fundamentals and applications*, Oxford university press, Oxford, **1987**.

11)  (a) Ortenwall, P.; Wadenvik, H.; Kutti, J.; Risberg, B. *J. Vasc. Surg.* **1987**, *6*, 17-25. (b) Singhvi, R.; Kumar, A.; Lopez, G. P.; Stephanopoulos, G. N.; Wang, D. I. C.; Whitesides, G. M.; Ingber, D. E. *Science* **1994**, *264*, 696-698.

12)  Andres, R. P.; Bein, T.; Dorogi, M.; Feng, S.; Henderson, J. J.; Kubiak, C. P.; Mahoney, W.; Osifchin, R. G.; Reifenberger, R. *Science* **1996**, *272*, 1323-1325.

13)  (a) Mulvaney, P. *Langmuir* **1996**, *12*, 788-800. (b) Siv Shankar, S.; Rai, A.; Ankamwar. B.; Singh, A.; Ahmad, A.; Sastry, M. *Nature Mater.* **2004**, *3*, 482-488.

14)  (a) Mandal, S.; Roy, D.; Chaudhari, R. V.; Sastry, M. *Chem. Mater.* 2004, 16, 3714-3724. (b) Mandal, S.; Selvakannan, PR.; Roy, D.; Chaudhari, R. V.; Sastry, M. *Chem. Comm.* **2002**, 3002-3003.

15)  (a) Klein, D. L.; Roth, R.; Kim, A. K. L.; Alivisatos, A. P.; McEuen, P. L. *Nature* **1997**, *389*, 699-701. (b) Ingram, R. S.; Hostetler, M. J.; Murray, R. W.; Schaaff, T. G.; Khoury, J. T.; Whetten, R. L.; Bigioni, T. P.; Guthrie, D. K.; First, P. N. *J. Am. Chem. Soc.* **1997**, *119*, 9279-9280. (c) Weller, H. *Angew. Chem. Int. Ed.* **1998**, *37*, 1658-1659.

16)  (a) Bandyopadhyay, K.; Patil, V.; Vijayamohanan, K.; Sastry, M. *Langmuir* **1997**, *13*, 5244-5248. (b) Sarathy, K. V.; Thomas, P. J.; Kulkarni, G. U.; Rao, C. N. R. *J. Phys. Chem. B* **1999**, *103*, 399-401.

17)  Andres, R. P.; Bein, T.; Dorogi, M.; Feng, S.; Henderson, J. I.; Kubiak, C. P.; Mahoney, W.; Osifchin, R. G.; Reifenberger, R. *Science* **1996**, *272*, 1323-1325.

18)  Long, B.; Nikitin, K.; Fitzmaurice. *J. Am. Chem. Soc.* **2003**, *125*, 15490-15498.

19)  Orlov, A. O.; Amlani, I.; Berstein, G. H.; Lent, C. S.; Snider, G. L. *Science* **1997**, *277*, 928-930.

20)  Feldheim, D. L.; Grabar, K. C.; Natan, M. J.; Mallouk, T. E. *J. Am. Chem. Soc.* **1996**, *118*, 7640-7641.

21)  Niemeyer, C. *Angew. Chem. Int. Ed.* **2001**, *40*, 4128-4158.

22)  (a) Heller, A. *J. Phys. Chem. 1992,* 96, 3579-3587. (b) Willner, I.; Riklin, A.; Shoham, B.; Rivenzon, D.; Katz, E. *Adv. Mater.* **1993**, *5*, 912-915. (c) Bardea, A.; Katz, E.; Tao, G.; Buckmann, A. F.; Heller, A. *J. Am. Chem. Soc.* **1997**, *119*, 9114-9119.

23)   Willner, I.; Riklin, A.; Shoham, B.; Rivenzon, D.; Katz, E. *Adv. Mater.* **1993**, *5*, 912-915.

24)  Bardea, A.; Katz, E.; Willner, I. *Electroanalysis* **2000**, *12*, 1097-1106.

25)  Patolsky, F.; Katz, E.; Willner, I. *Angew. Chem. Int. Ed.* **2002**, *41*, 3398-3402.

26)  Park, T. H.; Shuler, M. L. *Biotechnol. Prog.* **2003**, *19*, 243-253.

27) Bruchez Jr, M.; Moronne, M.; Gin, P.; Weiss, S.; Alivisatos, A. P. *Science* **1998**, *281*, 2013-2016.

28) Chan, W. C. W.; Nie, S. *Science* **1998**, *281*, 2016-2018.

29) Hainfeld, J. E. *Science* **1987,** *236*, 450-453.

30) Safer, D.; Hainfeld, J. H.; Wall, J. S.; Reardon, J. E. *Science* **1982**, *218*, 290-291.

31) Krisch, B.; Feindt, J.; Mentlein, R. *J. Histochem. Cytochem.* **1998**, *46*, 1233-1242.

32) Rembaum, A.; Dreyer, W. J. *Science* **1980**, *208*, 364-368.

33) Billsten, P.; Carlsson, U.; Jonsson, B. H. Olofsson, G.; Hook, F.; Elwing, H. *Langmuir* **1999**, *15*, 6395-6399.

34) (a) Karlsson, M.; Martensson, L. G.; Jonsson, B. H.; Carlsson, U. *Langmuir* **2000**, *16*, 8470-8479. (b) Maste, M. C. L.; Norde, W.; Visser, A. *J. Colloids Interface Sci.* **1997**, *196*, 224-230.

35) Albers, W. M.; Vikholm, I.; Viitala, T.; Peltonen, J. *Interfacial and materials aspects of the immobilization of biomolecules onto solid surfaces* Handbook of surfaces and interfaces of materials, Vol. 5, Chapter 1, Academic Press, San Diego, USA, **2001**.

36) Tischer, W.; Wedekind, F. *Top. Curr. Chem.* **1999**, *200*, 95-126.

37) (a) Langmuir, I.; Schaefer, V. J. *J. Am. Chem. Soc.* **1938**, *60*, 1351-1360. (b) Boussaad, S.; Dziri, L.; Arechabaleta, R.; Tao, N. J.; Leblanc, R. M. *Langmuir* **1998**, *14*, 6215-6219. (c) Nicolini, C.; Erokhin, V.; Antolini, F.; Catasti, P.; Facci, P. *Biochim. Biophys. Acta.* **1993**, *1158*, 273-278.

38) (a) Stenger, D. A.; Georger, J. H.; Dulcey, C. S.; Hickman, J. J.; Rudolph, A. S.; Nielsen, T. B.; McCort, S. M.; Calvert, J. M. *J. Am. Chem. Soc.* **1992**, *114*, 8435-8442. (b) Prime, K. L.; Whitesides, G. M. *J. Am. Chem. Soc.* **1993**, *115*, 10714-10721. (c) Xia, Y.; Rogers, J. A.; Paul, K. E.; Whitesides, G. M. *Chem. Rev.* **1999**, *99*, 1823-1848. (d) Roberts, C.; Chen, C. S.; Mrksich, M.; Martichonok, V.; Ingber, D. E.; Whitesides, G. M. *J. Am. Chem. Soc.* **1998**, *120*, 6548-6555. (e) Ghosh, P.; Amirpour, M. L.; Lackowski, W. M.; Pishko, M. V.; Crooks, R. M. *Angew. Chem. Int. Ed.* **1999**, *38*, 1592-1595.

39) (a) Hamachi, I.; Honda, T.; Noda, S.; Kunitake, T. *Chem. Lett.* **1991**, 1121-1125. (b) Hamachi, I.; Noda, S.; Kunitake, T. *J. Am. Chem. Soc.* **1990**, *112*, 6744-6745.

(c) Hamachi, I.; Fujita, A.; Kunitake, T. *J. Am. Chem. Soc*. **1994**, *116*, 8811-8812.
(d) Rusling, J. F. *Acc. Chem. Res*. **1998**, *31*, 363-369. (e) Chen, X.; Hu, N.; Zeng, Y.; Rusling, J. F.; Yang, J. *Langmuir* **1999**, *15*, 7022-7030. (f) Snejdarkova, M.; Rehak, M.; Otto, M. *Anal. Chem.* **1993**, *65*, 665-666. (g) Loidl-Stahlhofen, A.; Schmitt, J.; Noller, J.; Hartmann, T.; Brodowsky, H.; Schmitt, W.; Keldenich, J. *Adv. Mater.* **2001**, *13*, 1829-1835.

40) (a) Johnson, J. C. *Immobilized enzymes: Preparation and engineering, Recent advances*, Noyes data corporation, New Jersey, USA, **1979**. (b) Zoungrana, T.; Norde, W. *Colloids and Surfaces B* **1997**, *9*, 157-167. (c) Schmitt, A.; Fernandez-Barbero, A.; Cabrerizo-Vilchez, M.; Hidalgo-Alvarez, R. *Prog. Colloid Polym. Sci*. **1997**, *104*, 144-147. (d) Elgersma, A. V.; Zsom, R. L. J.; Norde, W.; Lyklema, J. *J. Colloid Interface Sci*. **1990**, *138*, 145-156. (e) Kamyshny, A.; Magdassi, S. *Colloids and Surfaces B* **1997**, *9*, 147-155. (f) Peula, J. M.; de las Nieves, F. J. *Colloids and Surfaces A* **1993**, *77*, 199-208. (g) Peula, J. M.; de las Nieves, F.J. *Colloids and Surfaces A* **1994**, *90*, 55-62. (h) Molina-Bolivar, J. A.; Ortega-Vinuesa, J. L. *Langmuir* **1999**, *15*, 2644-2653.

41) (a) Woodward, J. *Immobilized cells and enzymes: a practical approach*, IRL Press, Oxford, UK, **1985**. (b) Li, J.; Wang, J.; Gavalas, V. G.; Atwood, D. A.; Bachas, L. G. *Nano Lett.* **2003**, *3*, 55-58. (c) Kawasaki, K.; Kambara, M.; Matsumura, H.; Norde, W. *Colloids and Surfaces B* **2003**, *32*, 321-334. (d) Lundqvist, M.; Sethson, I.; Jonsson, B. *Langmuir* **2004**, DOI: 10.1021/la0484725. (e) Vertegel, A. A.; Siegel, R. W.; Dordick, J. S. *Langmuir* **2004**, *20*, 6800-6807.

42) (a) Dyal, A.; Loos, K.; Noto, M.; Chang, S. W.; Spagnoli, C.; Shafi, K. V. P. M.; Ulman, A.; Cowman, M.; Gross, R. A. *J. Am. Chem. Soc.* **2003**, *125*, 1684-1685. (b) Keating, C. D.; Kovaleski, K. M.; Natan, M. J. *J. Phys. Chem. B*. **1998**, *102*, 9404-9413. (c) Sasaki, Y. C.; Yasuda, K.; Suzuki, Y.; Ishibashi, T.; Satoh, I.; Fujiki, Y.; Ishiwata, S. *Biophys. J.* **1997**, *72*, 1842-1848. (d) Gole, A.; Dash, C.; Ramakrishnan, V.; Sainkar, S. R.; Mandale, A. B.; Rao, M.; Sastry, M. *Langmuir* **2001**, *17*, 1674-1679. (e) Gole, A.; Dash, C.; Sainkar, S. R.; Rao, M.; Sastry, M. *Bioconjugate Chem.* **2001**, *12*, 684-690. (f) Gole, A.; Vyas, S.; Phadtare, S.; Lachke, A.; Sastry, M. *Colloids and Surfaces B* **2002**, *25*, 129-138. (g) Bin, L.;

Xie, J.; Lu, C.; Wu, C.; Wie, Y. *Anal. Chem*. **1995**, *67*, 83-87. (h) O' Brien, J. C.; Jones, V. W.; Porter, M. D.; Mosher, C. L.; Henderson, E. *Anal. Chem*. **2000**, *72*, 703-710. (i) O' Shannessy, D. J.; Hoffman, W. L. *Biotechnol. Appl. Biochem*. **1987**, *9*, 488-496. (j) Viitala, T.; Vikholm, I.; Peltonen, J. *Langmuir* **2000**, *16*, 4953-4961. (k) Nakanishi, K.; Mvguruma, H.; Karube, I. *Anal. Chem*. **1996**, *68*, 1695-1700. (l) Vikholm, I.; Albers, W. M. *Langmuir* **1998**, *14*, 3865-3872. (m) Prisyazhnoi, V. S.; Fusek, M.; Alakhov, Y. B. *J. Chromat*. **1988**, *424*, 243-253.

43) (a) Anzai, J.; Kobayashi, Y.; Suzuki, Y.; Takeshita, H.; Chen, Q.; Osa, T.; Hoshi, T.; Du, X. *Sensors and Actuators B* **1998**, *52*, 3-9. (b) Niemeyer, C. M.; Ceyhan, B.; Blohm, D. *Bioconjugate Chem*. **1999**, *10*, 708-719. (c) Qhobosheane, M.; Santra, S.; Zhang, P.; Tan, W. *Analyst* **2001**, *126*, 1274-1278.

44) (a) Kumar, C. V.; Chaudhari, A. *J. Am. Chem. Soc*., **2000**, *122*, 830-837. (b) Kumar, C. V.; McLendon, G. L. *Chem. Mater*. **1997**, *9*, 863-870. (c) Kanzaki, Y.; Abe, M. *Bull. Chem. Soc. Jpn*. **1991**, *64*, 2292-2294. (d) Han, Y.; Stucky, G. D.; Butler, A. *J. Am. Chem. Soc*. **1999**, *121*, 9897-9898. (e) He, J.; Li, X.; Evans, D. G.; Duan, X.; Li, C. *J. Mol. Catal. B*. **2000**, *11*, 45-53.

45) (a) Decher, G. *Science* **1997**, *277*, 1232-1237. (b) Schmitt, J.; Decher, G.; Dressik, W. J.; Brandow, S. L.; Geer, R. E.; Shashidhar, R.; Calvert, J. M. *Adv. Mater*. **1997**, *9*, 61-65. (c) Lvov, Y.; Ariga, K.; Ichinose, I.; Kunitake, T. *J. Am. Chem. Soc*. **1995**, *117*, 6117-6123. (d) Caruso, F.; Niikura, K.; Furlong, D. N.; Okahata, Y. *Langmuir* **1997**, *13*, 3427-3433. (e) Caruso, F.; Mohwald, H. *J. Am. Chem. Soc*. **1999**, *121*, 6039-6046. (f) Caruso, F. *Adv. Mater.* **2001**, *13*, 11-22. (g) Lvov, Y.; Munge, B.; Giraldo, O.; Ichinose, I.; Suib, S. L.; Rusling, J. F. *Langmuir* **2000**, *16*, 8850-8857. (h) Ma, H; Hu, N.; Rusling, J. F. *Langmuir* **2000**, *16*, 4969-4975. (i) Lvov, Y. M.; Lu, Z.; Schenkman, J. B.; Zu, X.; Rusling, J. F. *J. Am. Chem. Soc*. **1998**, *120*, 4073-4080. (j) Franchina, J. G.; Lackowski, W. M.; Dermody, D. L.; Crooks, R. M.; Bergbreiter, D. E.; Sirkar, K.; Russell, R. J.; Pishko, M. V. *Anal. Chem*. **1999**, *71*, 3133-3139.

46) (a) Ganguly, P.; Pal, S.; Sastry, M.; Shashikala, M. N. *Langmuir* **1995**, *11*, 1078-1080. (b) Pal, S. *Ph.D. Thesis*, University of Pune, **1996**. (c) Gole, A**.;** Sastry, M.

*Inorg. Chem. Commun.* **2001, 4**, 568-570. (d) Gole, A.; Kumar, A.; Phadtare, S.; Sastry, M. US Patent and Indian Patent filed **2001**.

47) (a) Sastry, M. *Nanoparticles: Building block for Nanotechnology* **2004**, Ed. Rotello, V. Kluwer Academic/Plenum Publishers USA. (b) Mandal, S.; Damle, C.; Sainkar, S. R.; Sastry, M. *J. Nanoscience Nanotech.* **2001**, *1*, 281-285. (c) Mandal, S.; Sainkar, S. R.; Sastry, M. *Nanotechnology* **2001**, *12*, 358-362.

48) (a) Patil, V.; Mayya, K. S.; Sastry, M. *Langmuir* **1998, 14**, 2707-2711. (b) Sastry, M.; Patil, V; Mayya, K. S. *Langmuir* **1997**, *13*, 4490-4492. (c) Sastry, M.; Patil, V.; Sainkar, S. R. *J. Phys. Chem. B.*, **1998**, *102*, 1404-1410. (d) Patil, V.; Sastry, M. *Langmuir* **2000**, *16*, 2207-2212. (e) Patil, V.; Sastry, M. *Langmuir* **1997**, *13*, 5511-5513. (f) Patil, V.; Malvankar, R. B.; Sastry, M. *Langmuir* **1999**, *15*, 8197-8206. (g) Patil, V.; Sastry, M. *J. Chem. Soc. Faraday Trans.*, **1997**, *93*, 4347-4353. (h) Sastry, M. *Curr. Sci.* **2000**, *72*, 1089-1097. (i) Sastry, M. *Nanoparticle thin films: An approach based on self-assembly*, Handbook of surfaces and interfaces of materials, Vol. 3, Academic Press, San Diego, USA, **2001**.

49) (a) Kumar, A.; Damle, C.; Sastry, M. *Appl. Phys. Lett.* **2001**, *79*, 3314-3316. (b) Damle, C.; Kumar, A.; Sastry, M. *J. Phys. Chem. B*. **2002**, *106*, 297-302.

50) (a) Sastry, M.; Ramakrishnan, V.; Pattarkine, M.; Ganesh, K. N. *J. Phys. Chem. B* **2001**, *105*, 4409-4414. (b) Ramkrishnan, V. *Ph.D. Thesis*, University of Pune, **2003**.

51) (a) Sastry, M. *Trends Biotechnol.* **2002**, *20*, 185-189 and references therein. (b) Gole, A. *Ph.D. Thesis*, University of Pune, **2002**.

52) (a) Phadtare, S.; Vinod, V. P.; Muhkopadhyay, K.; Kumar, A.; Rao, M.; Chaudhari, R. V.; Sastry, M. *Biotechnol. Bioeng.* **2004**, *85*, 629-637. (b) Muhkopadhyay, K.; Phadtare, S.; Vinod, V. P.; Kumar, A.; Rao, M.; Chaudhari, R. V.; Sastry, M. *Langmuir* **2003**, *19*, 3858-3863.

53) Phadtare, S., Vinod, V. P., Wadgaonkar, P. P., Rao, M., Sastry, M. *Langmuir* **2004**, *20*, 3717-3723.

54) Phadtare, S.; Shah, S.; Prabhune, A.; Wadgaonkar, P. P.; Sastry, M. *Biotechnol. Prog.* **2004**, DOI 10.1021/bp049792h.

# Chapter II


# Characterization techniques

___

The different experimental techniques used during the course of the present work are discussed in this chapter

This thesis describes the formation of protein-lipid, protein-gold nanoparticle biocomposites, and whole cell immobilization on thermally evaporated fatty acid/amine lipid films and on the surface modified gold nanoparticle polymeric membrane. Various characterization techniques such as Quartz crystal microgravimetry (QCM), UV-visible spectroscopy, Fourier Transform Infrared Spectroscopy (FTIR), Fluorescence spectroscopy, Scanning Electron Microscopy (SEM), Transmission Electron Microscopy (TEM), X-ray diffraction, Contact angle measurements and Biocatalytic activity measurements have been used to characterize these biocomposites. This chapter is devoted to explain the basic principles and the techniques used for characterization. The basic requirement for the formation of protein-lipid biocomposite films is the preparation of thermally evaporated fatty acid/amine lipid films on solid support. Subsequent immersion of these lipid films in protein/electrolyte solution leads to the formation of *self-organized multilayers* (SOMs). Another part of the thesis describes the assembly of gold nanoparticles on massive polymer/silica microspheres and their subsequent use for the immobilization of the enzymes. Free-standing gold nanoparticle embedded polymeric membrane are also used as scaffolds for binding of enzyme and whole cells.

## 2.1 Thermal evaporation of fatty acid/ amine lipids

Thermally evaporated fatty acid and amine lipid films used for enzyme immobilization in this thesis have been deposited using Edwards E306 coating unit. The coating unit consists of a rotary pump used for backing and roughing the chamber where deposition is done and can produce a vacuum upto $10^{-3}$ Torr. Below this pressure, oil diffusion pump is employed to produce high vacuum of $10^{-7}$ Torr [1] and the deposition rate was 10 Å /min. Both these pumps are used in conjunction for backing and roughing of the deposition chamber. A liquid nitrogen trap was also used. Deposition of organic thin films is done under vacuum due to the following reasons:

1) The quality of deposition is better due to the increased mean free path of a molecule under vacuum as compared to atmosphere, resulting in a linear trajectory of the thermally evaporated molecule.

2)  The melting point of fatty acid/ amine lipids is reduced under vacuum, enabling low current requirements for thermal evaporation.

The fatty acid/amine lipids (amphiphilic molecules) used for deposition, were taken in a molybdenum boat and subjected to low tension DC of about 20 amps under $10^{-7}$ Torr vacuum and heated. The substrates such as Si(111), glass and quartz were kept at a suitable distance above the molybdenum boat. The molecules when heated evaporated and condensed onto these substrates giving nearly same thickness of the uniform films on each substrate. The rate of deposition and the thickness of the lipid films was monitored *in-situ* using Edwards FTM5 quartz crystal microbalance. The films were tested for stability by using infrared spectroscopy, and it was found that the films did not decompose on deposition in vacuum.

## 2.1.1 Amphiphilic molecules

An amphiphilic molecule has a hydrophobic and a hydrophilic part.  The hydrophobic end is normally a long chain of hydrocarbons called the tail and the hydrophilic moiety is called the polar head group as shown in Fig.2.1.
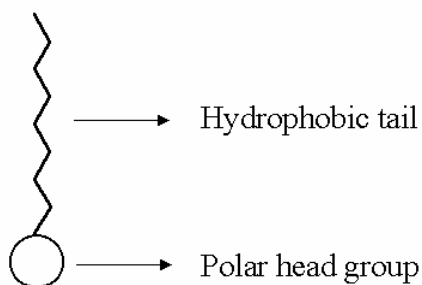


**Figure 2.1:** Schematic representation (not to scale) of an amphiphilic molecule showing the hydrophobic long chain hydrocarbons and hydrophilic head group.

The amphiphilic molecules we have used in this work are: Stearic acid [StA; $CH_3$-$(CH_2)_{16}$-COOH] and octadecylamine [ODA; $CH_3$-$(CH_2)_{17}$-$NH_2$].

*2.1.2 Self-organized Multilayers (SOMs)*

In earlier studies in this laboratory, it has been shown that the thermally evaporated films of fatty acids and amines can be spontaneously organized via selective ionic interaction of cations/anions by simple immersion of the lipid film in a suitable electrolyte [2]. This leads to an organized lamellar film structure similar to c-axis oriented Y-type LB films, which is termed as self-organized multilayers (SOMs). Recognizing this, approach was further extended to study the electrostatic binding of surface modified colloidal nanoparticles in thermally evaporated fatty acid and amine lipid films [3]. The various biomolecules such as DNA, proteins, enzymes, etc. have the dimensions same as that of colloidal nanoparticles. Thus, this technique was further extended to entrap biomolecules such as DNA and enzymes in thermally evaporated fatty acid/amine lipid films [4].

## 2.2 Quartz crystal microgravimetry (QCM)

Quartz crystal microgravimetry is extensively used to investigate adsorption of self-assembled monolayers (SAMs)[5], Langmuir-Blodgett films [6], nanoparticles [6,7], and biomolecules [8]. Jin *et al.* studied the high activity enzyme microcrystal multilayer films constructed by layer-by-layer (LbL) deposition of the polyelectrolyte coated catalase crystals and oppositely charged polyelectrolyte on QCM electrodes [9]. In this thesis, QCM have been used for calculating the exact amount of entrapped enzyme within the stacks of lipid bilayers. The knowledge of exact amount of the immobilized biocatalyst is important to compare the activity of the immobilized enzyme with the similar amount of the free enzyme in solution.

In 1880, Jacques and Pieree Curie discovered that mechanical stress applied to the surfaces of various crystals such as quartz, rochelle and tourmaline afforded a corresponding electrical potential across the crystal whose magnitude was proportional to the applied stress [10]. This behavior is referred to as the *piezoelectric effect*. This property exists only in materials that are acentric that is those crystallize in noncentrosymmetric space groups. A single crystal of an acentric material will possess a polar axis due to dipoles associated with the orientation of atoms in the crystalline lattice. When stress is applied across an appropriate direction, there is a shift of dipoles

resulting from the displacement of atoms. This atomic displacement leads to a corresponding change in the net dipole moment producing a net change in electrical charge on the faces of the crystal. The validity of the converse of this effect was also established wherein application of a voltage across these crystals afforded a corresponding mechanical strain. This inverse piezoelectric effect is the basis of the quartz crystal microgravimetry (QCM) technique. AT-cut quartz resonator, in which thin quartz wafer is prepared by slicing a quartz rod at an angle of $35^{\circ}$ with respect to the X-axis of the crystal, resonates in the *thickness shear mode*. Fig.2.2 shows a gold-coated QCM crystal.
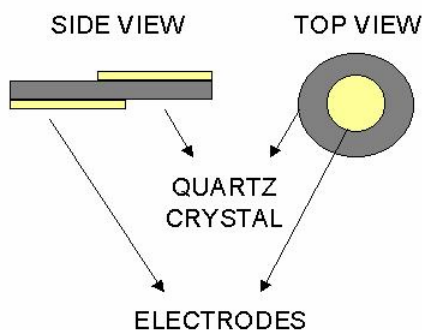


**Figure 2.2:** Diagram (not to scale) showing details of a quartz resonator

Application of electric field across the crystal causes a vibrational motion of the quartz crystal, with amplitude parallel to the surface of the crystal [5b]. The vibrational motion of the quartz crystal results in the establishment of transverse acoustic waves that propagates across the thickness of the crystal, reflecting back into the crystal at the surface. When a uniform layer of foreign material is added to the surface of the quartz crystal, the acoustic wave will travel across the interface and will propagate through the layer. This leads to decrease in the frequency of the crystal. The details have been depicted in the Fig.2.3. The Frequency changes on deposition of the film can be converted to mass loading by using the Saurbrey formula [11].

$$\Delta f = -\, 2\, f_o^2 \; x \frac{\Delta m}{A \; x \; (\mu \; x \; \rho)^{1/2}} \qquad \ldots(\,2.1)$$

where $\Delta f$ - frequency change, $f_o$ - frequency of the crystal prior to a mass change, $\Delta m$ - mass change, A - Piezo electrically active area, $\mu$ - shear modulus for quartz, $\rho$ - density of quartz ($\mu = 2.95 \; x \; 10^{11} \; g \; cm^{-1} \; s^{-2}$, $\rho = 2.65 \; g/cm^3$).
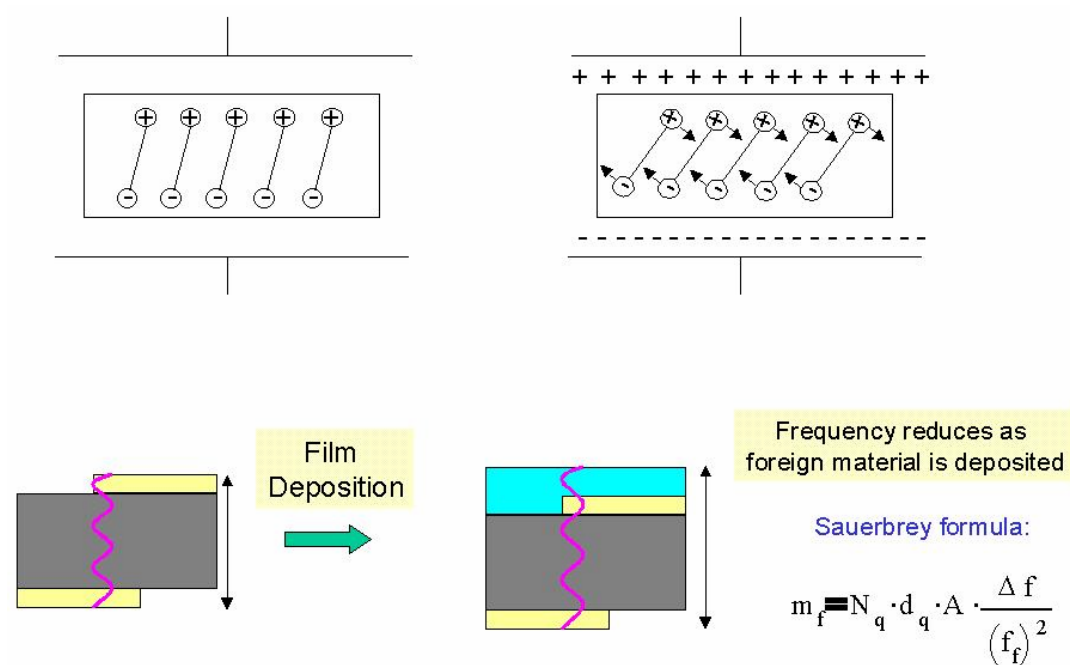


**Figure 2.3:** Schematic representation (not to scale) of the converse piezoelectric effect for shear motion. The electric field induces reorientation of the dipoles of the acentric material, resulting in a lattice strain and shear deformation of the material. Direction of shear is dependent upon the applied potential while the extent of shear strain depends on the magnitude of the applied potential.

The work described in this thesis, we have used gold-coated AT-cut 6 MHz quartz crystal. The frequency counter used was an Edwards FTM5 instrument operating at a frequency stability and resolution of $\pm$ 1 Hz. At this resolution and with the type of quartz crystal used, the mass resolution would be 12 ng/cm$^2$. The different thicknesses of lipid films were thermally evaporated on the QCM crystals. These crystals were

immersed into protein solution for different time intervals and the frequency changes were measured *ex-situ* after thorough washing with deionized water and drying in flowing nitrogen. The frequency changes were converted to a mass uptake by using the standard Saurbrey formula [11]. The "leaching out" of the proteins was also studied by QCM by immersing the enzyme incorporated lipid films in appropriate buffer solution and measuring the frequency change at different time intervals.

There may be errors in the interpretation of the QCM data using the simple Saurbrey formula. Most QCM investigations assume that the film layer shows rigid behavior and no slip at the resonator-fluid boundary, while using Saurbrey equation [11]. These assumptions are valid when dealing with studies on inorganic thin films, wherein the films deposited is rigid enough to be considered "quartz like". However, while dealing with lipid films that are being intercalated with biological molecules such as proteins and DNA, one would need to consider factors such as viscoelastic effects, high mass loadings, surface roughness, surface stress, interfacial slippage and non uniform mass distribution in any piezoelectric measurement [5a,b]. QCM measurements are considered accurate provided the mass of the film does not exceed 2 % of the mass of the crystal. The work discussed in this thesis, QCM plays an important role in determining the amount of enzyme entrapped within the stacks of lipid bilayers. The thin films of thickness 250 Å used in this study has mass loading of 6-12 $\mu g/cm^2$ as compared to total weight of the crystal. Assuming uniform mass distribution over the film surface supports the validity of the use of Saurbrey equation in our case.

## 2.3 UV-visible spectroscopy

The work described in this thesis, UV-visible spectroscopy is used for monitoring the signatures of gold nanoparticles and amount of enzyme bound to the gold nanoparticles.

### *2.3.1 Theory*

UV-visible spectroscopy is a powerful tool for the characterization of colloidal particles [12]. In particle, noble metal particles are ideal candidates for study with UV-

vis spectroscopy, since they exhibit strong surface plasmon resonance absorption in the visible region and are highly sensitive to the surface modification. The light absorption by small metal particles is described by Mie theory [12]. The absorption spectrum of particles in a given solvent can be calculated from optical constants of the bulk metal [13]. The absorption spectrum of spherical particles of sizes between 3 to 30 nm does not strongly depend on particle size. This is because the particles are below the size at which higher order term in the Mie formulae for the absorption constant becomes significant. Thus one has to regard only the dipole term, which depends only on the total metal concentration in the solution and not on particle size. The absorption coefficient $\alpha$ (mol$^{-1}$ L cm$^{-1}$) is calculated from the relation 2.2.

$$\alpha = \frac{18\,\pi}{\ln 10} \frac{10^5}{\lambda} \frac{M\,n_o^3}{\rho} \frac{\varepsilon_2}{(\varepsilon_1 + 2n_o^2) + \varepsilon_2^2} \qquad ....2.2$$

where $\lambda$ is the wavelength of light, M and $\rho$ are the molecular weight and density of the metal, $n_o$ is the refractive index of the solvent and $\varepsilon_1$ and $\varepsilon_2$ are the real and imaginary parts of the dielectric constant of the metal. When the size of the particles becomes smaller than the mean free path of the electrons, the absorption bands are broadened this is accounted by using size-corrected values of $\varepsilon_2$ [14].

$$\varepsilon_2 = \varepsilon_{2(bulk)} + (\omega_p^2 / \omega^3)\,(\nu_F / R) \qquad .....2.3$$

where $\omega$ is the frequency of light, $\omega_p$ the plasmon frequency, $\nu_F$ the electron velocity at the Fermi level and R the particle radius ($R/\nu_F$, mean time of the free movement of the electrons). Resonance with the incident light is reached at the wavelength where the negative value of $\varepsilon_1$ of the metal is equal to twice the dielectric constant of the medium.

Gold nanoparticles possess plasmon resonances in the visible range (~514 nm). Resonance is produced by a collective excitation of all the free electrons in the particles. As shown in Fig.2.4 the movement of the electrons under the influence of

electric field vector of the incoming light leads to a dipole excitation across the particle sphere, the positive polarization charge acting as a restoring force which makes the electrons oscillate. Thus the electron density within surface layer, the thickness of which is about equal to the screening length of a few angstroms, oscillate whereas the density in the interior of the particle remains constant ("surface plasmon"). Therefore, any changes in the electron density of this surface layer will lead to changes in the plasmon absorption.
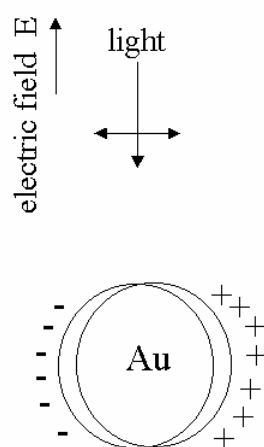


**Figure 2.4:** Schematic representation (not to scale) showing the polarization of a spherical metal nanoparticle by the electric field vector of the incoming light.

The work described in this thesis, UV-Vis spectroscopy was used to monitor the binding of gold nanoparticles to polyurethane and amine functionalized zeolite microsphers. UV-Vis spectra of gold nanoparticles bound to the surface of polyurethane microsphers was monitored on a quartz substrate. The mass loading of gold nanoparticles on polyurethane and amine functionalized zeolite was estimated by UV-vis spectra from the decrease in the intensity of the surface plasmon resonance of gold nanoparticles in the supernatant obtained after centrifugation of the microsphers. UV-vis spectra of gold nanoparticle polymeric membrane transferred on quartz substrate were recorded in transmission mode. These measurements were done on a JASCO V570 UV/VIS/NIR operated at a resolution of 1 nm.

*2.3.2 Protein quantitative analysis*

Any molecule absorbs light in some wavelength range. However, for any selected wavelength certain types of chemical groups usually dominate the observed spectrum. These groups are called chromophores. Typical chromophores found in proteins and nucleic acids absorb light only at wavelength less than 300 nm. The absorbance of a protein solution above 275 nm depends on three chromophores the side chains of tryptophan, tyrosine and cystine [15]. An average protein with no prosthetic groups has a $\lambda_{max}$ in the near UV at about 280 nm. Tryptophan, tyrosine and cystine have extinction coefficients at this wavelength of about 5700, 1300 and 130 $M^{-1}$ $cm^{-1}$ respectively. As a rough approximation one can assume that the extinction coefficients of these amino acids do not change drastically when they are incorporated into a protein.

In tyrosine the local symmetry is much lower and a much stronger transition ($\varepsilon$ 1300 $M^{-1}$ $cm^{-1}$) is observed at 274 nm. The absorption spectrum of indole side chain of trptophan is more complex with narrow wavelength region 240 to 290 nm consists of three or more electronic transitions. The resonance at about 280 nm arising from the $\pi \rightarrow \pi^{*}$ transitions in the tyrosine and tryptophan residues in proteins is a characteristic signature which has been probed by us. The concentration of a protein in a solution is determined by using Beer-Lambert law by measuring the absorbance at 280 nm.

$$A = \varepsilon\, c\, l \qquad \dots\dots 2.4$$

where, A is absorbance, $\varepsilon$ molar absorptive coefficient ($M^{-1}$ $cm^{-1}$), l path length (cm) and c protein concentration (M). The above relation is used to determine the amount of enzyme bound to the different scaffolds. After separation of the bioconjugates from the enzyme solution, the supernatant are analyzed for the enzyme quantitative analysis. The loss in absorbance at 280 nm in the supernatant (arising from $\pi$-$\pi$* transitions in tryptophan and tyrosine residues in proteins) was used to quantify

the amount of pepsin bound to the bioconjugates. These measurements were done on a JASCO V570 UV/VIS/NIR operated at a resolution of 1 nm.

## 2.4 Fourier transform infrared spectroscopy (FTIR)

The energy required exciting the bonds in a compound and making them to vibrate more energetically occurs in the infrared region of the spectrum (ca. 400-4000 $cm^{-1}$). If we pass a beam of infrared radiations of varying frequency through a sample then the energy of the beam is absorbed. This happen when the energy matches the difference between vibrational energy levels belonging to the bonds. The vibrational frequency of the molecule is given by simple harmonic equation 2.5.

$$\nu = \frac{1}{2\pi} \sqrt{\frac{k}{\mu}} \qquad \ldots.. \; 2.5$$

where $\nu$ is resonant frequency, k is force constant and $\mu$ is reduced mass.

Infra-red Spectroscopy (IR) affords an excellent insight into the organization of hydrophobic chain, transport and ion exchange properties of the LB film [16].

### 2.4.1 Peak assignments for fatty lipids

The fatty lipids used in this thesis are octadecylamine (ODA) and stearic acid (StA). The peak assignments have been discussed in general.

### 2.4.1 (A) C-H stretch

The two bands at 2920 and 2850 $cm^{-1}$ have been assigned to the antisymmetric and symmetric methylene ($CH_2$) stretching vibrations respectively and two weak bands at about 2960 and 2875 $cm^{-1}$ to the asymmetric/degenerate and symmetric methyl ($CH_3$) stretching vibrations respectively. The position of the peaks and the increase in intensity of the methylene stretching vibrations relative to methyl stretching vibration with chain length indicates structural integrity of the molecule. More interestingly,

actual peak values of the symmetric and antisymmetric $CH_2$ stretching vibrations can be used as a sensitive indicator of the ordering of the alkyl chains.

*2.4.1 (B) N-H vibrations*

Typical peaks for the free amine are seen at 3333 cm$^{-1}$. This band shifts to 3198 cm$^{-1}$ on salt formation of primary amine [17a,b]. $NH_3$ symmetric deformation band is observed at 1487 cm$^{-1}$ in case of pure amine and is absent in case of amine salts as observed in the case of chloroplatinic acid complexed with octadecylamine [17c]. The $NH_3$ antisymmetric deformation appears in the region of 1587 cm$^{-1}$ [18].

*2.4.2 Peak assignments for proteins*

FTIR is a powerful tool to study protein-lipid biocomposite films. The position of amide I, II and III bands in the FTIR spectra of proteins is a sensitive indicator of conformational changes in the protein secondary structure [19] and we have used this to study the conformational changes of protein molecules in the lipid matrix. The amide linkages between amino acid residues in polypeptides and proteins give rise to well-known signatures in the infrared region of the electromagnetic spectrum. The position of the amide I (C=O band in amide linkage at ca. 1650 cm$^{-1}$), amide II band (N-H stretch mode of vibration in the polypeptide linkage at ca. 1546 cm$^{-1}$) and amide III (C-N band in the polypeptide chain at ca. 1240 cm$^{-1}$) bands in the FTIR spectra of proteins is a sensitive indicator of conformational changes in the protein secondary structure [20]. These bands in the biocomposite films have been compared with drop dried proteins films on Si(111) substrates.

The work described in this thesis, 250 Å thick thermally evaporated fatty acid/amine lipid films were deposited on a Si(111) wafer. The silicon substrates were used in this study since they are chemically stable and generally are not reactive. It is excellent for optical studies of deposited films in the visible region using reflection techniques. It does not have strong lattice absorption bands in the useful regions of the infrared and thus can be used for transmission studies in this region. To correct for the lattice absorption bands in silicon, a reference silicon sample is used as a reference. FTIR measurements of 250 Å thick fatty acid/amine biocomposite lipid films on

Si(111) substrates were carried out *ex-situ* after immersion of the films in the aqueous enzyme solution and whole cells dispersed in deionized water. Through washing and drying of the films was done prior to FTIR measurements. For comparison FTIR measurements of as-deposited fatty acid/amine lipids films were also recorded. FTIR was used to study the binding of gold nanoparticles to amine-functionalized zeolite particles. A film of amine-functionalized zeolite before and after binding with gold nanoparticles was prepared on a Si(111) substrate by drop-casting from solution. FTIR measurements of gold nanoparticle polymeric membrane before and after binding with octadecylamine were also recorded by transferring the membranes on Si(111) substrate. These measurements were done in the diffuse reflectance mode on a Perkin-Elmer Spectrum One FTIR spectrometer operated at the resolution of 4 cm$^{-1}$. A total of 256 scans yielded a good signal to noise ratio of the IR spectra.

## 2.5 Fluorescence spectroscopy

Light emission can reveal properties of biological molecules quite different from the properties revealed by light absorption. The process takes place on a much slower time scale, allowing a much wider range of interactions and perturbations to influence the spectrum. The chromophores found in proteins are tryptophan and tyrosine. By and large, quantum yields ($\phi_F$) are low and lifetimes ($\tau_F$) are short given in Table 1. The fluorescence quantum yield ($\phi_F$) is equal to the ratio of photons emitted to photos absorbed by the system.

**Table 1**

Fluorescence characteristics of protein constituents

| Substance | Conditions | Abs. $\lambda_{max}$ (nm) | Abs. $\varepsilon_{max}$ (M$^{-1}$ cm$^{-1}$) | Fluore-scence* $\lambda_{max}$ (nm) | Fluore-scence* $\phi_F$ | $\tau_F$ (nsec) |
|---|---|---|---|---|---|---|
| Tryptophan | H$_2$O, pH 7 | 280 | 5600 | 348 | 0.20 | 2.6 |
| Tyrosine | H$_2$O, pH 7 | 274 | 1400 | 303 | 0.14 | 3.6 |

* Values shown for $\phi_F$ are the largest usually observed. In a given case actual values can be considered lower.
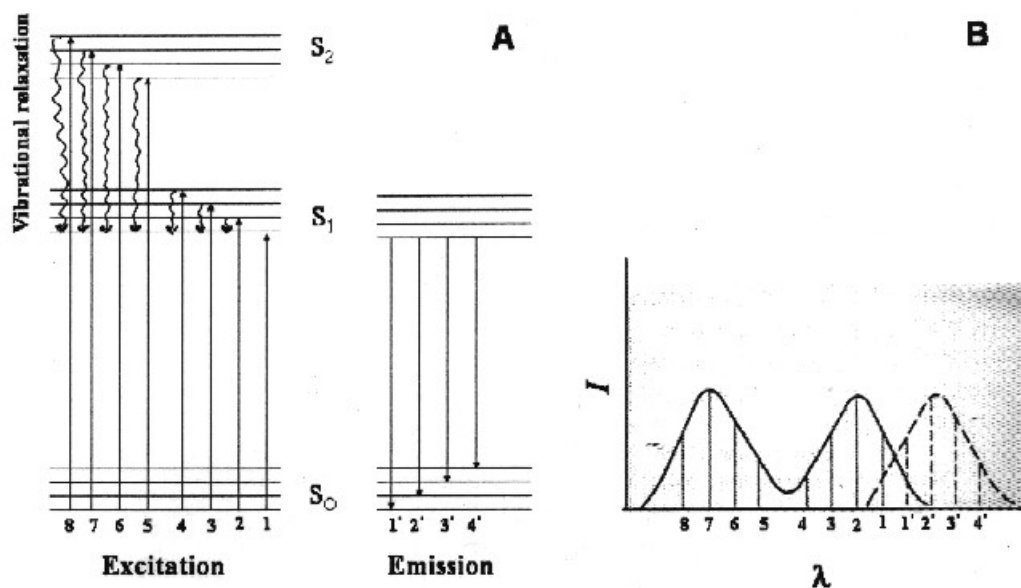
**Figure 2.5:** Excitation and emission of fluorescence. (A) Energy levels. (B) Spectra.

Initially molecules are in their electronic ground state and lowest vibrational energy level. After the absorption of energy, molecule will be in an excited electronic state depending on the energy absorbed. However, vibrational state will be different and a number of vibrations/rotations can occur during this time. When energy is dissipated the electron returns to the lowest vibrational energy level in the excited state. This energy is dissipated to neighboring solvent molecules. The transition to ground electronic state takes place, with a red shift in wavelength of emission (see Fig.2.5) [21]. It is well known that the tryptophan fluorescence emission is very sensitive to the changes in local environment of the enzyme. This fact has been successfully used by a number of researchers to probe the changes in the local protein environment variation by exciting the sample at 280 nm and monitoring the emission spectra [22]. Significant red/blue shifts in the emission spectra are observed depending on the local tryptophan variation and indicates whether the protein tertiary structure is stable or in denatured form [23].

The enzyme quantitative analysis in the bioconjugates was done by fluorescence measurements. Fluorescence measurements were carried out on initial concentration of

the enzyme in solution and supernatant of enzyme in solution after separation of bioconjugate. The enzyme solutions were excited at 280 nm and the emission band was monitored in the range 300 to 500 nm using a Perkin-Elmer Luminescence Spectrophotometer (model LS 50B).   The loss in  fluorescence intensity arising from $\pi \rightarrow \pi^*$ transitions in tryptophan and tyrosine residues in proteins was used to quantify the amount of enzyme bound to different immobilization templates.

## 2.6 Scanning electron microscopy (SEM)

Scanning Electron Microscopy is extremely useful for the direct observations of surfaces because they offer better resolution and depth of field than optical microscope. The two major components of an SEM are the electron column and control console [24]. The electron column consists of an electron gun and two or more electron lenses, which influence the path of electrons traveling down an evacuated tube. The control console consists of a cathode ray tube (CRT) viewing screen and computer to control the electron beam. The base of the column is usually taken up with vacuum pumps that produce a vacuum of about $10^{-6}$ Torr. The purpose of electron gun is to provide a stable beam of electrons. Generally, tungsten or Lanthanum hexaboride ($LaB_6$) thermionic emitters are used as electron gun. The most common electron gun consists of three components: tungsten wire filament serving as cathode, grid cap and anode. A tungsten filament is heated resistively by a current to a temperature of 2000-2700 K. This results in an emission of thermionic electrons from the tip over an area about 100 µm x 150 µm. The electron gun generates electrons and accelerates them to energy in the range 0.1 – 30 keV. The spot size from a tungsten hairpin gun is too large to produce a sharp image unless electron lenses are used to demagnify it and place a much smaller focused electron spot on the specimen. Most SEMs can produce an electron beam at the specimen with a spot size less than 10 nm that contains sufficient probe current to form an acceptable image. The beam emerges from the final lenses into the specimen chamber, where it interacts with the specimen to a depth of approximately 1 µm and generates the signals used to form an image.

The scanned image is formed point by point. The deflection system causes the beam to move to a series of discrete locations along a line and then along another line

below the first and so on, until a rectangular 'raster' is generated on the specimen. Simultaneously, the same scan generator creates a similar raster on the viewing screen. Two pairs of the electromagnetic deflection coils (scan coils) are used to sweep the beam across the specimen. The first pair of the coils deflects the beam off the optical axis of the microscope and the second pair bends the beam back onto the axis at the pivot point of the scan.

Contrast in an image arises when the signal collected from the beam specimen interactions varies from one location to another. When the electron beam impinges on the specimen, many types of signals are generated and any of these can be displayed as an image. The two signals most often used to produce SEM images are secondary electrons (SE) and backscattered electrons (BSE). Most of the electrons are scattered at large angles (from 0 to $180^{o}$) when they interact with the positively charged nucleus. These elastically scattered electrons usually called 'backscattered electrons' (BSE) are used for SEM imaging. Some electrons scatter inelastically due to the loss in kinetic energy upon their interaction with orbital shell electrons. Due to electron bombardment, phonons are set up in the specimen resulting considerable heating of the specimen. Incident electrons may knock off loosely bound conduction electrons out of the sample. These are secondary electrons (SE) and along with backscattered electrons are widely used for SEM topographical imaging. Both SE and BSE signals are collected when a positive voltage is applied to the collector screen in front of detector. When a negative voltage is applied on the collector screen only BSE signal is captured because the low energy SEs are repelled. Electrons captured by the scintillator/ photomultiplier are then amplified and used to form an image in the SEM.

If the electron beam knocks off an inner shell electron, the atom rearranges by dropping an outer shell electron to an inner one. This excited or ionized atom emits an electron commonly known as the Auger electron. Recently Auger electron spectroscopy (AES) is useful to provide compositional information. Instead of excited atom releasing Auger electron, it can release a photon of electromagnetic radiation. If the amount of energy released is high, the photon will be an X-ray photon. These

electrons are characteristic of the sample and can be used for analysis. This type of analysis is known as Energy Dispersive analysis of X-rays (EDAX).

The study of SEM in our case is important in order to rule out any surface adsorption of enzymes on the lipid surface. SEM and EDAX measurements were also used to confirm the binding of enzymes on gold nanoparticle surface. Samples for SEM and EDAX measurements were prepared by drop-coating a film of the PU-Au, and bioconjugates solutions on a Si(111) substrate. SEM and EDAX measurements were also used to confirm the binding of whole cells to the patterned thermally evaporated fatty lipid films and octadecylamine bound to gold nanoparticle polymeric membrane. SEM images of whole cells bound to as-prepared gold nanoparticle polymeric membrane were also recorded. These measurements were performed on a Leica Stereoscan-440 scanning electron microscopy (SEM) equipped with a Phoenix EDAX attachment.

## 2.7 Transmission electron microscopy (TEM)

TEM is a method of producing images of a sample by illuminating the sample with electronic radiation (under vacuum), and detecting the electrons that are transmitted through the sample. After 35 years from the discovery of electron by J. J. Thompson in 1897, Max Knoll and Ernst Ruska found a way to accelerate electrons through a sample to create an image in a way remarkably similar to optical microscopy in order to create the first TEM [25]. In 1938 the first commercial TEM instruments began to be produced by Siemens-Halske Company in Berlin. TEM is similar to optical microscopy, except that the photons are replaced by electrons. Higher resolution can be achieved in TEM instruments since electrons have a much smaller wavelength than photons.

The electron gun usually consists of a tungsten wire filament, which is bent into a hairpin ("V") shape and surrounded by a shield with a circular aperture (1-3 mm diameter) centered just below the filament tip. Electrons in the gun are accelerated across a potential difference of the order of 100,000 volts between the cathode (at high negative potential) and anode (at ground potential). The function of the condenser lens is to focus the electron beam emerging from the electron gun onto the specimen to

permit optimal illuminating conditions for visualizing and recording the image. The optical enlarging system of an electron microscope consists of an objective lens followed by one or more projector lenses. The objective lens determines resolution and contrast in the image, and all subsequent lenses bring the final image to a convenient magnification for observation and recording. The objective lens is most critical lens since it determines the resolving power of the instrument and performs the first stage of imaging. The specimen image generated by the objective lens is subsequently magnified in one or two more magnification stages by the intermediate and projector lens and projected onto a fluorescent screen or photographic plate.

The work described in this thesis, TEM is used to confirm the binding of gold nanoparticles to polyurethane and zeolite microsphers. Samples for TEM analysis were prepared by placing a drop of the polyurethane and amine functionalized zeolite solutions before and after binding with gold nanoparticles on a carbon-coated TEM copper grid. The drop was allowed to dry for 1 min following which the extra solution was removed using a blotting paper. TEM is also used to determine the particle size of gold nanoparticles embedded in polymeric membrane. Samples for TEM analysis were prepared by transferring the gold nanoparticle polymeric membrane from the liquid-liquid interface onto carbon-coated copper TEM grids. TEM micrographs of the gold nanoparticles leached from the polymeric membrane and only the polymeric membrane were also recorded. These measurements were performed on a JEOL Model 1200EX instrument operated at an accelerating voltage of 120 kV.

## 2.8 Contact angle measurements

Contact angle measurements are sensitive to changes on the surface and one can probe any changes in surface hydrophobicity by this technique [8c]. We have performed contact angle measurements of sessile water drop (1 μl) our thermally evaporated lipid films before and after enzyme intercalation using a Rame Hart 100 Goniometer. In all the studies herein, there is substantial incorporation of the enzyme molecules in the lipid matrix. There are two possible modes by which the enzymes may be immobilized in the thermally evaporated fatty acid/amine lipid films, viz., purely surface binding and entrapment within the stacks of lipid bilayers. In order to resolve

this issue, contact angle measurements were done on a 250 Å thick stearic acid (StA) and octadecylamine (ODA) lipid films on a Si(111) substrate before and after immersion of the lipid film in enzyme solution. These values represent averages over 10 measurements carried out over the whole film surface.
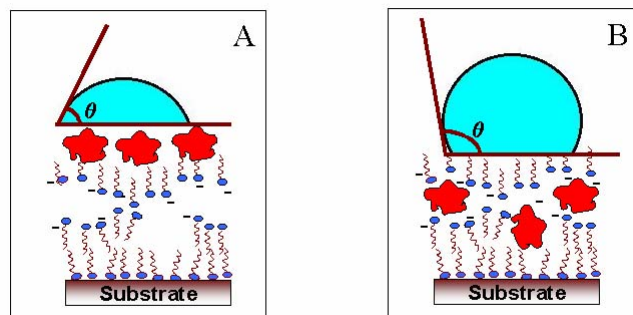


**Figure 2.6:** Schematic representation (not to scale) showing the contact angle measurements of lipid films with (A) enzyme adsorbed on surface and (B) enzyme within the stacks of lipid bilayers.

We believe that enzyme molecules are intercalated within the stacks of lipid bilayers and not on the film surface. Contact angle measurements give an indirect evidence for this assumption. If the protein were adsorbed on the film surface, the surface would be hydrophilic and hence the contact angle would be less than 90° as shown in Fig.2.6A. However, if the enzyme molecules are immobilized within the stacks of lipid bilayers (Fig.2.6B), the surface is hydrophobic and hence the contact angle is greater than 90°.

## 2.9 X-ray diffraction

X-rays are electromagnetic radiation with typical photon energies in the range of 100 eV - 100 keV. For diffraction applications only short wavelength x-rays in the range of a few angstroms to 0.1 Å are used. Since the wavelength of x-rays is comparable to the size of atoms they are ideally suited for probing the structural arrangement of atoms and molecules in a wide range of materials. The energetic x-rays

can penetrate deep into the materials and provide information about the bulk structure. X-rays are generated when a focused electron beam accelerated across a high voltage field bombards a stationary or rotating solid target. As electrons collide with atoms in the target and slow down, a continuous spectrum of x-rays are emitted, which are termed Bremsstrahlung radiation. The high energy electrons also eject inner shell electrons in atoms through the ionization process. When a free electron fills the shell, x-ray photon with energy characteristic of the target material is emitted. Common targets used in x-ray tubes include Cu and Mo, which emits 8 keV and 14 keV x-rays with corresponding wavelengths of 1.54 Å and 0.8 Å, respectively.

X-rays primarily interact with electrons in atoms. When x-ray photons collide with electrons, some photons from the incident beam will be deflected away from the direction where they original travel. If the wavelength of these scattered x-rays did not change (x-ray photons does not lose any energy) the process is called elastic scattering where only momentum has been transferred in the scattering process. These are the x-rays we measure in diffraction experiments since the scattered x-rays carry information about the electron distribution in materials.

We have used XRD for the determination of the lamellar lipid bilayer structure. When lead ions are intercalated in the self-organized multilayers (SOMs) films or LB films, XRD analysis gives spectra of (0,0,l) reflections arising due to the layer-by-layer structure similar to the *c*-axis oriented LB films [2, 26]. The spacing between the reflections can be converted to their 'd' values by using Bragg's law. This spacing gives us an idea whether the periodicity of the stacks of lipid bilayers is maintained or if there is some tilt in the chains of the stacks of lipid bilayers. The cystallinity of the amine functionalized zeolite before and after binding with gold nanoparticle was confirmed from peak positions and peak intensities of the Bragg reflections observed in zeolite [27]. XRD measurements of amine-functionalized zeolite before and after binding with gold nanoparticles were done. XRD measurements of gold nanoparticles embedded in the polymeric membrane were also recorded. These measurements were done on a Philips PW 1830 instrument operating at 40 kV and a current of 30 mA with Cu K$_\alpha$ radiation.

**2.10 Mass spectrometry**

Mass spectrometers are used to measure the masses of atoms and molecules with great accuracy [28]. They are also capable of detecting remarkably small amounts of an element or compound in the range $10^{-6} - 10^{-12}$ g. In 1919, Aston invented the first mass spectrometer although his apparatus is known as a mass spectrograph. His method and modern mass spectrometer, makes use of the fact that when charged particles move in a magnetic field they traveled in a curve paths. The heavier the particle the harder it is to make it turn and vice-versa. Gaseous can directly let in to the apparatus, although precautions are necessary to prevent air getting inside the chamber. Owing to the vacuum in the spectrometer liquids will usually give off sufficient molecules from their surfaces to provide a reasonable level of vapor. The next task is to turn the atoms or molecules into ions. The high energy electrons generated by the electron gun collide with the atoms or molecules. When they collide one or sometimes two electrons are knocked out and the atoms and molecules turn into positive ions. Thereafter, ions pass between a series of negatively charged metal plates. These plates accelerate the ions to high speed. In the analyzer the positive ions pass through another electric field. This field makes the particles to move in curved path. All the ions that emerge from the analyzer have the same kinetic energy. By changing the magnitude of electric field, ions with different kinetic energy can be sent into the region of the magnetic field. Here analyzer acts as an ion filter. On entering the magnetic field the ions begin to move in circular path. The path depends on the ratio of their mass and charge (m/z). By changing the size of the magnetic field ions with different masses are detected by the detector.

In this thesis, the biotransformation of the arachidonic acid to sophorolipids by using cytochrome P450 enzyme present in the yeast cells is described. Thereafter, the acid hydrolysis of these sophorolipids yields 20-hydroxyeicosatetraenoic acid (20-HETE). The hydroxyl group present at the 20 carbon position is confirmed by conversion of 20-HETE to methyl ester silyl ether of 20-hydroxy-5Z,8Z,11Z,14Z-eicosatetraenoic acid and thereafter analyzed by mass spectrometer [29]. These measurements were done on Shimadzu GCMS QP 5050 automated quadrupole mass

spectrometer operating in the electron impact mode. GC parameters: column used, BP-5 fused silica column (30 m x 0.25 mm, 0.25 mm, 0.25 mm coatings); He carrier at 14 kPa head pressure; injector at 250 °C; column initially at 150 °C for 1 min (rate 35 °C/min) and then increased to 220 °C for 5 min (rate 5 °C/min) and then at 280 °C and then held at these conditions for 10 min; injection volume, 1 $\mu$L. MS parameters: interface temperature 250 °C, ionization mode electron impact, scan range 70-800 amu (arbitrary mass units) $s^{-1}$.

**References:**

1)   Maissel, L. I.; Glang, R. *Handbook of thin film technology*, McGraw Hill Book Company, NewYork, **1970**.

2)   (a) Ganguly, P.; Pal, S.; Sastry, M.; Shashikala, M. N. *Langmuir* **1995**, *11*, 1078-1080. (b) Pal, S. *Ph.D. Thesis*, University of Pune, **1996**. (c) Gole, A.; Sastry, M. *Inorg. Chem. Commun*. **2001,** *4*, 568-570.

3)   Sastry, M.; Rao, M.; Ganesh, K. N. *Acc. Chem. Res.* **2002**, *35*, 847-855 and references therein.

4)   Sastry, M. *Trends Biotechnol.* **2002**, *20*, 185-189 and references therein.

5)   (a) Wang, J.; Frostman, L. M.; Ward, M. D. *J. Phys. Chem.* **1992**, *96*, 5224-5228. (b) Buttry, D. A.; Ward, M. D. *Chem. Rev.* **1992**, *92*, 1355-1379. (c) Geddes, N. J.; Urquhart, R. S.; Furlong, D. N.; Lawrence, C.R.; Tanaka, K.; Okahata, Y. *J. Phys. Chem*. **1993**, *97*, 13767-13772.

6)   (a) Brust, M.; Etchonique, R.; Calvo, E.J.; Gordillo, G. J. *Chem. Commun.* **1996**, 1949-1950. (b) Patil, V.; Mayya, K. S.; Pradhan, S. D.; Sastry, M. *J. Am. Chem. Soc*. **1997**, *119*, 9281-9282.

7)   (a) Bright, R. M.; Musick, M. D.; Natan, M. J. *Langmuir* **1998**, *14*, 5695-5701. (b) Sastry, M.; Patil, V.; Sainkar, S. R. *J. Phys. Chem. B* **1998**, *102*, 1404-1410. (c) Gole, A.; Sainkar, S. R.; Sastry, M. *Chem. Mater*. **2000**, *12*, 1234-1239.

8)   (a) Caruso, F.; Niikura, K.; Furlong, D. N.; Okahata, Y. *Langmuir* **1997**, *13*, 3427-3433. (b) Caruso, F.; Rodda, E.; Furlong, N. D.; Niikura, K.; Okahata, Y. *Anal. Chem.* **1997**, *69*, 2043-2049. (c) Gole, A.; Dash, C.; Mandale, A. B.; Rao, M.; Sastry, M. *Anal. Chem.* **2000**, *72*, 4301-4309. (d) Gole, A.; Chaudhari, P.; Kaur, J.; Sastry, M. *Langmuir* **2001**, *17*, 5646-5656.

9)   Jin, W.; Shi, X.; Caruso, F. *J. Am. Chem. Soc.* **2001**, *123*, 8121-8122.

10)  Curie, P.; Curie, J. C. R. *Acad. Sci.* **1880**, *91*, 294.

11)  Sauerbrey, G. *Z. Phys. (Munich)* **1959**, *155*, 206-222.

12)  (a) Mie, G. *Ann. Phys*. **1908**, *25*, 377. (b) Greighton, J. A.; Eadon, D. G. *J. Chem. Soc. Faraday Trans.* **1991**, *87*, 3881-3891. (c) Mulvaney, P. *Langmuir* **1996**, *12*, 788-800.

13)  Johnson, P. B.; Christy, R. W. *Phys. Rev. B* **1972**, *6*, 4370-4379.

14)  Henglein, A. *J. Phys. Chem.* **1993**, *97*, 5457-5471.

15)  (a) Nick Pace, C.; Vajdos, F.; Fee, L.; Grimsley, G.; Gray, T. *Protein Science* **1995**, *4*, 2411-2423. (b) Stoscheck, C. M. *Meth. Enzymol.* **1990**, *182*, 50-68.

16)  (a) Marshbanks, T. L.; Ahn, D. J.; Franses, E. I. *Langmuir* **1994**, *10*, 276-285. (b) Marshbanks, T. L.; Ranses, E. I. *J. Phys. Chem*. **1994**, *98*, 2166-2173.

17)  (a) Bardosova, M.; Tredgold, R. H.; Ali-Adib, Z. *Langmuir* **1995**, *11*, 1273-1276. (b) Pal, S. *Ph. D. Thesis*, **1996**, University of Pune. (c) Ganguly, P.; Paranjape, D. V.; Sastry, M. *J. Am. Chem. Soc.* **1993**, *115*, 793-794.

18)  Ning, G.; Guangfu, Z.; Shiquan, X. *J. Mol. Struct*. **1992**, *275*, 85-94.

19)  Timasheff, S. N.; Fasman, G. D. *Structure and stability of biological macromolecules*, Marcel Dekker Inc; New York, **1969**.

20)  (a) Dong, A.; Huang, P.; Caughey, W. S. *Biochemistry* **1992**, *31*, 182-189. (b) Kumar, C. V.; McLendon, G. L. *Chem. Mater.* **1997**, *9*, 863-870. (c) Templeton, A. C.; Chen, S.; Gross, S. M.; Murray, R. W. *Langmuir* **1999**, *15*, 66-76. (d) Caruso, F.; Furlong, D. N.; Ariga, K.; Ichinose, I.; Kunitake, T. *Langmuir* **1998**, *14*, 4559-4565.

21)  Rendell, D.; Mowthorpe, D. *Fluorescence and Phosphorescence Spectroscopy*: *Analytical Chemistry by open learning*. John Wiley & Sons, USA, **1987**.

22)  (a) Eftink, M. R; Ghiron, C. A. *Anal. Biochem*. **1981**, 199-227. (b) Bortoleto, R. K.; de Oliveira, A. H. C.; Ruller, R.; Arni, R. K.; Ward, R. J. *Archives Biochem. Biophys*. **1998**, *351*, 47-52.

23)  Reynolds, J. A.; Gallagher, J. P.; Steinhardt, J. *Biochemistry* **1970**, *9*, 1232-1238.

24)  Lawes, G. *Scanning electron microscopy and X-ray microanalysis: Analytical chemistry by open learning*, John Wiley & sons, **1987**.

25) (a) Knoll, M., Ruska, E. *Z. Phys (Munich)* 1932, *78*, 318-339. (b) Williams, D. B. *Transmission Electron Microscopy, A textbook for Material Science,* Plenum Press. New York and London. **1996**.

26) Shiv Shankar, S.; Rautaray, D.; Pasricha, R.; Pavaskar, N. R.; Mandale, A. B.; Sastry, M. *J. Mater. Chem.* **2003**, *13*, 1108-1111.

27) (a) Kaleta, W.; Nowinska, K. *Chem. Commun.* **2001**, 535-536. (b) Prouzet, E.; Pinnavaia, T. J. *Angew. Chem. Int. Ed.* **1997**, *36*, 516-518.

28) Roboz, J. *Introduction to mass spectrometry: Instrumentation and technique*, New York: John Wiley and Sons Inc. **1968**.

29) (a) Prabhune, A.; Fox, S. R.; Ratledge, C. *Biotechnol. Lett.* **2002**, *24*, 1041-1044. (b) Phadatre S.; Parekh, P.; Shah, S.; Tambe, A.; Joshi, R. Sainkar, S. R.; Prabhune, A.; Sastry, M. *Biotechnol. Prog.* **2003**, *19*, 1659-1663.

# Chapter III

# Protein immobilization in thermally evaporated fatty acid/amine lipid films: Characterization and biocatalytic activity studies

This chapter discusses the formation of penicillin G acylase, invertase and fungal protease - fatty lipid biocomposite films. The immobilization of cationic protein (penicillin G acylase, fungal protease) into anionic lipid matrix (stearic acid; StA) and anionic protein (invertase) into cationic matrix (octadecylamine; ODA) has been demonstrated. Analysis of the influence of protein solution pH, role of buffers and thickness of the lipid films on the diffusion process has been discussed. It has been shown that protein diffusion into the lipid films is governed to a large extent by electrostatic interactions. Secondary interactions such as hydrophobic and hydrogen bonding are also responsible for biocomposite formation. The entrapment of the reactants and inefficient release of the products are responsible for the decrease in the biocatalytic activity of the immobilized enzyme in the lipid matrix relative to the free enzyme in solution. The lead ion ($Pb^{2+}$) lamellar ordered structure of the lipid films enhances the diffusivity of the protein fungal protease in the lipid matrix (anionic, StA) compared to the as-deposited unordered lipid film. The ordered lamellar structure of the PbStA-F-prot biocomposite films showed enhanced biocatalytic activity of the entrapped enzyme relative to that of the free enzyme in solution. Enzyme immobilized in PbStA SOM lipid film showed highly improved shelf-life/reusability as compared to enzyme immobilized in unordered StA lipid film. This was possible due to the easy accessibility of the substrates to the entrapped enzyme and efficient release of the products during the biocatalytic reactions.

## 3.1 Introduction

Cell membranes are composed of complex and dynamic patterns of lipids and proteins. The proteins serve as enzymes, carry molecules and provide the membrane with distinctive structural properties. Lipids have several important biological functions, serving as structural component of the membrane, as storage and transport forms of metabolic fuel, as a protective coating on the surface of many organisms and as cell-surface components involved in cell recognition [1]. Supported lipid bilayers are useful model membranes that have been used extensively to study the structure and function of the biomembranes [2]. Moreover, it possesses a unique combination of physical properties, which make them well suited to serve as cell membrane mimics. Supported lipid membranes can be assembled by spontaneous adsorption and fusion of unilamellar phospholipid vesicles with an appropriate substrate [3]. Alternative methods such as Langmuir-Blodgett dipping [4], membrane spreading [5] can also produce high quality of supported membranes. Phosphate bearing synthetic bilayer membrane plays a more positive role in the function of myoglobin molecules [6].

While research efforts are oriented towards understanding the fundamental properties of protein-lipid interactions is important, another aspect that also needs to be pursued is the patterning of proteins. The field of protein patterning was originally conceived as a critical technology for the integration of biological molecules into miniature biological-electronics devices [7]. Recent developments in the field of protein microarrays show applications of enzyme-substrate, DNA-protein and different types of protein-protein interactions. Moreover, there is a greater interest in the development and applications of techniques for protein patterning, especially for *in vitro* studies of protein function and for applications outside of the biological context (e.g. for artificial biomineralization and in biochemical sensors). General techniques for producing two dimensional patterns of functional protein on silicon dioxide surfaces are by using a combination of self-assembled monolayers (SAMs) of alkylsilane, albumin alkyl adsorption, and biotin-avidin interactions [8]. Thermally evaporated fatty acid/amine lipids (stacks of lipid bilayers prepared on solid support) are also used for the generation of patterned protein films by encapsulation in arrays [9]. This approach

is closely related to the work described in this chapter is based on the use of electrostatic interactions and secondary interactions between the proteins and stacks of lipid bilayers for the immobilization onto 2-D supports. The inefficient release of the products or the slow diffusion of the substrates in the lipid films during the biocatalytic reactions is studied. The activity of the enzyme after immobilization depends not only on losses caused by the binding procedure but may be further reduced as a result of diminished availability of enzyme molecules entrapped or from slowly diffusing substrate molecules. Such limitations are summarized as mass transfer effects and lead to lowered efficiency. The mass transport problem associated with the immobilized enzyme in thermally evaporated lipid films is easily overcome by pre-ordering the lipid films. The biocomposite film formation has been characterized by QCM, FTIR, contact angle, UV-visible and XRD measurements.

## 3.2 Preparation of biocomposite lipid films

In earlier studies carried out in this laboratory (1996), it has been established that thermally evaporated fatty acid/amine lipid films can be spontaneously organized via selective ionic interactions of cations/anions by immersion of the film in a suitable electrolyte solution [10]. This leads to an organized lamellar film structure similar to *c*-axis oriented Y-type LB films. The generality of this protocol was extended in 1997 to the incorporation of surface modified colloidal nanoparticles in thermally evaporated ionizable fatty lipid films [11]. It was demonstrated that both positively and negatively charged colloidal nanoparticles of silver, gold and cadmium sulfide (CdS) could be incorporated into fatty acid/amines via selective electrostatic interactions [11]. It was found that the modulation of solution pH, film thickness and particle size, varied the amount of loading in the lipid films. The important question was whether the simple solution-based extraction protocol could work with more delicate guests such as proteins/enzymes? Would the entrapped proteins/enzymes be able to perform their biological functions without hindrance? We found the answer to be affirmative as has been explained in detail in this chapter. The encapsulated enzyme is accessible to substrates and protects the enzyme against harsh environmental conditions. In fact, the lipid bilayers host enhances the temporal, pH and temperature stability of the

encapsulated enzyme, thus making the protocol of self-organized multilayers (SOMs) suitable in biocomposite formation for industrial applications. In a more generalized way, it has been demonstrated in the work discussed in this chapter, that positively or negatively charged enzymes (depending on the isoeletric point, pI of the enzymes) can be incorporated into ionizable thermally evaporated fatty lipid films by immersion of the films in the enzyme solution at particular pH. The ability to tailor the extent of enzyme loading in the biocomposite by simple variation in the thickness of the thermally evaporated lipid films is an important advantage of our protocol.

## 3.3 Immobilization of Penicillin G acylase (PGA) in thermally evaporated fatty acid/amine lipid films
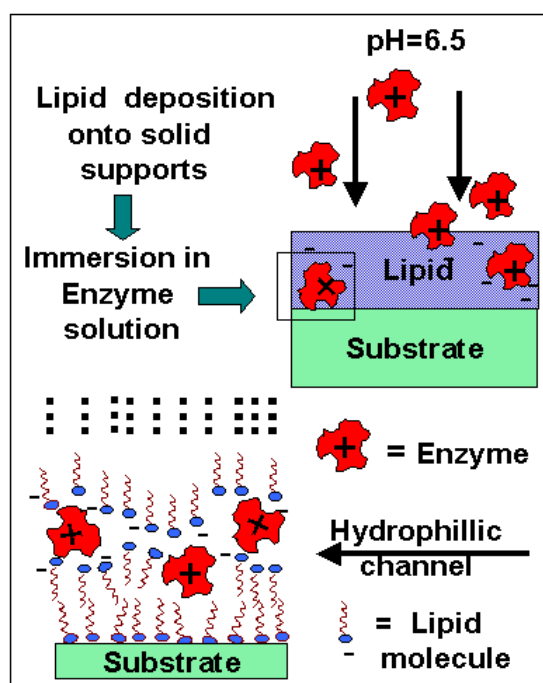


**Figure 3.1:** Schematic (not to scale) showing the various steps involved in the formation of PGA-lipid biocomposite film. A possible microscopic structure of the enzyme-lipid composite films is also shown.

Penicillin G acylase (PGA) (EC 3.5.1.11) is an enzyme of tremendous biomedical and industrial potential due to its use in the hydrolysis of penicillin G to 6-

amino penicillanic acid, the key intermediate for the production of semisynthetic penicillin's. A 1.5 mg/mL aqueous solution of PGA was prepared in potassium phosphate buffer (0.05 M, pH 6.5). The 250 and 500 Å thick lipid films were immersed in the aqueous enzyme solution, thereafter the enzyme diffuses into the thermally evaporated stacks of lipid bilayers under enzyme friendly conditions (see Fig.3.1).

### 3.3.1 Determination of protein isoelectric point

The isoelectric point of PGA was determined using a mini-scale isoelectric focusing unit built in-house [12] in the pH range 3-10 (Pharmalyte) to be 8.1.

### 3.3.2 Quartz Crystal Microgravimetry (QCM)

Thin films of stearic acid (StA) and octadecylamine (ODA) of thickness 250 and 500 Å were deposited on Si(111) substrates and gold coated 6 MHz AT cut quartz crystals as discussed in Section 2.1. After deposition of the StA and ODA, the kinetics of enzyme incorporation was followed by immersing the StA and ODA film coated quartz crystal in the enzyme solution of concentration of 1.5 mg/mL prepared in potassium phosphate buffer (0.05 M, pH 6.5) and measuring the frequency change ex-situ after thorough washing and drying of the crystals. The change in the quartz crystal resonance frequency was measured using an Edwads FTM5 QCM having frequency resolution and stability of $\pm$ 1 Hz. For the 6 MHz crystal used in this study, this yields a mass resolution of 12 ng/cm$^2$. The frequency change was converted to mass loading using the standard Sauerbrey formula [13]. The kinetics of mass uptake was determined from QCM for the following experimental conditions:

1) StA films of 250 and 500 Å thickness immersed in PGA solution at pH 6.5.

2) ODA films of 250 Å thickness immersed in PGA solution at pH 6.5.

The kinetics of enzyme incorporation into a StA film of 250 and 500 Å and 250 Å ODA films at pH 6.5 are shown in Fig.3.2A. It is observed that the enzyme readily diffuses into 250 Å thick both cationic/anionic lipids and the equilibrium mass loading is observed to be 8 $\mu$g/cm$^2$. At a solution pH of 6.5, the enzyme molecules would bear a net positive charge (pI of PGA ~ 8.1) while ODA and StA would be cationic and anionic respectively. Considering purely electrostatic interactions to be the driving

mechanism for diffusion of the PGA molecules into the lipid films, it is expected that the enzyme would preferably diffuse into an anionic matrix. This result highlights the fact that diffusion of the enzyme from solution into the lipid films is governed by secondary interactions such as hydrophobic and hydrogen bonding rather than pure electrostatics interactions.
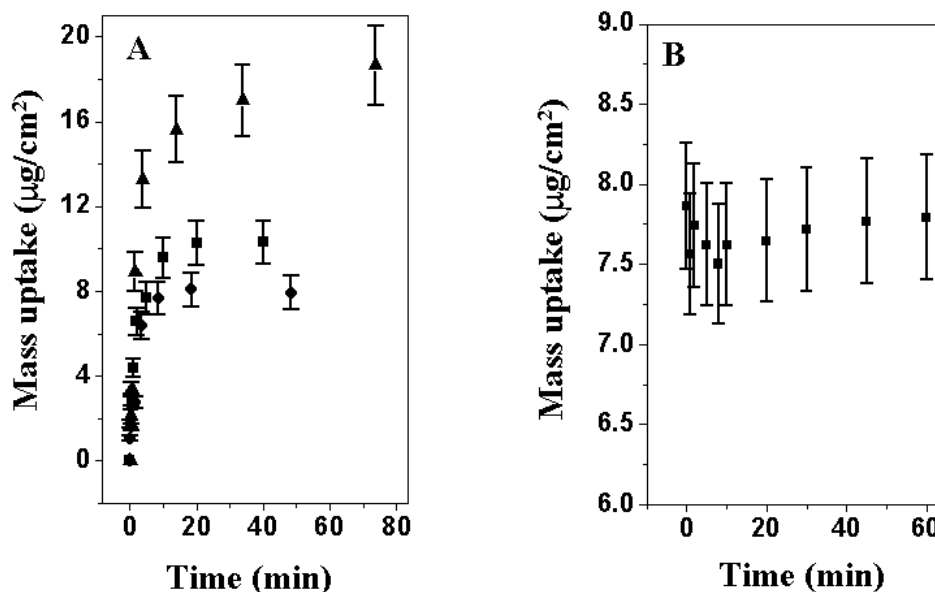


**Figure 3.2:** (A) Mass uptake with time measured with QCM for 250 Å thick StA lipid films (circles), 500 Å thick StA lipid films (triangles) and 250 Å thick ODA films (squares) at pH 6.5 (0.05 M potassium phosphate buffer) during immersion in PGA solution. (B) QCM kinetics of leaching out of PGA at pH 7.5 from a fully loaded 250 Å thick PGA-StA biocomposite film. The error bars indicate 10% deviation to the data from their mean values as determined from three separate measurements in each case.

In our earlier work on studies of immobilization of proteins in lipid films, the major driving force for the immobilization was electrostatic, with some contributions due to other secondary interactions [14,15]. Furthermore, the process of immobilization was reversible, i.e. the proteins could be "leached out" by alteration of electrostatic interaction by pH modulation [14,15].

In the case of PGA-lipid composites, we observe no such reversibility, further highlighting the role of other secondary interactions responsible for PGA entrapment.

Furthermore, we have also studied the kinetics of possible removal, if any, of the immobilized PGA at pH 7.5. PGA was immobilized into 250 Å thick StA lipid film at pH 6.5. To understand whether the activity obtained is due to the substrates diffusing inside the matrix or the enzyme diffusing out into the solution for reaction, QCM leaching out kinetics was performed. The fully loaded 250 Å thick PGA-StA biocomposite film was immersed into a buffer solution at pH 7.5 and 40 °C, since the biological activity of the enzyme is performed under these experimental conditions, and the variation in the mass was calculated. As can be seen from the Fig.3.2B, no mass loss was observed thus ruling out any possibility of enzyme leaching during the reaction process. Furthermore the time required for the biocomposite formation is less as compared to our earlier studies, 10 min for PGA-lipid films as compared to 1-3 h required for earlier studies [14a,c,d]. The QCM kinetics of diffusion of PGA into a thicker film of StA (500 Å) shows a higher mass loading in comparison with the 250 Å thick film (Fig.3.2A, triangles). The film thickness dependent mass loading of PGA indicates that the immobilization of the enzyme molecules is not just on the surface of the lipid film but within the stacks of lipid bilayers as illustrated in Fig.3.1. Since hydrophobic interactions may contribute to the diffusion of PGA into the lipid films, it is possible that the protein molecules may also be entrapped partially within the hydrophobic regions of the lipid bilayers (Fig.3.1). At this stage, we are unable to make an unequivocal statement on the exact location of the PGA molecules in the lipid bilayers. The ability to tailor the extent of enzyme loading in the biocomposite by simple variation in the thickness of the thermally evaporated lipid films is an important advantage of our protocol. Such control over the amount of protein loading has been achieved by layer-by-layer deposition technique demonstrated by Caruso *et al.* [17].

### 3.3.3 Contact angle measurements

Contact angle measurements of sessile water drop (1 μl) on 250 Å thick PGA StA/ODA biocomposite lipid films deposited on Si(111) substrates were carried out on a Rame Hart 100 Goniometer. For comparison, the contact angles were recorded from PGA solution drop-dried on Si(111) substrate as well as on 250 Å as-deposited thick StA/ODA lipid films. The contact angles of a sessile water drop (1 μl volume) on 250

Å thick as-deposited StA and ODA lipid films were ~ 100° indicating a hydrophobic surface. After formation of PGA-lipid biocomposites, the contact angles were found to be ~105° (StA matrix) and ~ 85° (ODA matrix). These measurements indicate that the PGA molecules are not adsorbed on the surface of the lipid films. It is pertinent to mention here that the contact angles measured for the bare Si(111) surface and a PGA film deposited on the Si(111) substrate by evaporation of a drop of the enzyme solution yielded average values of 15° and 12° respectively, further strengthening the conclusion mentioned above. The above results clearly indicate that the enzyme molecules are immobilized within the stacks of lipid bilayers (possibly in the hydrophilic regions) as indicated in the scheme of Fig.3.1 (expected microscopic film structure) and not on the film surface.

*3.3.4 Fourier Transform Infrared Spectroscopy (FTIR)*
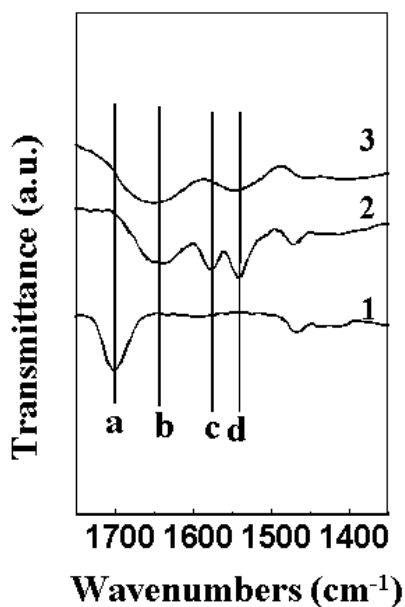


**Figure 3.3:** FTIR spectra recorded from a 250 Å thick as-deposited StA film (curve 1), a 250 Å thick PGA-StA biocomposite film grown at pH 6.5 (curve 2), and a drop-dried film of PGA formed on Si(111) substrate.

Fig.3.3 shows the FTIR spectra recorded from the as-deposited 250 Å thick StA film (curve 1) and 250 Å thick PGA-StA biocomposite films (curve 2) in the range 1350 to 1750 cm$^{-1}$. For comparison, the FTIR spectra of a drop of PGA film deposited

directly onto Si(111) substrate were also recorded (curve 3). The amide linkages between amino acid residues in polypeptides and proteins give rise to characteristic signatures in the infrared region of the electromagnetic spectrum. The position of the amide I and II bands in the FTIR spectra of proteins is a sensitive indicator of changes in the protein secondary structure [18] and may be used to study the stability of enzymes in the biocomposite films. The peak at 1650 cm^{-1} corresponds to the amide I band, which is assigned to the stretch modes in the carbonyl group in the amide linkage (Fig.3.3, feature b). This band is clearly absent in the as-deposited StA film (Fig.3.3, curve 1). The position of this band is close to that reported for native proteins in earlier papers [14], and indicates that the secondary structure of the enzyme in the StA environment is unperturbed. The amide II band, which arises due to the N-H stretching modes of vibration in the amide linkage, occurs at 1540 cm^{-1} (Fig.3.3, feature d) and can also be clearly seen for the biocomposite (curve 2) and the PGA drop-dried film (curve 3) and is close to that reported in earlier studies of native proteins [14]. The band at 1700 cm^{-1} (Fig.3.3, feature a) arises from the carbonyl stretch modes from the carboxylic acid groups in the StA matrix [19]. On complexation of the StA matrix with the PGA molecules, this band shifts to ca. 1570 cm^{-1} (feature c, Fig.3.3) and is indicative of fairly strong interaction of the StA 'host' with the protein 'guest'. Thus, FTIR spectroscopy clearly brings out the fact that the enzyme secondary structure is not compromised on formation of biocomposite films with lipids.

## 3.4 Biocatalytic activity measurements

PGA activity of the free enzyme in solution and in the immobilized form (250 Å thick PGA-StA films on Si(111) substrates, 4 cm$^2$ film area) was determined at 40 $^o$C with 2% (w/v) potassium salt of penicillin G in potassium phosphate buffer (0.1 M, pH 7.5). The 6-aminopenicillanic acid (6-APA) formed in the reaction was estimated spectrophotometrically at 415 nm by the method of Bomstein and Evans [20], modified by Sehwale *et al.* [21]. The biocatalytic activity of the free enzyme in solution was 7.5 ± 0.5 U (units/10μg/h) and that of PGA- StA biocomposite lipid film was 8.2 ± 0.5 U (units/10μg/h). The increase in the biocatalytic activity in the biocomosite lipid films is within experimental uncertainty.

*3.4.1 Long-term stability of the biocomposite films*
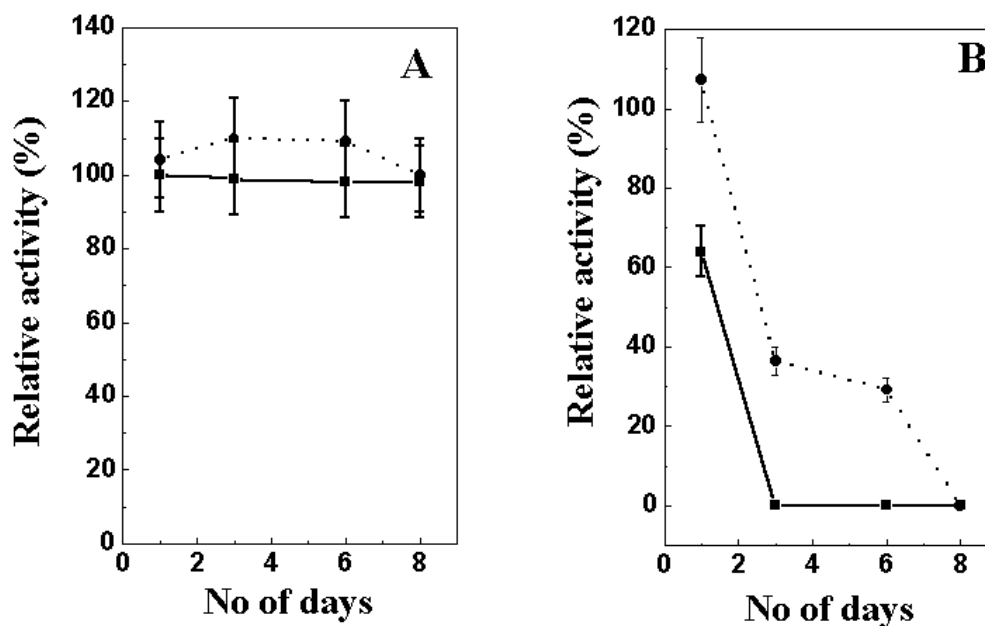


**Figure 3.4:** Comparison of the bio-catalytic activity of 250 Å thick PGA-StA biocomposite films (circles) with the free enzyme in solution (squares) at (A) 4 °C and (B) 25 °C. The solid lines in all the case is aid to the eye and have no physical significance.

The biocomposite films (250 Å thick PGA-StA films on Si(111) substrates, 4 cm$^2$ film area) were checked for biocatalytic activity as a function time of storage at 4 °C and 25 °C. The stability of PGA in the lipid can be clearly seen from Fig.3.4A and B, which shows plots of the biocatalytic activity with time of aging of the biocomposite films stored at 4 °C and films stored at 25 °C respectively. It is observed that there is a steady loss in biological activity of the PGA-StA biocomposite film stored at 25 °C as compared to the biocomposite films stored at 4 °C. The free enzyme stored at 4 °C showed similar stability as compared to biocomposite films (Fig.3.4A). The biocatalytic activity of free enzyme stored at 25 °C reduced to 64 % after one day of aging and showed a complete loss of biocatalytic activity after two days (Fig.3.4B, squares). This indicates a slightly better stability of the biocomposite films as compared to free enzyme in solution stored at 25 °C. Such a stabilizing effect has been observed by some researchers using controlled multipoint covalent attachment of Penicillin G

acylase enzyme to agarose-aldehyde gels [22]. The reduced degrees of freedom brought about by the entrapment of the enzyme in the matrix is expected to be responsible for this increased temporal/temperature stability of the composite material and is well known in immobilized protein systems [23-24].

*3.4.2 Reusability of the biocomposite lipid films*

The main advantage of immobilized biocatalysts is the ease of separation of the enzyme from the product and their reuse [23]. Table 1 shows the versatility of our approach for reuse of the PGA-lipid biocomposite films. Even after five cycles of reuse, there is little drop in the biocatalytic activity of the biocomposite films. In our earlier studies with fungal protease-StA biocomposite films, we had observed a steady decrease in the biocatalytic activity on reuse [15]. We had attributed this to be due to the replacement of enzyme molecules by its substrate hemoglobin (Hb), or possibly due to hindered accessibility of the enzyme due to the presence of the Hb molecules that effectively 'poisoned' the biocomposite films. In the present case, we observe no such loss in biological activity. This can also be attributed to the smaller size of the substrate molecules (Mol. Wt ~ 372.4) as compared to the F-Prot case [15] wherein Hb is the substrate (Mol. Wt ~ 66,000). The smaller size of penicillin G promotes facile and faster access to immobilized PGA as compared to the access of bulky Hb molecules to F-prot. In our earlier studies on F-prot immobilization, electrostatic interactions were observed to be important indicating some degree of locking of the orientation of F-prot molecules within the lipid bilayers. Thus, access of substrates to the F-prot enzyme molecules would not be as easy as in the case of PGA molecules which are expected to be randomly oriented within the lipid bilayers.

*3.4.3 Temperature dependent biocatalytic activity of biocomposite lipid films*

The temperature profile of biocatalytic activity of the biocomposite films and that of free PGA enzyme in solution is shown in Table 2. The reproducibility of the data was confirmed by checking the biocatalytic activity for three similarly loaded films for each of the temperature values mentioned. The activity of the system in terms of relative percent activity has also been displayed in Table 2.

**Table 1**

Comparison of enzymatic activity of PGA in solution and in PGA-StA biocomposite films using Penicillin G as substrate

| System | Specific activity[*] (units/10μg/h) | Relative activity[#] (%) |
|---|---|---|
| PGA in solution | $7.5 \pm 0.5$ | 100 |
| PGA-StA biocomposite film | $8.4 \pm 0.5$ | 110 |
| StA film (blank) | 0 | 0 |
| PGA-StA (run 1) | 7.9 | 105 |
| PGA-StA (run 2) | 6.5 | 87 |
| PGA-StA (run 3) | 8.8 | 117 |
| PGA-StA (run 4) | 9.8 | 130 |
| PGA-StA (run 5) | 8.8 | 117 |

**Table 2**

Comparison of temperature profile of biobatalytic activity of PGA in solutions and in PGA-StA biocomposite films using Penicillin G as substrate

| Temperature (°C) | Specific activity[*] (units/10μg/h) Free enzyme | Specific activity[*] (units/10μg/h) Immobilized enzyme | Relative activity[#] (%) Free enzyme | Relative activity[#] (%) Immobilized enzyme |
|---|---|---|---|---|
| 30 | 4.4 | 4.0 | 85 | 70 |
| 40 | 5.2 | 5.6 | 100 | 100 |
| 50 | 5.9 | 7.0 | 113 | 126 |
| 60 | 6.0 | 8.3 | 117 | 148 |

*One unit of enzyme activity is defined as the amount of enzyme that produces 1 μmol of 6-aminopenicillanic acid (6-APA) formed by reaction with Penicillin G for 30 min and estimated spectrophotometrically at 415 nm.

# Relative activity (percent) is the biocatalytic activity of the enzyme in the encapsulated form relative to that of the free enzyme in solution under ambient assay conditions. The maximum enzyme activity in solution at pH 6.5 at 40 °C is taken to be 100%.

It can be clearly seen from Table 2 that the biocatalytic activity at each temperature is greater in the case of the PGA-StA biocomposite films compared to that of free enzyme in solution. This fact is true for immobilized PGA for the range 40-60 °C. Surprisingly, the biological activity of immobilized PGA at 30 °C is less as compared to free PGA at that temperature. This may be due to the fact that upon immobilization the optimum temperature conditions for biological activity would shift to higher temperature values. We have observed such a shift in our earlier study [14c]. This clearly brings out the role of the lipid in shielding the enzyme from external harsh conditions. Furthermore, it is well known that immobilized enzyme molecules have restricted mobility that prevents structural changes. The enhanced thermal stability of the PGA-lipid biocomposite films of this study may be due to the hindered mobility of the entrapped enzyme molecules [23,24]. The decrease in the biocatalytic activity of the immobilized enzyme in the stacks of the lipid bilayers after few reuse cycles was observed. The decrease in the biocatalytic activity of the enzyme during the each reuse cycles was due to the inefficient release of the products during the biocatalytic reaction. Hence the substrate molecules were not easily accessible to the entrapped enzyme.

This feature was confirmed by immobilization of another enzyme Invertsae in the ODA lipid films. Invertase is an enzyme used for the hydrolysis of the disaccharides such as sucrose to give glucose and fructose. The product formed during the biocatalytic reaction when reacted with 2,3,5-triphenyl 2H-tertazonium chloride (TPTZ) to form a water-insoluble, deep red pigment triphenyl formazan. This deep red pigment can be easily detected by UV-vis spectroscopy.

## 3.5 Immobilization of Invertase enzyme in thermally evaporated octadecylamine (ODA) lipid films

In the following work, electrostatically controlled diffusion of the enzyme Invertase (β-fructofuranosidase, EC 3.2.1.26.) in thermally evaporated ODA lipid films has been studied as a function of pH of the solution. The aqueous solution of Invertase (0.1 mg/mL) was prepared in sodium acetate buffer (0.05 M, pH 4.5) and potassium phosphate buffer (0.05 M, pH 7). The mass uptake of the enzyme in 250 and 500 Å

ODA lipid films was studied by immersion in the aqueous enzyme solution at different pH.

### 3.5.1 Determination of protein isoelectric point

The isoelectric point of invertase was determined using a mini-scale isoelectric focusing unit built in-house [12] in the pH range 2-8 (Pharmalyte) to be 3.5.

### 3.5.2 Quartz Crystal Microgravimetry (QCM)

Thin films of ODA of thickness 250 and 500 Å were deposited on Si(111) substrates and gold coated 6 MHz AT cut gold coated quartz crystals as discussed in Section 2.1. The kinetics of diffusion of invertase enzyme in ODA lipid films were studied using QCM for the following experimental conditions:

1) ODA films of 250 Å thickness immersed in invertase enzyme at pH 4.5 (0.05 M sodium acetate buffer).

2) ODA films of 500 Å thickness immersed in invertase enzyme at pH 4.5 (0.05 M sodium acetate buffer).

3) ODA films of 250 Å thickness immersed in invertase enzyme at pH 7 (0.05 M potassium phosphate buffer).

In all the cases, the mass uptake measurements were performed after immersion of the films in the respective solutions for 35 min at similar time intervals. The kinetics of mass uptake determined using QCM for a 250 and 500 Å thick ODA film immersed in invertase solution at pH 4.5 and 7.5 are shown in Fig.3.5A. The error bars in each case are based on an analysis of 3 separate QCM measurements for each of the above experiments. It is clearly seen that the extent of loading and the time required for loading of the enzyme in the ODA lipid films is dependent on the pH of the solution. The amount of enzyme loaded in the 250 Å thick ODA lipid films at pH 4.5 ($\sim$ 9 $\mu g/cm^2$) is greater than at pH 7 ($\sim$ 6 $\mu g/cm^2$). This emphasizes the role of electrostatic interactions in directing the assembly of invertase enzyme in ODA lipid films and may be rationalized as follows.
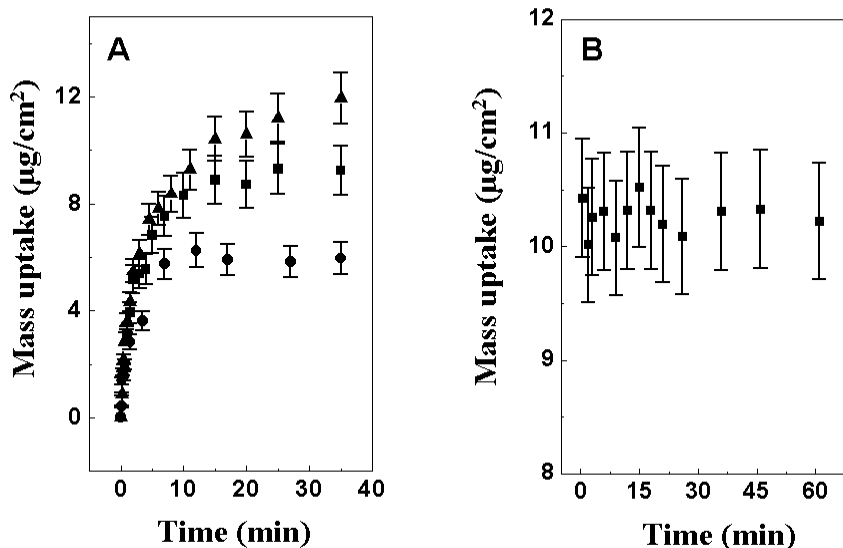
**Figure 3.5:** (A) QCM kinetics of formation of invertase-ODA lipid biocomposite during immersion of ODA films in invertase solution (0.1 mg/mL) at different pH. Circles - 250 Å thick ODA film at pH 7; squares - 250 Å thick ODA film pH 4.5 and triangles - 500 Å thick ODA pH 4.5. (B) QCM kinetics of leaching out of invertase enzyme at pH 4.5 from a fully loaded 250 Å thick invertase-ODA biocomposite lipid film. The error bars indicate 10 % deviation in the data from their mean values as determined from three separate measurements in each case.

In a solution of pH 4.5 invertase would bear a net negative charge (pI of invertase ~ 3.5) while the ODA film would be cationic (pKa of ODA ~ 10.2). The extent of protonation of the ODA molecules in the film host would clearly be higher at pH 4.5 than at pH 7 and hence the net electrostatic interaction between invertase and ODA would expect to be greater at pH 4. The entrapment of invertase in the ODA films at different pH is quite rapid and equilibration of enzyme concentration in the lipid matrix is achieved within 35 min of immersion. To rule out the possibility of purely surface binding of the invertase molecules on the ODA film, QCM kinetics of diffusion of invertase into 500 Å thick ODA was measured (Fig.3.5A, triangles). It is observed from this data that the extent of loading of invertase is enhanced (~ 12 $\mu$g/cm$^2$) relative to the 250 Å thick ODA film. This could happen only if the invertase is immobilized within the lipid bilayers. Based on the structure of ODA thin films, which are known to

self-organize into lamellar structures, we speculate that the invertase molecules populate the hydrophilic regions of the ODA bilayer lamellae (Fig.3.6, b). By analogy with earlier work on immobilization of inorganic ions such as $TiF_6^{2-}$ in ODA films where such a lamellar structure was conclusively shown to form [25], we believe entrapment of invertase in the hydrophilic ODA channels is the most likely scenario that would also explain the thickness-dependent loading of invertase observed. Thermally evaporated StA lipid films were also used for the immobilization of the invertase. Since the loading of the enzyme was not sufficient in the StA lipid films for the biocatalytic activity measurements, the results are not reported. This may be due to the fact that, at pH 4.5 the StA molecules in lipid film are not ionized, hence the enzymes are not immobilized by electrostatic interactions.
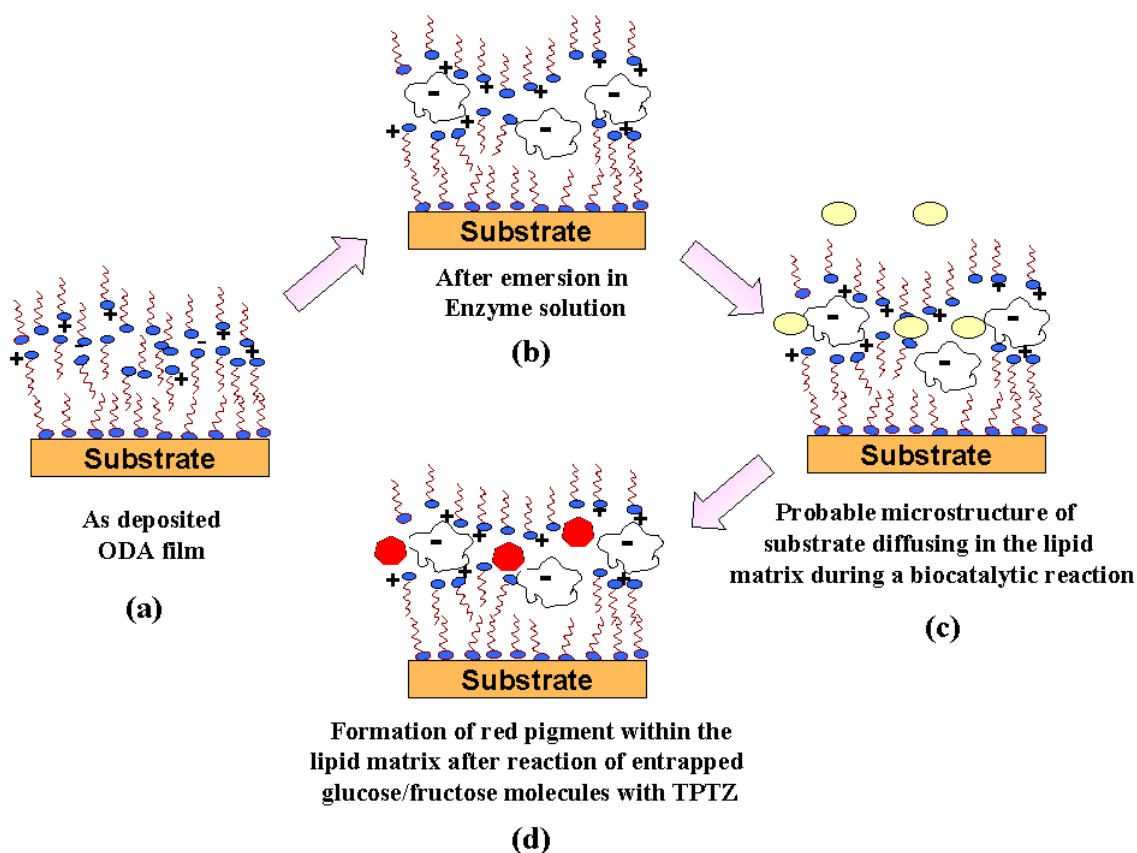


**Figure 3.6:** The probable microstructure of the invertase-ODA lipid biocomposite film during the different stages of reactions (not to scale).

*3.5.3 Contact angle measurements*

Contact angle measurements were also performed to rule out surface adsorption of invertase on the lipid films and were done as described in Section 3.3.3. The average contact angle of a sessile water drop (1 μl volume) on a 250 Å thick as-deposited ODA lipid film was ~100° indicating a hydrophobic surface. After formation of the invertase-ODA biocomposite film, the average contact angle was measured to be ~105°. These measurements indicate that invertase is not adsorbed on the surface of the lipid films. It is pertinent to mention here that the contact angles measured for the bare Si(111) surface and an invertase film deposited on the Si(111) substrate by evaporation of a drop of the enzyme solution, yielded average values of 15° and 20° respectively. The contact angle results clearly indicate that the enzyme molecules are immobilized within the lipid matrix possibly in the hydrophilic regions (Fig.3.6, b).

## 3.6 Biocatalytic activity measurements

The biocatalytic activity of invertase enzyme in the immobilized and free form was estimated according to the method described by Gascon and Lampsen [26]. The biocatalytic activity of biocomposite films (250 Å thick invertase-ODA films on Si(111) substrates, 4 cm$^2$ film area) in sodium acetate buffer (0.05 M, pH 4.5) was determined by reaction with 1 mL of 2 % sucrose at 50 °C for 10 min. After this incubation time, an equal volume of 0.2 M dipotassium hydrogen phosphate was added to the reaction solution to quench the reaction. The reducing sugars were estimated by the DNSA method (3,5-Dinitrosalicylic acid) [27]. The biological activity of an enzyme depends to a large extent on the intactness of its tertiary structure and is an important prerequisite for any enzyme immobilization procedure. A comparison of the biocatalytic activity of free enzyme in solution and the invertase-ODA biocomposite films was possible since an accurate estimate of the amount of immobilized enzyme in the 250 Å thick ODA films could be made from the QCM measurements (Fig.3.5A). In all the biocatalytic activity measurements, care was taken to use biocomposite films loaded under similar experimental conditions (250 Å thick invertase-ODA films on Si(111) substrates, 4 cm$^2$ film area). The biocatalytic activity of free invertase in solution at pH 4.5 and 50 °C was determined to be 9 ± 1.0 U/μg (Units per microgram)

and that of the enzyme in ODA was 8.5 ± 1.0 U/µg. It is clear that the biological activity of the enzyme in the biocomposite films is not compromised after entrapment in the ODA matrix. The marginal decrease of the biological activity in the biocomposite film is within experimental uncertainty. The main advantage of immobilized biocatalysts is their ease of separation from the products in the reaction medium leading to the possibility of reusing them [23,24].

*3.6.1 Reusability of biocomposite lipid films*

Table 3 lists the results obtained from experiments carried out on the reuse of a 250 Å thick invertase-ODA biocomposite film over 5 sequential runs. It can be clearly seen that even after three cycles of reuse, the biocomposite film retains 93 % of the initial biocatalytic activity. The invertase-ODA biocomposite film exhibits only a 30 % loss in biocatalytic activity by the 4th reuse cycle and retains 37 % of the original biocatalytic activity after the 5th cycle of reaction. These results clearly underline the excellent reuse characteristics till three reuses and thereafter there is drop in the biocatalytic activity of the invertase-ODA biocomposite lipid film. In our earlier studies with fungal protease-StA biocomposite films, we had observed a steady decrease in the biocatalytic activity on reuse [15]. We had attributed this to the replacement of enzyme molecules by its substrate hemoglobin (Hb), or possibly due to hindered accessibility of the enzyme due to the presence of the Hb molecules that effectively "poisoned" the biocomposite films. In the present case, we observe no such loss in biological activity. This difference may be attributed to the smaller size of the sucrose substrate molecules (Mol. Wt. ~ 342.3) of this study in comparison with F-Prot studies wherein Hb was the substrate (Mol. Wt. ~ 66,000) [15]. The smaller size of sucrose is expected to promote facile and faster access to immobilized invertase molecules. Similar results were also observed for the PGA-StA biocomposite lipid films, where the substrate used was penicillin G (Mol. Wt. 372.4, Section 3.4). However, the perceptible loss in biocatalytic activity of the invertase-ODA biocomposite films after 3 reuse cycles needs elaboration. It is possible that the enzyme leaches out from the ODA lipid films during successive reaction cycles.

**Table 3**

Specific activity of Invertase in solution and Invertase-ODA biocomposite films using sucrose as substrate at pH 4.5 and 50 $^{o}$C

| System | Specific activity[*] (units/µg) | Relative activity[#] (%) |
|---|---|---|
| Invertase in solution | $9.0 \pm 1.0$ | 100 |
| Invertase-ODA biocomposite film | $8.5 \pm 1.0$ | 100 |
| ODA film (blank) | 0 | 0 |
| Invertase-ODA (run 1) | 8.5 | 94 |
| Invertase-ODA (run 2) | 8.5 | 94 |
| Invertase-ODA (run 3) | 8.3 | 93 |
| Invertase-ODA (run 4) | 5.8 | 64 |
| Invertase-ODA (run 5) | 3.4 | 37 |

**Table 4**

Temperature profile of biocatalytic activity of invertase in solution and Invertase-ODA biocomposite film using sucrose as substrate at pH 4.5

| Temperature ($^{o}$C) | Specific activity[*] (units/µg) Free enzyme | Specific activity[*] (units/µg) Immobilized enzyme | Relative activity[#] (%) Free enzyme | Relative activity[#] (%) Immobilized enzyme |
|---|---|---|---|---|
| 40 | 8.7 | 8.0 | 88 | 77 |
| 50 | 9.0 | 8.4 | 100 | 93 |
| 60 | 9.0 | 10.0 | 100 | 111 |
| 70 | 2.0 | 2.3 | 22 | 25 |

* One unit of enzyme activity is defined as the amount of enzyme that produces 1 µmol of glucose by reaction with sucrose for 30 min and estimated spectrophotometrically at 504 nm.

# Relative activity (percent) is the biocatalytic activity of the enzyme in the encapsulated form relative to that of the free enzyme in solution under ambient assay conditions. The maximum enzyme activity in solution at pH 4.5, 50 $^{o}$C is taken to be 100 %.

Other factors such as mass transport of the substrate into the biocomposite films are also expected to play a role in defining the effective catalytic activity of the biocomposite material. In order to distinguish between the two mechanisms, a fully loaded 250 Å thick invertase-ODA biocomposite film was immersed into a buffer solution at pH 4.5, 50 $^{o}$C and the variation in the mass was measured by QCM (Fig.3.5B). As seen from the Fig.3.5B, no mass loss was observed even after 60 min of immersion (twice the reaction time in biocatalytic activity measurement) thus ruling out any possibility of enzyme leaching during the reaction process. This result points to the entrapment of the substrate or products of the reaction of sucrose with invertase within the ODA films as possible contributors to loss in biocatalytic activity of the invertase-ODA film with reuse. To confirm the entrapment of the reaction products such as glucose/fructose in the ODA films, a 250 Å thick ODA-invertase film deposited on quartz substrate was reacted with 2,3,5-Triphenyl 2H-tertazonium chloride (TPTZ) and analyzed by UV-vis absorption spectroscopy. The TPTZ reacts with glucose and fructose to form a water-insoluble, deep red pigment triphenyl formazan [28].
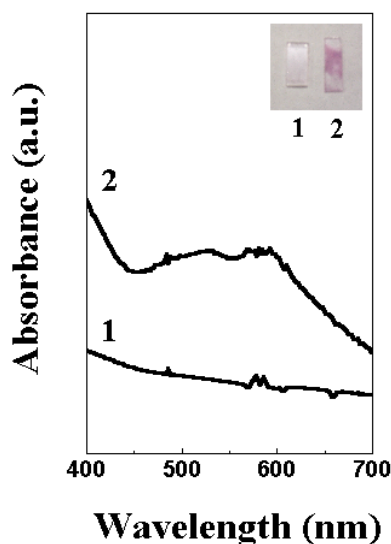


**Figure 3.7:** UV-visible absorption spectra recorded from a 250 Å thick invertase-ODA lipid biocomposite film incubated at pH 4.5 for 30 min (curve 1) and after reaction with TPTZ (curve 2). The inset shows pictures of a 250 Å thick invertase-ODA biocomposite film before (1) and after (2) reaction with TPTZ.

Fig.3.7 shows the UV-vis spectra of the invertase-ODA biocomposite film after reaction with sucrose (pH 4.5, 30 min reaction time) measured before (curve 1) and after (curve 2) reaction with TPTZ. The 250 Å thick invertase-ODA biocomposite films shows a strong and broad absorption centered at ca. 535 nm (curve 2) due to the complex formed by glucose/fructose molecules entrapped in the biocomposite lipid films with the TPTZ to give a deep red pigment, triphenyl formazan (Fig.3.6c,d). Such absorption at 535 nm is not seen in the invertase-ODA biocomposite film before reaction with TPTZ (curve 1) as expected. The inset in the Fig.3.7 shows the pictures of the invertase-ODA film before (1) and after (2) reaction with TPTZ clearly showing the reddish hue in the biocomposite film further to formation of triphenyl formazan. These results confirm the presence of entrapped glucose/fructose after reaction of the invertase-ODA biocomposites with sucrose indicating that reduction in biocatalytic activity of the films is due to glucose/fructose mediated blockage of diffusion pathways to sucrose during successive reuse.

### 3.6.2 Temperature dependent biocatalytic activity of biocomposite lipid films

The temperature profile of biocatalytic activity of 250 Å thick invertase-ODA biocomposite film compared with that of free invertase in solution at pH 4.5 is shown in Table 4. The reproducibility of the data was confirmed by checking the biocatalytic activity for three similarly loaded films at each of the temperatures mentioned. It can be clearly seen from Table 4 that invertase in the immobilized form showed biocatalytic activity similar as compared to the free enzyme in solution. The biological activity of immobilized invertase at 60 $^{\circ}$C is high as compared to free invertase in solution at that temperature. This may be due to the fact that upon immobilization the optimum temperature conditions for biological activity would shift to higher temperature values. We have observed such a shift in our earlier studies on endoglucanase enzyme immobilized in thermally evaporated ODA lipid films [14c]. The stability of the invertase enzyme in the immobilized form may be attributed to conformational integrity of the enzyme structures brought about by the reduced degrees of freedom of the entrapped enzyme. The lipid matrix clearly serves to restrict the mobility of the entrapped enzyme molecules thus preventing structural changes and loss of biological

activity [23,24]. Such increase in the thermal stability is also observed for enzymes immobilized in different matrixes/solid supports [29]. The decrease in the biocatalytic activity of the entrapped enzyme in the lipid bilayers was attributed to the inefficient release of the products during the reaction. The decrease in the biocatalytic activity was also attributed to the inaccessibility of the substrates to the enzyme.These various phenomena are refereed as mass transfer effects. These mass transfer effects are responsible for the decrease in the efficiency of the immobilized enzyme as compared to the free enzyme in solution. The question is what are the reasons for restriction caused by mass transfer, and how can they be avoided if necessary? Mass transfer effects are easily overcome in stirred tanks by stirring the reaction liquids sufficiently. At lower substrate concentrations pore diffusion leads to low efficiency of the immobilized enzyme. In such cases increasing the substrate concentration to about 100 folds of the $K_M$ (Michaelis constant) is generally preferred.

The decrease in biocatalytic activity of biocomposite lipid films is mainly due to the substrate diffusivities and can easily overcome by cation/anion induced pre-ordering the fatty lipid films. The efficiency of the pre-ordered (SOMs) was confirmed by immobilization of Fungal protease enzyme in lead ions induced pre-ordered StA lipid films. Thereafter, these biocomposite lipid films were used for the biocatalytic activity measurements using hemoglobin as a substrate (Mol. Wt. 64,000).

## 3.7 Preparation of Self organized multilayers (SOMs)

In the previous section we had seen the biocatalytic activity of the biocomposite lipid films were reduced after certain reuses due to the 'mass transfer problem'. The reduced biological activity of the entrapped enzyme is due to the slow diffusion of the substrate molecules into the biocomposite matrix and therefore inefficient access of the substrate to the enzyme. This diffusion-limited problem can be circumvented by enhancing the substrate diffusivities for the entrapped enzyme by different processes such as shaking the reaction mixtures, increasing the interfacial area of contact etc. [23]. We have recently shown that the diffusivity of the protein cytochrome *c* into thermally evaporated fatty acid films of stearic acid (StA) may be significantly enhanced by lead cation-induced pre-ordering of the lipid film [14d]. This was

attributed to facile access of the protein to the hydrophilic carboxylic acid groups of the fatty acid matrix due to $Pb^{2+}$-induced lamellar ordering of the lipid structure and the consequent creation of uninterrupted 'water channels' for protein diffusion [14a]. In this part we will see how the mass transfer effects are overcome by simply pre-ordering the lipid films to form self-organized multilayers (SOMs). This method reduces the mass transfer problem and thus overcomes the drawbacks in the thermally evaporated fatty acid/amine lipid films.

### 3.7.1 Lamellar structure studies of PbStA SOM films

StA lipid films of 250 Å thick were deposited as discussed in Section 2.1. The ordering of thermally evaporated StA films was done by simple immersion of the 250 Å thick as-deposited StA lipid films in $10^{-4}$ M aqueous $PbCl_2$ solution at pH 5.5.
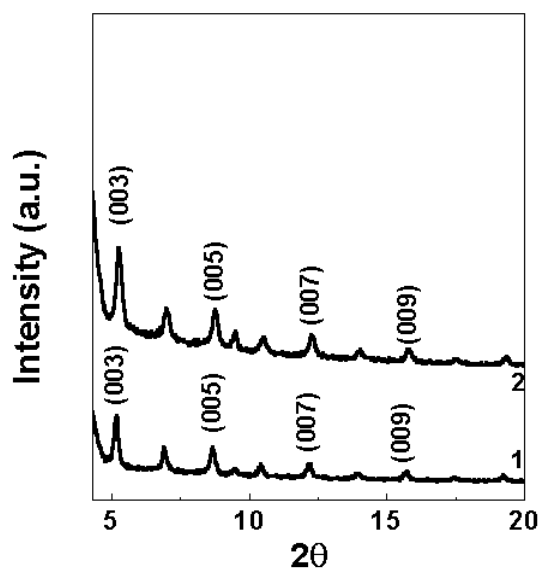


**Figure 3.8:** XRD patterns recorded from 250 Å thick PbStA SOM films (curve 1) and PbStA-Fprot SOM biocomposite film (curve 2).

The intercalation of F-prot into the pre-ordered PbStA-SOM films was achieved by immersion of these films into (0.37 mg/mL) F-prot solution (0.05 M sodium phosphate buffer, pH 6). The XRD measurements of ca. 250 Å thick PbStA SOM films before and after incorporation of F-prot were recorded. Fig.3.8 shows the comparison

of the two patterns that there is little change in intensity of the (0 0 l) Bragg reflections. This is somewhat surprising given the fact that radius of the F-prot molecules is 2.6 nm [15] and its accommodation in the hydrophilic regions of the bilayers would presumably lead to distortion of the lamellae and a consequent in loss in intensity of the (0 0 l) Bragg reflections. This result indicates that the enzyme may be entrapped in such a way that it spans the bilayer either partially or fully. This aspect is not fully understood at the moment. However, the fact that the bilayer lamellar structure of the SOM film after F-prot intercalation is maintained indicates the availability of uninterrupted water channels and is extremely important for easy accessibility of substrate molecules (Hb) to the entrapped enzyme.

*3.7.2 Quartz Crystal Microgravimetry (QCM)*
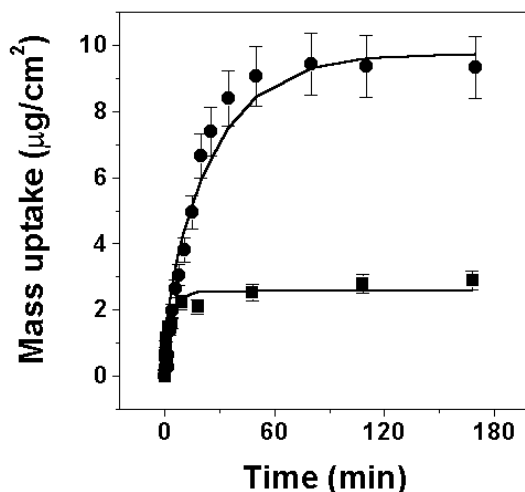


**Figure 3.9:** QCM mass uptake kinetics of incorporation of F-prot into 250 Å thick as-deposited StA film (circles) and into 250 Å thick PbStA SOM films (squares) during immersion in F-prot solution at pH 6. The solid line is based on a 1-D diffusion analysis of the data. The error bars to the data are roughly 10 % deviation of the data from the mean values obtained from 3 separate experiments under similar conditions.

The kinetics of incorporation of the enzyme into the SOMs film was studied using QCM for the following experiments:

1)  StA films of 250 Å thickness immersed in F-prot enzyme at pH 6 (0.05 M sodium phosphate buffer).

2)  PbStA SOM films of 250 Å thickness immersed in F-prot enzyme at pH 6 (0.05 M sodium phosphate buffer).

Fig.3.9 shows the QCM kinetics data of the intercalation of F-prot (pH 6) into the 250 Å thick as-deposited StA film (circles) and PbSt SOM film (squares). The solid lines in both Fig.3.9 are based on a 1-D diffusion analysis of the mass uptake data and will be discussed below. The error bars shown in both the cases are a 10% deviation of the data from the mean values obtained from three separate experiments carried out under nearly identical conditions. It is interesting to note that the final enzyme loading for the two films is different (3 $\mu$g/cm$^2$ for the Pb-StA SOM pre-ordered lipid film compared to 9.3 $\mu$g/cm$^2$ for as-deposited StA unordered lipid film). The extent of loading of enzyme is expected to dominate the neutralization of the negative charge in the fatty acid matrix by the cationic F-prot molecules. Consequently, the presence of Pb$^{2+}$ ions in the StA film would lead to an effective reduction in the negative charge in the lipid film and a smaller loading with F-prot is observed.

### 3.7.3 One-dimensional (1-D) Diffusion Model

Recently, Frances and co-workers [30] have studied the process of ion exchange and water transport in Langmuir Blodgett (LB) films of calcium stearate using infrared spectroscopy. An analysis of the ion diffusion process in terms of a 1-D diffusion model was done taking into account a reaction term (due to salt formation) and it was shown that the model did not adequately account for the IR intensity variations observed. A possible explanation put forward was that ion (and water) diffusion could occur through defects such as pores in the film as well as through the hydrophilic lamellar spaces present in the LB films studied resulting consequently in two simultaneous 1-D diffusion processes. In the present situation, the thermally evaporated StA lipid films are not disordered as evidenced by the Bragg peaks in the XRD patterns and therefore, a 1-D model may be appropriate. To simplify the calculations, we have omitted the reaction term in the diffusion equation. We feel this is justified given that the electrostatic interaction between the proteins/enzymes and the lipid molecules is

weak when compared to the energies involved in salt formation. The equation for simple 1-D diffusion is written as:

$$\frac{\partial\, C(x,t)}{\partial t} = D\, \frac{\partial^2\, C(x,t)}{\partial\, x^2} \qquad \ldots\ldots(1)$$

where $C(x,t)$ is the time and distance dependent protein concentration in the film and D is the protein diffusivity. Fig.3.10 shows the physical situation in this protein incorporation study and leads naturally to the following boundary conditions:

$$\partial C(0,t)/\, \partial x = 0 \qquad \ldots(2a)$$

$$C(L,t) = \begin{cases} 0 & t < 0 \\ C_0 & t \geq 0 \end{cases} \qquad \ldots(2b)$$

where $C_o$ is the protein concentration at the film/protein solution interface (Fig.3.10, $x = L$) and condition (2a) is a consequence of the fact that the quartz crystal substrate is impervious to protein diffusion (at $x = 0$, the film/quartz substrate interface, Fig.3.10). The solution of Eq.1 subject to the above boundary conditions (Eq.2) is given by [31]:

$$C(x,t) = C_o \left[ 1 + 4 \cdot \left[ \sum_{n=0}^{\infty} e^{\left[ -D \cdot (2 \cdot n + 1)^2 \cdot \frac{\pi^2}{4 \cdot L^2} \right] \cdot t} \cdot \cos\left[ \frac{(2 \cdot n + 1) \cdot \pi \cdot x}{2 \cdot L} \right] \cdot \frac{(-1)^{n+1}}{(2 \cdot n + 1) \cdot \pi} \right] \right]$$

.....(3)

In QCM studies, one observes a mass uptake over the whole length of the film covering the sensing electrode. The total mass uptake recorded as a function of time, M(t), is therefore :

$$M(t) = m_o \cdot \int_0^L C(x,t)\, dx \qquad \ldots\ldots(4)$$

where $m_o$ is the mass per protein. In the calculation of the QCM mass uptake from Eq.4, knowledge of molecular weight of protein can help to calculate the mass of the single protein molecule (in ng). As the protein molecules diffuse into the matrix, the films swell.
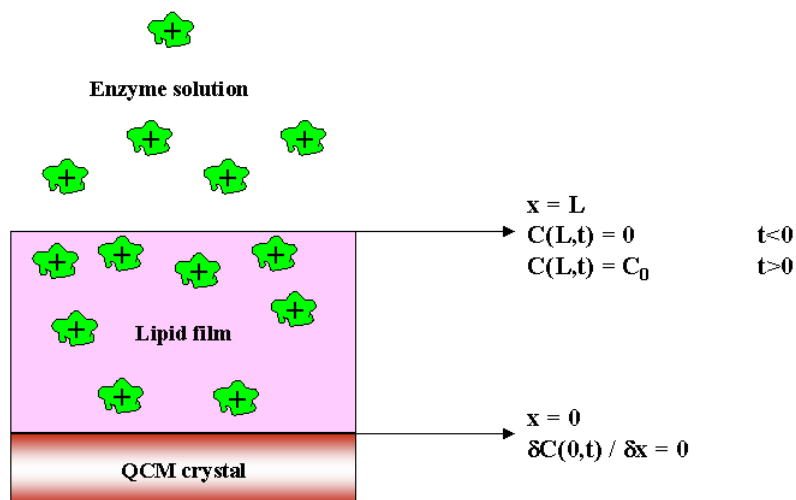


**Figure 3.10:** Scheme (not to scale) of enzyme incorporation in a thermally evaporated StA lipid film during immersion in the enzyme solution.

Ellipsometry was used to determine the film thickness before and after protein incorporation. The final thickness values thus determined (L) were used in Eq.3 and the QCM kinetics results fitted to Eq.4 using a non-linear least squares procedure using an application written in Mathcad by Dr. Murali Sastry. Mathcad is a commercial mathematical software package for the PC available from Mathsoft Inc., Cambridge, MA 02142, USA.

*3.7.4 Analysis of the QCM diffusion data*

The QCM data on the incorporation of F-prot into the as-deposited unordered StA film and the pre-ordered PbStA SOM film (Fig.3.9) may be conveniently analyzed in terms of a one-dimensional (1-D) diffusion model. The mathematical details of the 1-D diffusion model and discussion pertaining to the appropriate boundary conditions in

the model (Section 3.7.3) are also available from our earlier work on intercalation of proteins and enzymes [14d].

**Table 5**

Parameters obtained from 1-D diffusion analysis of QCM mass uptake measurements during incorporation of F-prot in 250 Å thick PbStA SOM and as-deposited StA films.

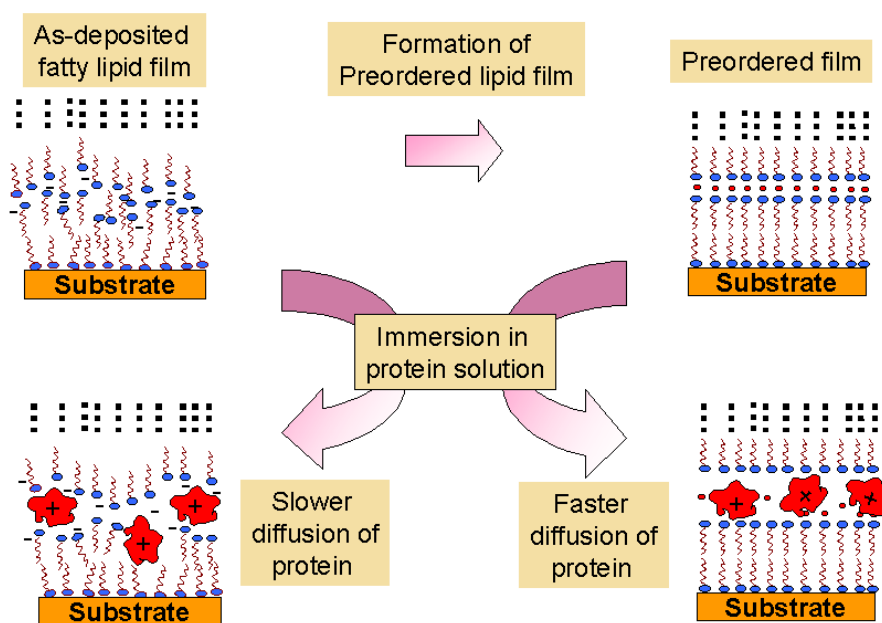| Diffusing system | Final protein loading ($\mu g/cm^2$) | D ($\text{Å}^2 \, min^{-1}$) |
|---|---|---|
| F-prot into as-deposited StA film | 9.3 | $5.7 \times 10^3$ |
| F-prot into pre-ordered PbStA SOM film | 3 | $2.4 \times 10^4$ |



**Figure 3.11:** Intercalation of F-prot in as-deposited StA lipid film versus that in pre-ordered PbStA SOM lipid films. Expected microscopic structures of enzyme-lipid biocomposite films also shown (not to scale).

Table 5 lists the values for diffusion coefficient (D) for these two films. It can be clearly seen that the diffusivity of the enzyme into the PbStA-SOM (pre-ordered film) is 4.2 times larger than in the as-deposited unordered StA lipid film. In Fig.3.11, we have attempted to explain this enhancement. In PbStA-SOM films, the $Pb^{2+}$ ions lead to lamellar ordering in the films and to a *c*-axis oriented structure. The presence of stacks of uniform bilayers results in the creation of uninterrupted water channels that facilitate the diffusion of the enzyme molecules into the lipid matrix. The as-deposited StA films also would be solvated however, lack of a lamellar structure would prevent facile access of the carboxylate groups in the acid matrix to the enzyme molecules and thus lead to a lower diffusivity of the enzyme molecules in the lipid matrix.

*3.7.5 Fourier Transform Infrared Spectroscopy (FTIR)*

FTIR measurements of the biocomposite films on Si(111) substrates were made after immersion of 250 Å thick Pb-StA SOM films in the F-prot solutions for 1 h and thereafter rinsing and drying the films in flowing nitrogen for 5 minutes.
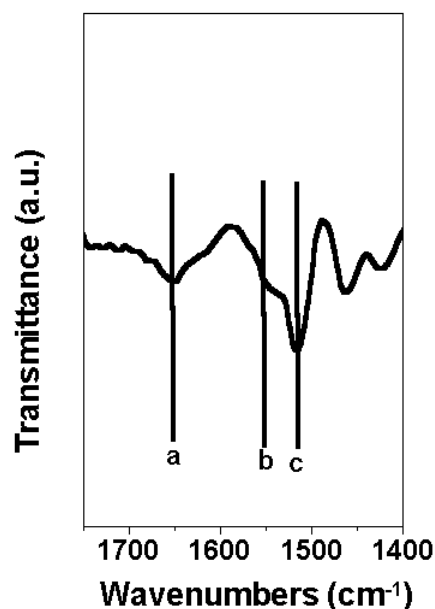


**Figure 3.12:** FTIR spectra of PbStA-Fprot SOM after incorporation of F-prot.

The confirmation of the presence of enzyme in the Pb-StA SOM films and the secondary structure of the immobilized F-prot was obtained by monitoring the amide

bands from the polypeptide chains in the enzyme molecules using FTIR spectroscopy. Fig.3.12 shows the FTIR spectra of Pb-StA SOM film on Si(111) after incorporation of F-prot. The amide I band can be clearly seen at 1650 cm$^{-1}$ (feature a). The amide II band arising due to excitation of N-H stretch vibrations in the amide linkage can be seen at ca. 1545 cm$^{-1}$ (feature b). This band partially coincides with the carboxylate asymmetric stretch bands arising due to the coordination of Pb$^{2+}$ ions with the acid matrix. The feature at 1512 cm$^{-1}$ (band c) is also attributed to carboxylate asymmetric stretch mode of vibration. (The 1541 and 1512 cm$^{-1}$ carboxylate asymmetric bands appear as doublets) [19b,c]. The presence of well defined amide I and II bands thus indicates the intactness of the secondary structure of F-prot in the Pb-StA-SOM [18].

## 3.8 Biocatalytic activity measurements.

Biocatalytic activity of F-prot in both unordered StA-F-prot film and pre-ordered PbStA-F-prot film (substrate area 4 cm$^2$) was determined by reacting with a solution of hemoglobin (Hb) a concentration of 5mg/mL. The reaction is carried out in sodium phosphate buffer (pH 6). The $k_M$ for this reaction is determined to be 3.5 mg/ml. Thus the reaction was carried out at concentration greater than the $k_M$ of F-prot. The biocatalytic activity of the F-prot-StA bomposite film of the dimensions mentioned above was carefully immersed in 1 mL of the hemoglobin solution and the reaction mixture was incubated at 37 °C for 1 h. After the incubation time, the film was removed and equal volume of 1.7 M perchloric acid was added to the reaction solution to precipitate the remaining hemoglobin. After 1 h, the precipitate was removed by centrifugation and the optical absorbance of the filtrate measured at 280 nm. F-prot digests hemoglobin and yields acid-soluble products (tryptophan and tyrosine residues), which are readily detected by their strong UV signatures at 280 nm [15,16].

### 3.8.1 Operational stability of the immobilized F-prot in StA lipid matrix

In the case of immobilized enzymes, the biocatalytic activity of the entrapped enzyme is normally reduced/underestimated due to the diffusion-limited access of the substrate molecules to the entrapped enzyme [23]. It is reasonable to believe that the enhanced diffusivity of the F-prot molecules into the pre-ordered PbStA SOM films (Table 5) would extend to enhance diffusivity of the substrate molecules (Hb in this

study) in the biocomposite films as well. That this is true can be verified by checking the biocatalytic activity of the F-prot-StA biocomposite films as a function of time of reaction with Hb.

*3.8.1 (A) Biocatalytic activity as a function of time*

In these experiments, free F-prot in solution and unordered StA-F-prot and pre-ordered PbStA-F-prot biocomposite films were assayed using Hb as substrate for 1 and 2 h. This would give an idea as to the enhancement/reduction of the biological activity of the entrapped enzyme due to diffusion-limited accessibility of the Hb molecules (the well-known mass transport problem). Here the free enzyme, StA F-prot and PbStA-Fprot SOM pre-ordered biocomposite films were carefully immersed in 1 mL of Hb solution, and the reaction mixture was incubated at 37 °C for 1 and 2 h. Thereafter, the biocatalytic was done as described above. Three separate measurements were performed to check the reproducibility of the data. It is observed from Table 6, that the biocatalytic activity of the PbStA-F-prot biocomposite film is enhanced by a factor of ca. 36 % relative to the free enzyme in solution during the first and 26% during the second hours of reaction with Hb. Furthermore, the biocatalytic activity of the unordered biocomposite film is comparable to that of the free enzyme in solution and is a result in accordance with our earlier findings on F-prot-StA biocomposites [15]. The pre-ordering greatly improves accessibility of the substrate molecules (Hb) to the entrapped F-prot molecules and results in enhanced reactivity and faster production of the products. This development in our lipid-based enzyme immobilization protocol is expected to be of great importance in dealing with the mass transport problem and practical industrial application of the process.

A control experiment was performed wherein the enzyme in solution was assayed with Hb in the presence of $10^{-4}$ M concentration of lead chloride solution. It was found that the biological activity of free enzyme in solution (assay time = 1 h) was 58 units whereas, the free enzyme in solution in the presence of lead ions was 60 units. This clearly indicates that the metal ions do not play a significant role in enhancing/reducing the enzymatic activity of entrapped F-prot molecules and that the enhancement observed is due to pre-ordering of the lipid matrix as discussed above.

**Table 6**

Specific biocatalytic activity of enzymes as a function of time of reaction

| Reaction Time (h) | F-prot in solution (units/mg)[#] | StA-Fprot (unordered) biocomposite film (units/mg)[#] | Pb-StA SOM (pre-ordered) biocomposite film (units/mg)[#] |
|---|---|---|---|
| 1 | 58 | 56 | 79 |
| 2 | 68 | 23 | 36 |

**Table 7**

Specific biocatalytic activity of biocomposite lipid films upon reuse.

| No. of reuse cycles | StA-Fprot (unordered) biocomposite film (units/mg)[#] | Pb-StA SOM (pre-ordered) biocomposite film (units/mg)[#] |
|---|---|---|
| 1 | 64 | 77 |
| 2 | 30 | 73 |
| 3 | 10 | 68 |

**Table 8**

Specific biocatalytic activity of biocomposite lipid films as a function of time of storage at 4 °C

| Time of aging (h) | StA-Fprot (unordered) biocomposite film (units/mg)[#] | Pb-StA SOM (pre-ordered) biocomposite film (units/mg)[#] |
|---|---|---|
| 1 | 68 | 78 |
| 5 | 33 | 74 |
| 12 | 15 | 70 |
| 24 | 7 | 68 |
| 48 | 3 | 63 |

# One unit of the enzyme will produce a change in absorbance at 280 nm of 0.001 per minute at pH 6.0 and 37 °C measured as acid soluble products using hemoglobin as the substrate.

*3.8.1 (B) Reusability of the PbStA-F-prot biocomposite films*

Reusability of the unordered StA-F-prot biocomposite film and pre-ordered PbStA-F-prot biocomposite film (substrate area 4 cm$^2$) was done at 37 $^o$C for 1 h as described above for three different cycles. Care was taken to rinse the biocomposite films with copious amount of deionised water prior to reuse. The pre-ordered PbStA-F-prot biocomposite films were checked for their reusability and the data obtained are shown in Table 7 along with the data for the unordered biocomposite film. It can be clearly seen that there is little drop in the biocatalytic activity of the pre-ordered biocomposites upon reuse while there is a drastic drop in biological activity of the entrapped F-prot molecules in unordered StA films. We believe that the pre-ordered lamellar structure of the PbStA-SOM biocomposite film not only enhances the accessibility of the substrates towards the entrapped enzyme, but also facilitates the release of the products. The ease with which the reactants can escape from the ordered lipid film considerably reduces the possibility of 'poisoning/fouling' of the biocomposite film due to the presence of unreacted/reacted trapped Hb molecules in the lipid matrix.

*3.8.2 Storage Stability of biocomposite films*

The stability of the biocomposite film was analysed as a function of time interval 1-48 h at 4 $^o$C. Here the unordered StA-F-prot and pre-ordered PbStA-F-prot biocomposite films (substrate area 4 cm$^2$) were prepared and stored at 4 $^o$C. At different time interval films were used for biocatalytic activity with Hb at 37 $^o$C for 1 h as described above. A control experiment was also performed wherein a lead chloride solution (final concentration of $10^{-4}$ M) was added to the F-prot solution (pH 6) and the biocatalytic activity measured after incubation with Hb as described above. The stability of the immobilized enzymes is a key issue where increased shelf life of the biocomposites is being sought. Three separate measurements were performed to check the reproducibility of the data. Table 8 shows the results of our investigations into the stability of the PbStA-F-prot SOM biocomposite films upon storage at 4 $^o$C for different time intervals. While the biological activity of the unordered biocomposite film drops rapidly with time to 4 % of its original value upon aging at 4 $^o$C for 48 h, the

biocatalytic activity of the pre-ordered biocomposite film is fairly steady with time of storage ultimately reaching 81 % of original activity upon aging under similar conditions. The drop in the biological activity of the unordered biocomposite films upon aging was attributed to the dehydration of the lipid films as observed in our earlier studies [15]. While this aspect is not entirely clear to us at present, one possibility is the long-term retention of water due to the presence of the $Pb^{2+}$ ions in the lipid matrix along with the entrapped enzyme molecules. Whatever be the exact mechanism leading to the improved shelf-life of the F-prot-lipid biocomposite film, it is clear that this is a significant feature of the work that adds considerably to the lipid-based protocol for entrapment of enzymes.

## 3.9 Summary

We have demonstrated the formation of enzyme-lipid biocomposite films by a simple beaker-based immersion process. The non-specificity of the lipid matrix (cationic or anionic) in the entrapment of PGA and the irreversible binding of the enzyme to the lipid matrix highlights the role of hydrophobic and hydrogen bonding interactions in the biocomposite formation. The entrapment of invertase enzyme in the fatty amine lipid matrix occurs primarily due to attractive electrostatic interaction between the invertase guest and the fatty amine host. The lipid biocomposite films show biocatalytic activity and temporal/temperature stability superior to that of the free enzyme in solution. An important feature of the PGA-lipid biocomposite films is the excellent reusability of the films marking this protocol for potential commercial application. However, after certain number of reuses the biocomposite lipid films showed decrease in the activity. The decrease in the biocatalytic activity is attributed to inefficient release of the product during the reaction. The mass transfer effect was studied by using invertase enzyme. The entrapped products such as glucose and fructose in the invertase-ODA lipid films during the biocatalytic reaction was confirmed by reacting the biocomposite films with 2,3,5-triphenyl 2 H-tetrazolium chloride (TPTZ) to produce an insoluble red pigment.

Mass transfer effects are observed in the fatty lipid biocomposite films and hence, reduce the efficiency of the enzyme. It has been shown that pre-ordering of

thermally evaporated StA films by intercalation of lead ion results in the formation of self organized multilayers (SOMs) and enhances the diffusion of the F-prot enzyme into the lipid matrix during immersion in the protein solution. Other salient features associated with the ordered lamellar structure of the F-prot-fatty acid biocomposite film include enhanced biocatalytic activity of the entrapped enzyme relative to that of the free enzyme in solution as well as the enzyme in unordered fatty lipid films and a highly improved shelf-life/reusability of the biocomposite lipid film. This was possible due to the easy accessibility of the substrates to the entrapped enzyme and efficient release of the products during the biocatalytic reactions.

**References:**

1) (a) Singer, S. J.; Nicolson, G. L. *Science* **1972**, *175*, 720-751. (b) Jost, P. C.; Griffith, O. H. *Lipid-Protein Interactions*, Vol. 2, John Wiley & Sons, USA, **1982**. (c) Mouritsen, O. G.; Bloom, M. *Biophys. J.* **1984**, *46*, 141-153.

2) (a) Sackmann, E. *Science* **1996**, *271*, 43-48. (b) Tamm, L. K.; McConnell H. M. *Biophys. J.* **1985**, *47*, 105-113.

3) (a) Brian, A. A.; McConnell, H. M. *Proc. Natl. Acad. Sci. U.S.A.***1984**, *81*, 6159-6163. (b) Salafsky, J.; Groves, J. T.; Boxer, S. G. *Biochemistry* **1996**, 35, 14773-14781.

4) (a) Langmuir, I.; Schaffer, V. J. *J. Am. Chem. Soc.* **1938**, *60*, 1351-1360. (b) Ramsden, J. J. *Biosensors and Bioelectronics* **1996**, *11*, 523-528.

5) Radler, J.; Strey, H.; Sackmann, E. *Langmuir* **1995**, 11, 4539-4548.

6) Hamachi, I.; Fujita, A.; Kunitake, T. *J. Am. Chem. Soc.* **1994**, *116*, 8811-8812.

7) Haddon, R. C.; Lamola, A. A. *Proc. Natl. Acad. Sci. USA* **1985**, *82*, 1874-1878.

8) Mooney, J. F.; Hunt, A. J.; Mcintosh, J. R.; Liberko, C. A.; Walba, D. M.; Rogers, C. T. *Proc. Natl. Acad. Sci. USA* **1996**, *93*, 12287-12291.

9) Gole, A.; Sastry, M. *Biotechnol. Bioeng.* **2001**, *74*, 172-178.

10) Ganguly, P.; Pal, S.; Sastry, M.; Shashikala, M. N. *Langmuir* **1995**, *11*, 1078-1080.

11) Sastry, M.; Rao, M.; Ganesh, K. N. *Acc. Chem. Res.* **2002**, *35*, 847-855 and references therein.

12) (a) Sathivel, C.; Lachke, A.; Radhakrishnan, S. *J. Chromat. A* **1995**, *705*, 400-402. (b) Gole, A.; Sathivel, C.; Lachke, A.; Sastry, M. *J. Chromat. A* **1999**, *848*, 485-490.

13) Sauerbrey, G. *Z.Phys. (Munich)* **1959**, *155*, 206-222. (b) Buttry, D. A.; Ward, M. D. *Chem. Rev.* **1992**, *92*, 1355-1379. (c) Wang, J.; Frostman, L. M.; Ward, M. D. *J. Phys. Chem.* **1992**, *96*, 5224-5228.

14) (a) Gole, A.; Chaudhari, P.; Kaur, J.; Sastry, M. *Langmuir* **2001**, *17*, 5646-5656. (b) Gole, A.; Dash, C.; Rao, M.; Sastry, M. *Chem. Commun.* **2000**, 297-298. (c) Gole, A.; Vyas, S.; Sainkar, S. R.; Lachke, A. L.; Sastry, M. *Langmuir* **2001**, *17*, 5964-5970. (d) Gole, A.; Kaur, J.; Pavaskar, N.; Sastry, M. *Langmuir* **2001**, *17*, 8249-8253.

15) Gole, A.; Dash, C.; Mandale, A. B.; Rao, M.; Sastry, M. *Anal. Chem.* **2000**, *72*, 4301-4309.

16) Anson, M. *J. Gen. Physiol.* **1938**, *22*, 79-89.

17) (a) Jin, W.; Shi, X.; Caruso, F. *J. Am. Chem. Soc.*, **2001**, *123*, 8121-8122. (b) Caruso, F.; Furlong, D. F.; Ariga, K.; Ichinose, I.; Kunitake, T. *Langmuir* **1998**, *14,* 4559-4565.

18) (a) Dong, A.; Huang, P.; Caughey, W. S. *Biochemistry* **1992**, *31*, 182-189. (b) Templeton, A. C.; Chen, S.; Gross, S. M.; Murray, R. W. *Langmuir* **1999**, *15*, 66-76. (c) Kumar, C. V.; McLendon, G. L. *Chem. Mater.* **1997**, *9*, 863-870.

19) (a) Rabolt, J. F., Burns, F. C., Schlotter, N. E., Swalen, J. D. *J. Chem. Phys.* **1983**, 78, 946-952. (b) Ganguly, P.; Sastry, M.; Pal, S.; Shashikala, M. N. *Langmuir* **1995**, *11*, 1078-1080. (c) Pal, S. *Ph.D. Thesis*, University of Pune, **1996**.

20) Bomstein, J.; Evans, W. G. *Anal. Chem.* **1965**, *37*, 576-578.

21) Shewale, J. G.; Kumar, K. K.; Ambekar, G. R. *Biotechnol. Tech.* **1987**, *1*, 69-72.

22) Guisán, J. M.; Alvaro, G.; Fernandez-Lafuente, R.; Rosell, C. M.; Garciá, J. L.; Tagliani, A. *Biotechnol. Bioeng.* **1993**, *42*, 455-464.

23) (a) Tischer, W.; Wedekind, F. *Top Curr Chem.* **1999**, *200*, 95-126. (b) Tischer, W.; Kasche, V. *Trends. Biotechnol.* **1999**, *17*, 326-335.

24) (a) Avnir, D.; Braun, S. *Biochemical Aspects of Sol-Gel Science and Technology*; Kluwer: Hingham, MA, **1996**. (b) Weetal, H. H. *Science* **1969**, *166*, 615-616. (c)

Hernaiz, M. J.; Crout, D .H. G. *Enzyme. Microb. Technol.* **2000**, *27*, 26-32. (d) Heller, J.; Heller, A. *J. Am. Chem. Soc.* **1998**, *120*, 4586-4590.

25) Shiv Shankar, S.; Rautaray, D.; Pasricha, R.; Pavaskar, N. R.; Mandale, A. B.; Sastry, M. *J. Mater. Chem.* **2003**, *13*, 1108-1111.

26) Gascon, S.; Lampben, O. *J. Bio. Chem.* **1968**, *243*, 1567-1572.

27) Somogyi, N. *J. Bio. Chem.* **1952**, *195*, 19-23.

28) Yamanaka, K. *Meth. Enzymol.* **1975**, *41*, 466-471.

29) (a) Li, J.; Wang, J.; Gavalas, V. G.; Atwood, D. A.; Bachas, L. G. *Nano. Lett.* **2003**, *3*, 55-58. (b) Arica, M. Y.; Hasirci, V.; Alaeddinoglu, N. G. *Biomaterials* **1995**, *16*, 761-768. (c) Akgol, S.; Yalcinkaya, Y.; Bayramoglu, G.; Denizli, A.; Arica, M. Y. *Process Biochem.* **2002**, *38*, 675-683. (d) Takahashi, H.; Li, B.; Sasaki, T.; Miyazaki, C.; Kajino, T.; Inagaki, S. *Chem. Mater.* **2000**, *12*, 3301-3305.

30) (a) Marshbanks, T. L.; Ahn, D. J.; Franses, E. I. *Langmuir* **1994**, *10*, 276-285. (b) Marshbanks, T. L.; Frances, E. *J. Phys. Chem.* **1994**, *98*, 2166-2173.

31) Carslaw, H. S.; Jaeger, J. C. *Conduction of Heat in Solids*, (Clarendon Press, Oxford) Pg: 101, **1960**.

# Chapter IV

## Assembly of gold nanoparticles on polyurethane and zeolite microspheres: Template for enzyme immobilization

This chapter deals with immobilization of pepsin on gold nanoparticles assembled on submicron polyurethane and amine functionalized zeolite spheres. Gold nanoparticles provide a biocompatible surface for the binding of biomolecules such as DNA, enzymes, etc. To overcome the *mass transport problem*, we have immobilized enzymes on the surface of the polymer-gold nanoparticle and zeolite-gold nanoparticle 'core-shell' structures. The binding of gold nanoparticles on the polyurethane microspheres occurs through the nitrogen present in the polymer backbone, whereas in amine functionalized zeolite it occurs through the free amine groups of 3-amino propyltrimethoxy silane (3-APTS). The binding of the enzyme to the gold nanoparticles in turn occurs through the amine groups and the cysteine residues present in the enzyme. The biocatalytic activity of the enzyme bound to the surface of the core-shell conjugate material is comparable to free enzyme in solution. A major advantage of this strategy is that the enzyme on the surface of the gold nanoparticles behaves as free enzyme in solution. Moreover, the substrates are easily accessible to the immobilized enzyme for biocatalytic reactions. The bioconjugates are easily separated from the reaction medium and exhibit excellent reuse characteristics.

## 4.1 Introduction

Metal and semiconductor nanoparticles are exciting building blocks for the emerging and rapidly progressing field of nanotechnology [1-2]. Various biomolecules such as enzymes, antigens, antibodies, DNA, etc., have dimensions in the range of 2 to 100 nm. These dimensions are comparable to those of nanoparticles and thus the synthetic nanostructures and the biomaterial units exhibit structural compatibility. The conjugation of nanoparticles with the biomolecules is an exciting area of research since it may provide new dimensions to the area of nanobiotechnology. The utility of nanoscale curved surfaces such as those provided by colloidal particles in immobilizing biomolecules for immunoassays has been recognized in the early 1980's [3]. Rembaum, *et al.* demonstrated the formation of immunomicrospheres, which are specially designed microscopic particles that have antibodies or similar molecules chemically bound to their surfaces [3]. The antibody coated microspheres react in a highly specific way with target cells, viruses or other antigenic agents. Furthermore, the high surface-to-volume ratio offered by colloidal particle result in the concentration of the immobilized entity being considerably higher than that afforded by protocols based on immobilization on planar, 2-D surfaces resulting in enhanced detection signals.

Metal nanoparticles have potential biological applications especially in labeling biomolecules since metal nanoparticles make detection possible, easier and with greater sensitivity. Gold nanoparticles that are functionalized with proteins have long been tools in the biosciences. Antibodies adsorbed on colloidal gold are routinely used in histology [4], thus allowing the biospecific labeling of distinguished regions of tissue samples and subsequent TEM analysis. More advanced small gold clusters with a diameter of 0.8 or 1.4 nm can be used for the site-specific labeling of biological macromolecules [4]. Mirkin and co-workers reported a DNA sensor based on the dramatic red shift in the absorbance upon hybridization-driven gold nanoparticles aggregation [5]. Gold nanoparticles functionalized with biotin molecules have been successfully used for the cross linking the gold nanoparticles using the avidin molecules and semiempirical flocculation parameters were used to quantify the avidin induced aggregation of biotinylated gold colloids [6]. Recently, Hirsch *et al.* have designed $SiO_2$ core/Au shell composites, which absorb in the near-infrared where

interference from cell and tissues absorption in minimal [7]. Gold nanoshells which have tunable optical resonances in the near-infrared region have been used for treating the cancer cells [8]. Human breast carcinoma cells incubated with nanoshells in vitro were found to have undergone photothermally induced morbidity on exposure to near-infrared light.

In the area of metal nanoparticle-enzyme conjugate materials, Crumbliss, Stonehuerner and co-workers have studied the formation and enzymatic activity of gold nanoparticles complexed with horseradish peroxidase [9], xanthine oxidase [10] as well as glucose oxidase and carbonic anhydrase molecules [11]. A salient feature of their work is that the enzymes are bound tightly to gold nanoparticles and retain significant biocatalytic activity in the conjugated form while the enzyme molecules denature on adsorption to planar surfaces of gold. In our laboratory, we have reported the conjugation of pepsin [12], fungal protease [13] and endoglucanase enzymes [14] with gold nanoparticles, with excellent stability and biological activity of the immobilized enzymes. An important feature of this work was that the enzyme retains significant biocatalytic activity after adsorption on the surface of the gold nanoparticles. However, one major drawback of this approach is that the gold nanoparticle bioconjugate material was not easily separated from the reaction mixture and hence showed poor reuse characteristics. To overcome this problem, we have developed a protocol for the assembly of gold nanoparticle "shells" on massive polyurethane [15] and zeolite submicronsphere [16] "cores". Binding of the gold nanoparticles to the polymer surface occurs through nitrogen present in the polymer backbone and thus obviates the need for surface modification of the polymer spheres, which is required in other polymer microsphere-based nanoparticle immobilization methods [17-18]. In the case of zeolite the binding occurs through the free amine groups of 3-aminopropyltrimethoxy silane (3-APTS) present on the surface. In this manner gold nanoparticles assembled on the surface of these microspheres acts as the bulkier scaffolds for the immobilization of enzymes. These bulkier microspheres bound enzyme molecules are easily separated from the reaction mixture and hence are subsequently reused.

**4.2 Preparation of Polyurethane-gold nanoparticle 'core-shell' material**

The polyurethane (PU) microspheres of 2 μm mean diameter was synthesized as described in earlier work [19]. 10 mg of the PU microsphere powder was dispersed in 10 mL of hexane following which the dispersion was taken in a separating funnel along with 10 mL of the colloidal gold solution. Gold nanoparticles were synthesized by a procedure given by Sastry and co-workers [20]. A 100 mL of a $1.25 \times 10^{-4}$ M concentrated aqueous solution of chloroauric acid ($HAuCl_4$) was reduced by 0.01 g of sodium borohydride ($NaBH_4$) at room temperature to yield a ruby red solution containing $35 \pm 7$ Å diameter gold nanoparticles [20].
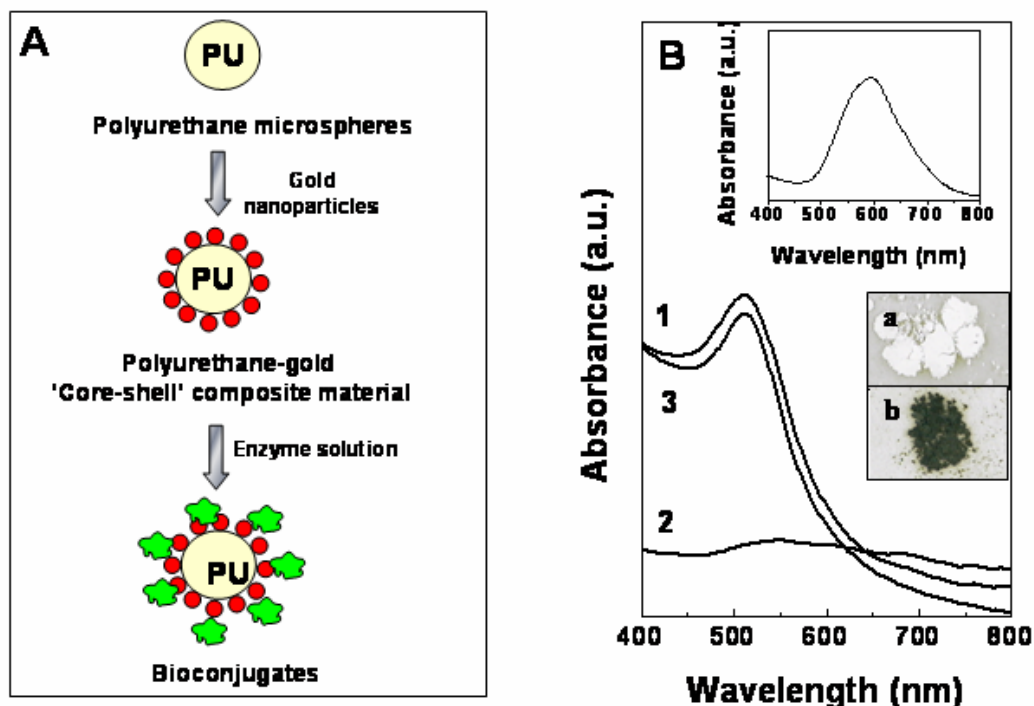


**Figure 4.1:** (A) Schematic (not to scale) showing the binding of gold nanoparticles to PU microspheres and thereafter their use for enzyme immobilization. (B) UV-vis spectrum of the as-prepared colloidal gold solution (curve 1) and the gold solution after addition of polyurethane microspheres and filtration (curve 2). Curve 3 shows the gold nanoparticle solution after vigorous mixing with hexane without PU microspheres. The inset shows the UV-vis spectrum recorded from a film of gold nanoparticle shell-PU core spheres on a quartz substrate. Inset shows a photograph of PU before (a) and after (b) binding with gold nanoparticles.

Vigorous shaking of the biphasic mixture for ca. 10 minutes yielded an emulsion-like phase that rapidly phase separated upon cessation of shaking. The originally ruby-red colloidal gold solution was now colorless and the PU powder had attained a purple color and had accumulated at the hexane-water interface. The gold nanoparticles coated-PU microspheres were separated by filtration, washed with double distilled water and dried in air for further use.

*4.2.1 UV-visible spectroscopy*

Fig.4.1B shows UV-vis spectra of the as-prepared colloidal gold solution (curve 1) and colloidal gold solution after addition of PU spheres and filtration (curve 2). The surface plasmon resonance in the as-prepared colloidal gold solution can be clearly seen at ca. 520 nm (curve 1) [20]. After shaking the colloidal gold solution with the PU dispersed in hexane, there is loss in intensity of the surface plasmon resonance due to a decrease in the concentration of gold nanoparticles in the aqueous solution (curve 2). This indicates binding of gold nanoparticles to the surface of PU microspheres through nitrogen atoms in polyurethane (see scheme in Fig.4.1A). The purple-colored PU spheres capped with gold nanoparticles were observed to assemble at the interface between the two liquids and could be separated and cast in the form of a film. The inset of Fig.4.1B shows the UV-vis spectrum recorded from a film of the PU spheres taken from the hexane-water interface after drying the film. A broad absorption band centered at ca. 600 nm is observed and arises from the gold nanoparticle 'shell' surrounding the PU 'core' spheres. The shift in the resonance wavelength indicates considerable aggregation of the gold nanoparticles consequent to binding with the PU surface (Fig.4.1A) [20,21].

Control experiments were done where only hexane (without PU microspheres) and aqueous colloidal gold solution were vigorously mixed, where aggregation of the gold nanoparticles at the liquid-liquid interface and the decrease in the intensity of the surface plasmon resonance in the aqueous solution of gold nanoparticles was not observed (Fig.4.1B, curve 3). This confirms the decrease in the surface plasmon resonance (Fig.4.1B, curve 2) in the aqueous solution is due to the binding of the gold nanoparticles to the PU microsphers and not due to the aggregation.

*4.2.2 Transmission Electron Microscopy (TEM)*

Fig4.2A and B show TEM micrographs of PU microspheres before and after binding to gold nanoparticles on a carbon-coated copper grid respectively. In Fig4.2B, the gold nanoparticles (dark spots) bound to the surface of the originally featureless PU particles (Fig.4.2A) can clearly be seen. As mentioned previously, the gold nanoparticles bind to the polymer surface through nitrogen atoms in PU.
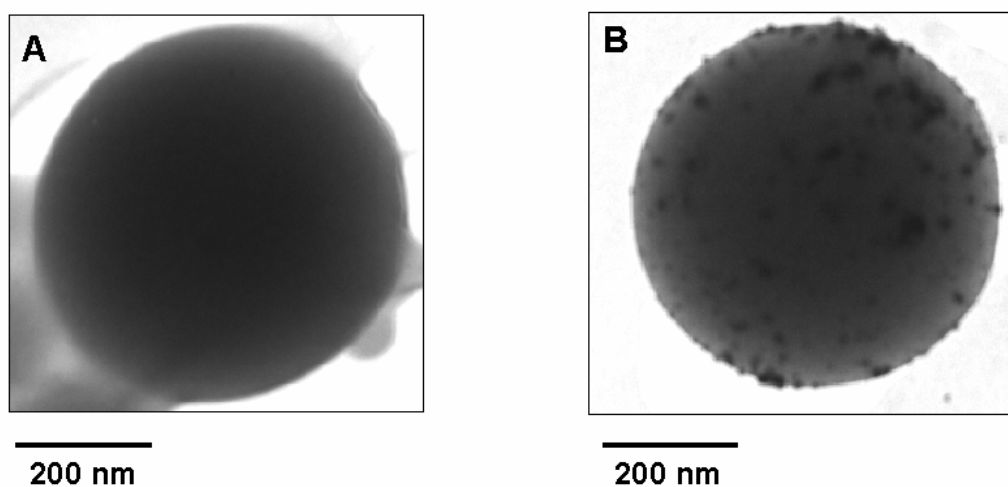


**Figure 4.2:** TEM images of polyurethane before (A) and after binding of gold nanoparticles (B) 'core-shell' particles on a carbon-coated TEM grid.

The structure of the PU-Au composite is illustrated in Fig.4.1A. It is well known that pyridine [22] and primary amines [23] bind to colloidal gold through nitrogen atoms. We believe a similar mechanism involving nitrogen atoms in PU in the entrapment of gold nanoparticles on the microspheres is operative in this study.

*4.2.3 Quantitative analysis of gold nanoparticles bound to PU microspheres*

The amount of gold nanoparticles bound to the PU microspheres was estimated by atomic absorption spectroscopy (AAS). 10 mg of gold nanoparticle-PU microsphere sample was dissolved in 20 mL of aqua-regia (concentrated HCl/concentrated $HNO_3$, 3:1) and the volume was made up to 100 mL using deionized water. The solution was

analyzed by a CHEMITO 201 atomic absorption spectrophotometer and was compared with the standard gold sample to estimate the weight percent of the loading of the gold nanoparticles in PU microspheres. The weight percent loading was estimated to be ca. 10 % by this procedure.

## 4.3 Preparation of Pepsin-PU-gold nanoparticle bioconjugate

10 mg of the gold nanoparticles bound to PU microsphere powder was dispersed in 2 mL of KCl-HCl buffer (0.02 M, pH 2), and to this dispersion 100 μL of ethanol was added to aid in the dispersion of the PU microspheres. To this solution, 100 μL of a stock solution consisting of 10 mg/mL of pepsin in KCl-HCl buffer (0.02 M, pH 2) was added under vigorous stirring. After 1 h of stirring, the bioconjugate were separated by centrifugation. The bioconjugate obtained was rinsed several times with KCl-HCl buffer (0.02 M, pH 2) solution and was re-suspended in buffer (pH 2) solution, and stored at 4 °C prior to further experiments.

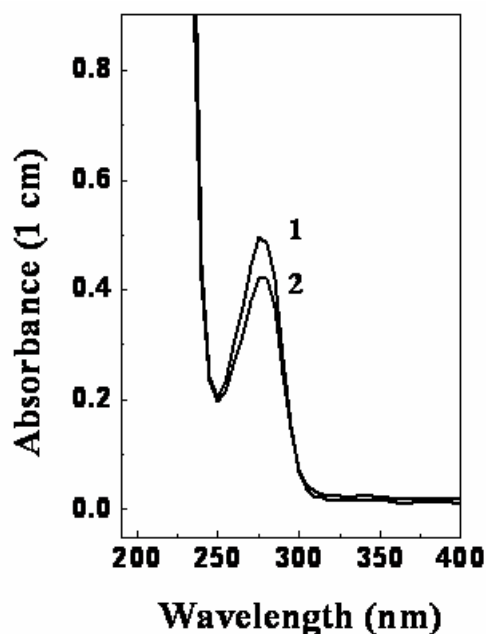### 4.3.1 Enzyme quantitative analysis in the bioconjugate



**Figure 4.3:** UV-vis spectra of pepsin solution in buffer (pH 2, curve 1) and supernatant of the PU-Au-pepsin bioconjugate solution after centrifugation (curve 2).

Fig.4.3 shows the UV-vis spectra of initial concentration (0.5 mg/mL) of free pepsin in buffer (curve 1) and the supernatant after centrifugation of bioconjugates (curve 2). The concentration of the enzyme in the bioconjugate was determined from a calibration curve of the absorbance of different concentrations of pepsin in KCl-HCl buffer (0.02 M, pH 2). From the decrease in the intensity of the enzyme in the supernatant at 280 nm, the amount of the enzyme bound to the PU-Au composite material was found to be 110 μg/10 mg of PU-Au [24].

*4.3.2 Scanning Electron Microscopy (SEM) and Energy dispersive analysis of X-rays (EDAX)*
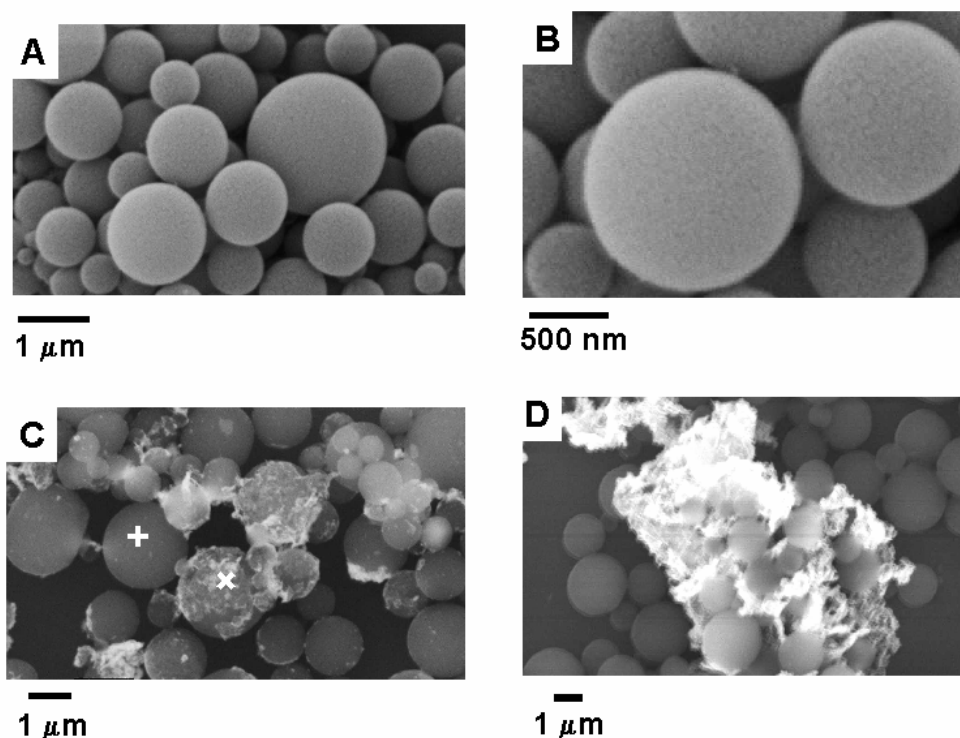


**Figure 4.4:** SEM images of PU-Au 'core-shell' composite material before (A and B) and after (C and D) binding of the enzyme pepsin.

Fig.4.4A and B show representative SEM images of drop-cast films of the PU-Au 'core-shell' material and the PU-Au-pepsin bioconjugate material (Fig.4.4C and D) on Si(111) substrates. While the surface texture of the PU spheres capped with gold

nanoparticles is quite smooth (Fig.4.4B, the gold nanoparticles are not clearly visible at the resolution of the SEM measurement), after conjugation with pepsin, thin sheets of presumably the aggregated enzyme are seen together with smooth PU-Au microspheres (Figs.4.4C and D). Spot profile EDAX analysis of the sheets (marked by an 'X' in Fig.4.4C) confirmed that they were composed of only the enzyme (through a strong sulfur signal from cysteine residues of pepsin). These sheets thus correspond to highly aggregated pepsin molecules, such protein aggregation having been observed by Caruso *et al.* in multilayer films of polymer-anti-IgG composites [25].

Spot profile EDAX analysis of the smooth gold nanoparticle-capped PU spheres away from the pepsin sheets (marked by a '+' in Fig4.4C) also showed the presence of sulfur indicating binding of the enzyme to the gold nanoparticles even though not visible by SEM imaging. The sulfur signal was absent in the PU-Au 'core-shell' material as expected.

## 4.4 Biocatalytic activity measurements

The biocatalytic activity of free pepsin in solution and of the PU-Au-pepsin bioconjugate in KCl-HCl buffer (0.02 M, pH 2) was determined by reaction with 0.6 % casein at 37 $^{o}$C for 1 h [12]. Carefully weighed amount of the PU-Au-pepsin bioconjugate in KCl-HCL buffer was reacted with 1 mL of casein solution at 37 $^{o}$C for 1 h. After this incubation time, equal volume of 1.7 M perchloric acid was added to the reaction solution to precipitate the residual casein. After 1 h, the precipitate was removed by centrifugation and the optical absorbance of the filtrate was measured at 280 nm. Pepsin digests casein and yields acid soluble products (tryptophan and tyrosine residues) that are readily detected by their strong UV signatures at 280 nm [26]. The amount of pepsin in the PU-Au-pepsin bioconjugate material was quantitatively estimated during preparation of the bioconjugate material as briefly mentioned earlier. For comparison, the biocatalytic activity of an identical concentration of the free enzyme in solution under identical experimental conditions was recorded. In order to determine the confidence limits of the biocatalytic activity measurements for the PU-Au-pepsin bioconjugate material, separate measurements of the biocatalytic activity (IU/μg) were made as described above for 6 different PU-Au-pepsin bioconjugate

materials. Biocatalytic activity of the bioconjugate was found to be 13.2 IU/μg and that of free enzyme in solution was 11.2 IU/μg. Indeed, there is a marginal enhancement in the biocatalytic activity in the bioconjugate material that is outside experimental uncertainty.

*4.4.1 Reusability of the bioconjugate*

The most significant part of the enzyme immobilization on PU microspheres is the easy separation of the enzyme from the products and reuse of the enzyme. The PU-Au-pepsin bioconjugate material was separated from the reaction medium by mild centrifugation for recycling studies.

**Table 1**

Biocatalytic activity of the PU-Au pepsin bioconjugate over six sequential reuses.

| System | Biocatalytic activity[#] (IU/μg) |
|---|---|
| Pepsin in solution | 11.2 |
| PU-Au-pepsin bioconjugate, run 1 | 13.2 |
| PU-Au-pepsin bioconjugate, run 2 | 10.2 |
| PU-Au-pepsin bioconjugate, run 3 | 8.0 |
| PU-Au-pepsin bioconjugate, run 4 | 7.2 |
| PU-Au-pepsin bioconjugate, run 5 | 4.3 |
| PU-Au-pepsin bioconjugate, run 6 | 3.6 |

# One unit of protease activity is measured as a change in absorbance at 280 nm of 0.001 per minute at pH 2 and 37 °C measured as acid soluble products using casein as the substrate.

Table 1 shows the results of 6 cycles of reuse of the PU-Au-pepsin bioconjugate. It is seen that there is a small, monotonic decrease in the biocatalytic activity of the enzyme with reuse, the biocatalytic activity falling to ca. 28 % of the starting activity after 6 cycles of reuse. This excellent retention of biocatalytic activity

of pepsin in the PU-Au-pepsin bioconjugat with reuse is to be contrasted with the almost complete loss in activity as seen in our earlier work of the same enzyme immobilized in thermally evaporated fatty amine films after just 3 cycles of reuse [26]. Clearly the blockage of diffusion pathways of substrate molecules implicated in the earlier study for loss in activity with recycling is not operative in the bioconjugation strategy presented in this work. This is a salient feature of the work with immense commercial implications. However, the monotonic and perceptible loss in catalytic activity of the PU-Au-pepsin bioconjugate material as a function of reuse needs elaboration.

It is possible that the gold nanoparticles detach from the surface of the PU microspheres during successive reaction cycles. Another possibility is the leaching out of pepsin from the bioconjugate material in successive reactions. In order to distinguish between the two mechanisms, atomic absorption spectroscopy (AAS) measurements were performed on the supernatant obtained after centrifugation of the reaction medium during each of the reaction cycles. Gold could not be detected by AAS [detection sensitivity ~ parts per million (ppm)] in any of the reaction cycles clearly showing that the nanoparticles are strongly bound to the underlying PU microsphere template. This results points to loss of enzyme from the nanoparticle surface during reaction. UV-vis spectroscopy measurements were carried out on the supernatant from 10 mg of the PU-Au-pepsin bioconjugate material immersed in 2 mL of pH 2 buffer solution. 1 ml of the supernatant was analyzed in intervals of 1 h, which is characteristic of the reaction times in the reuse measurements. After each measurement, the analyte was added back to the original buffer solution to simulate the reaction conditions precisely. It was observed that after 1 h of immersion, roughly 35 % of the total pepsin loading was released into solution (estimated from the absorbance at 280 nm) [24]. Thereafter, no further loss of enzyme occurred for longer times of immersion of the bioconjugate material. This percentage loss of enzyme correlates well with degree of loss of biocatalytic activity during the first reuse cycle (Table 1).
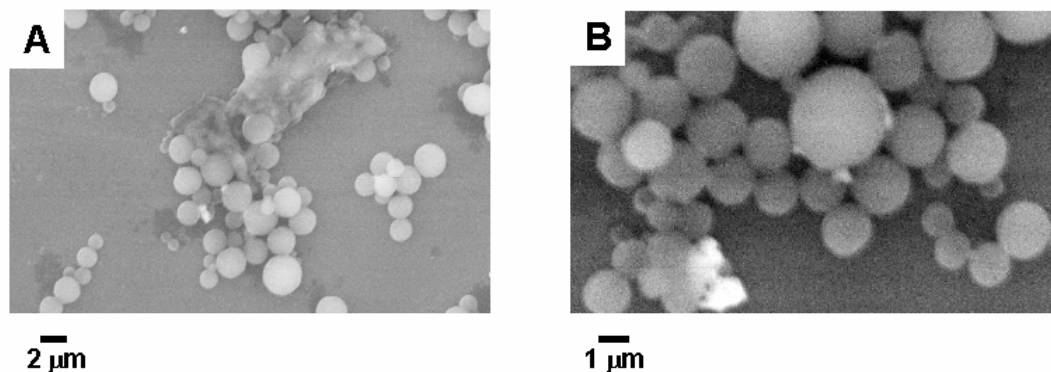
**Figure 4.5:** Low (A) and high (B) magnification SEM images of PU-Au-pepsin bioconjugate after one cycle of reaction.


We believe the initial loss of pepsin corresponds to loss of weakly bound enzyme from the bioconjugate. It is likely that the sheets of aggregated pepsin molecules observed in the SEM images of the PU-Au-pepsin bioconjugate (Fig.4.4C and D) correspond to the weakly bound enzyme that leaches out in the first reaction cycle. That is indeed the possible mechanism is indicated by the SEM images recorded from the PU-Au-pepsin bioconjugate material after one cycle of reuse (Fig.4.5A and B). It is clearly seen from this figure that the percentage of aggregated pepsin sheets observed in the as-prepared bioconjugate material has reduced drastically after one reaction cycle.

*4.4.2 pH dependent biocatalytic activity*

Many applications of immobilized enzymes require their operation under pH and temperature conditions far removed from optimum operating conditions. We have recently observed that the enzyme, endoglucanase, when immobilized in fatty lipid films, exhibited significant catalytic activity under highly alkaline conditions as well as enhanced temperature stability [27]. This feature is tremendously exciting for application of this enzyme in the paper pulp and fabric treatment industries where such harsh conditions are normally encountered [27]. While enhanced biocatalytic activity of the enzyme pepsin over a large pH range may not conceivably have an immediate application, such a variation in reactivity of the enzyme under different conditions of

immobilization would shed some light on the nature of interaction of the enzyme with the host matrix.

Fig.4.6A shows the biocatalytic activities (IU/µg) of the PU-Au-pepsin bioconjugate material (squares) along with that of the free enzyme in solution (triangles) as a function of solution pH in the range 2 to 10. Three separate measurements at each pH were performed to check the reproducibility of the data. The optimum biocatalytic activity in both cases is at pH 2 with a marginal fall in activity observed at pH 5. There is retention of nearly 40 % of the optimum biocatalytic activity by the PU-Au-pepsin bioconjugate at pH 8. Under these pH conditions, free pepsin in solution showed no catalytic activity at all (Fig.4.6A). A small biocatalytic activity was observed in the PU-Au-pepsin bioconjugate even at pH 10. We are unable to explain the stability of pepsin immobilized on the PU-Au surface as a function of pH at present, but speculate that this could be due to the ionic environment around the enzyme active site in the immobilized form.
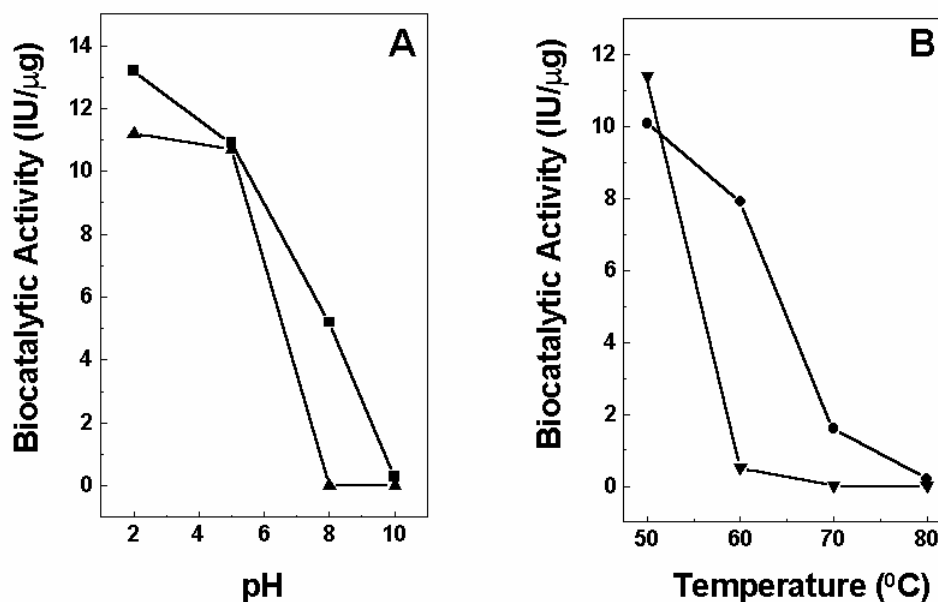


**Figure 4.6:** (A) pH dependent biocatalytic activity of free enzyme in solution (triangle) and PU-Au-pepsin bioconjugate (squares). (B) Temperature dependent biocatalytic activity of free enzyme in solution (triangle) and PU-Au-bioconjugate (circles). Solid lines are an aid to eye and have no physical significance.

*4.4.3 Temperature dependent biocatalytic activity*

Fig.4.6B shows the temperature variation in biocatalytic activity (IU/μg) of free pepsin in solution (triangles) and the PU-Au-pepsin bioconjugate material (circles) determined at pH 2 in the temperature range 50-80 $^o$C. Three separate measurements at each temperature were performed to check the reproducibility of the data. The free enzyme in solution is intolerant to even a 10 $^o$C increase in temperature of the reaction medium and biocatalytic activity of free enzyme in solution at 60 $^o$C is only 4 % of that observed at 50 $^o$C. However, pepsin in the bioconjugate material showed only a 32 % fall in biocatalytic activity under similar temperature rise conditions (Fig.4.6B). Indeed, the bioconjugate material showed a significantly high biocatalytic activity even at 70 $^o$C (Fig.4.6B, ca. 14 % of the specific biocatalytic activity at 50 $^o$C) under conditions where free pepsin showed no biocatalytic activity at all. Thus, complexation of the pepsin molecules with gold nanoparticles capping PU microspheres considerably increases the temperature and pH stability of the enzyme. The increase in the thermal stability of the enzyme in the bioconjugates is from the conformational integrity of the enzyme structures after binding the gold nanoparticles through the amine groups and cysteine residues present in the enzymes. Such increase in the thermal stability has also been observed for pepsin immobilized on the surface of alumina nanoparticles [28].

**4.5 Preparation of Zeolite-gold nanoparticle 'core-shell' material**

Silica is readily suspended in aqueous solution. Moreover, the silica surface can be easily derivatized with an enormous variety of chemical functional groups using simple silane chemistry with commercial available reagents [29]. Functionalized hexagonal SBA-15 with different functional groups such as chloride, thiol, amine and carboxylic acid were used for the immobilization of the enzyme trypsin [30]. By introducing 2 % coverage of HOOC-CH$_2$-CH$_2$- groups on the internal silanol wall of mesoporous silica, is used for the immobilization of the enzyme organophosphorous hydrolase (OHP) [31]. The organic functionalization provides the enzyme with a benign surrounding microenvironment, showing higher affinity for the protein. Silica nanotubes functionalized selectively to give hydrophilic chemistry on their outer

surface and hydrophobic chemistry on their inner surface are shown ideal for extracting lipophilic molecules from the aqueous solution [32].

In an earlier report by Westcott *et al.* silica nanoparticles synthesized using the Stöber method were functionalized with a mixture of 2 % 3-aminopropyltrimethoxysilane (APTS) and 98 % n-propyltrimethoxysilane (PTMS). The mixture yielded silica nanoparticles whose surfaces were terminated with the amine groups. Since gold nanoparticles can be bound to substrate via amine groups [33], mixing the gold nanoparticles with the functionalized silica nanoparticles would result in immobilization of a dilute coverage of gold nanoparticles onto the silica nanoparticles. Chen *et al.* reported the synthesis of gold-silica 'core-shell' nanoparticles with a mercaptosiliane layer between the core and shell [34]. This requires synthesis of mercaptosilane monolayer on colloidal gold and thereafter, sol-gel-hydrolysis and condensation to form gold-silica 'core-shell' structures.
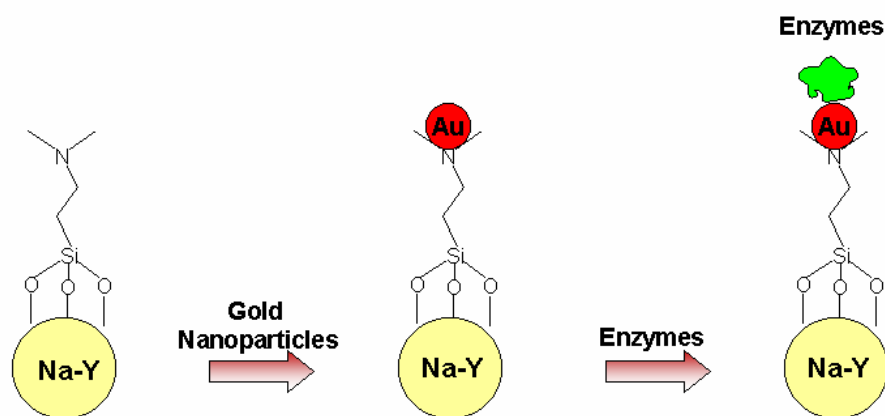


**Figure 4.7:** Schematic (not to scale) showing the binding of gold nanoparticles to APTS functionalized zeolite and thereafter their use for enzyme immobilization.

In this chapter, we demonstrate the assembly of gold nanoparticles on amine-functionalized zeolite. The silanol groups of the zeolite are functionalized by amine groups using 3-aminopropyltrimethoxysilane (3-APTS). Thereafter, the free amine

groups on the surface of the zeolite are used for binding of gold nanoparticles, which would thereafter serve as an excellent scaffold for enzyme immobilization.

*4.5.1 Synthesis of APTS Functionalized Spherical Faujasite (zeolite Y) Particles*

The process for the synthesis of spherical zeolite Na-Y was based on the report of Prouzet *et al.* [35]. To 1.0 g of the calcined Na-Y zeolite powder, 1 mL of 3-aminopropyltrimethoxysilane (APTS) in 30 mL of dicholoromethane (DCM) was added and the slurry stirred for 16 h at room temperature. The white APTS functionalized zeolite powder was then repeatedly washed with DCM and dried in vacuum. The samples thus obtained were used for further experiments. 10 mg of the amine-functionalized zeolite was dispersed in 50 mL of the colloidal gold solution under continuous stirring. After ca. 12 h of stirring, the originally ruby-red colloidal gold solution turned colorless, while the zeolite had attained a reddish hue. The zeolite particles capped with gold nanoparticles were separated by mild centrifugation, washed with double distilled water and dried in air for further use.

*4.5.2 UV-visible spectroscopy*

Fig.4.8A shows UV-vis spectra recorded from the as-prepared colloidal gold solution (curve 1) and the gold solution after stirring with zeolite for 12 h and filtration (curve 2). The surface plasmon resonance in the as-prepared colloidal gold can be clearly seen at ca. 520 nm (curve 1) [20]. After stirring the colloidal gold solution with the zeolite for 12 h, it is seen that there is loss in intensity of surface plasmon resonance due to decrease in the concentration of gold nanoparticles in aqueous solution (curve 2). This clearly indicates binding of the gold nanoparticles to the amine-functionalized zeolite through free amine groups of APTS [23]. The probable structure of the binding of gold nanoparticles to zeolite material is illustrated in Fig.4.7. The inset shows the photograph of as-prepared amine functionalized zeolite (a), which is white in color. After stirring amine-functionalized zeolite in gold nanoparticles solution for 12 h it attains a reddish hue (b) and confirms the binding of gold nanoparticles to the zeolite, possibly through the amine groups.
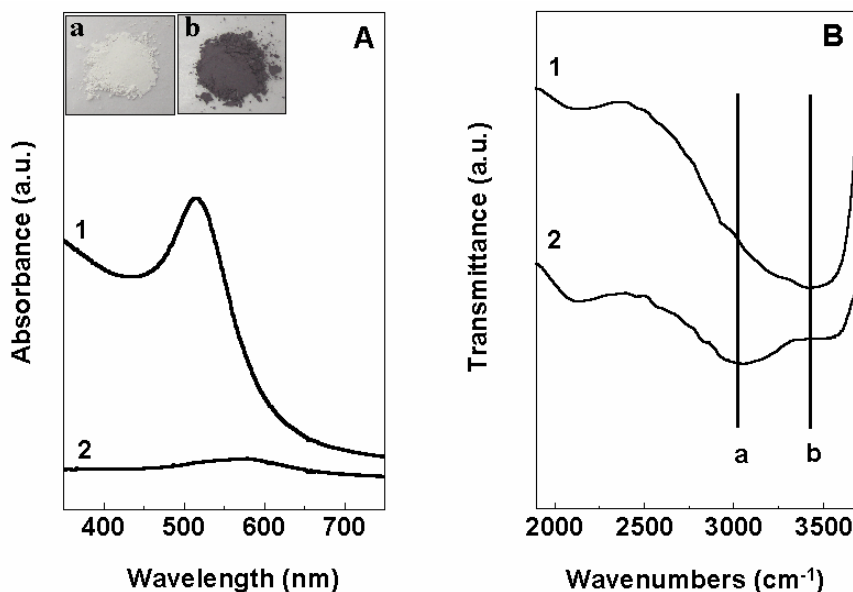
**Figure 4.8:** (A) UV-vis recorded from the as-prepared colloidal gold solution (curve 1) and gold solution after stirring with amine-functionalized zeolite for 12 h and centrifugation (curve 2). Inset shows a photograph of as-prepared zeolite before (a) and after (b) binding with gold nanoparticles. (B) FTIR spectra recorded from drop-coated films of amine-functionalized zeolite (curve 1) and gold nanoparticle-bound zeolite material (curve 2) on Si(111) substrates.

Control experiments were done where the pure zeolite (without amine-functionalization) and aqueous gold nanoparticle solution were stirred for 12 h. A decrease in the intensity of the surface plasmon resonance in the aqueous solution of gold nanoparticles was not observed. This confirms that the decrease in the surface plasmon resonance (Fig.4.8A, curve 2) in the aqueous solution is due to the binding of the gold nanoparticles to the amine groups of APTS present on the surface of zeolite and not to the zeolite directly.

*4.5.3 Fourier transform infrared spectroscopy (FTIR)*

Fig.4.8B shows FTIR spectrum of the amine-functionalized zeolite film (curve 1) shows an asymmetric, broad band centered at around 3450 cm$^{-1}$. This broad resonance arises from excitation of N-H stretch vibrations of the amine groups (usually centered at ca. 3350 cm$^{-1}$) [36] and O-H stretch vibrations from silanol groups in the zeolite material (3400 – 3600 cm$^{-1}$ region). In the film of amine-functionalized zeolite bound with gold nanoparticles (curve 2, feature a), a well defined band appears at ca.

3050 cm$^{-1}$ and is assigned to the N-H stretch vibrational mode of the free amine group of APTS after binding to gold nanoparticles. The shift in the N-H stretch band from 3350 cm$^{-1}$ to 3050 cm$^{-1}$ after stirring with gold nanoparticles indicates binding of the gold nanoparticles to the zeolite particles through the amine groups, such shifts having been observed in Langmuir-Blodgett films of octadecylamine after formation of complexes with PtCl$_6^-$ ions [36]. Due to the shift in the N-H stretch vibration in the gold nanoparticle-capped sample (curve 2), the O-H stretch band sharpens and a well defined resonance at ca. 3350 cm$^{-1}$ is now observed (curve 2, feature b).

*4.5.4 Quantitative analysis of gold nanoparticles bound to the zeolite*

The mass loading of the zeolite particles by gold nanoparticles was estimated to be 5 % by weight from the decrease in the intensity of the surface plasmon resonance of gold nanoparticles in the supernatant obtained after centrifugation of the zeolite (Fig.4.8A). Atomic absorption spectrometery (AAS) was also used to estimate the mass loading of the gold nanoparticles on the amine functionalized Na-Y zeolite. 60 mg of amine functionalized Na-Y zeolite bound with gold nanoparticles was dissolved in 10 mL agua regia (conc.HCl : conc. HNO$_3$, 3:1) and volume was made up to 100 mL by using deionized water. The solution was analyzed by CHEMITO 201 Atomic Absorption Spectrophotometer and was compared with a standard gold solution to estimate the weight percent of gold in zeolite. The weight percent loading of gold nanoparticles in the zeolite was estimated to be 5.8 % by this procedure. The result is comparable to the one estimated from the UV-visible spectroscopy. The small difference in the mass loading may be attributed to the aggregation of gold nanoparticles as seen in the supernatant (Fig.4.8A, curve 2) after centrifugation.

*4.5.5 Transmission Electron Microscopy (TEM)*

Fig.4.9A show representative TEM micrographs of the as-prepared amine functionalized zeolite particles. The particles are fairly spherical, with slightly irregular edges. Analysis of many similar TEM images indicated that the particles were quite uniform in size, with an average diameter of ca. 800 nm. TEM images recorded from the amine-functionalized zeolite particles after complexation with gold nanoparticles is

shown in Fig.4.8B. In this image, gold nanoparticles (dark spots) decorating the surface of the zeolite particles can clearly be seen.
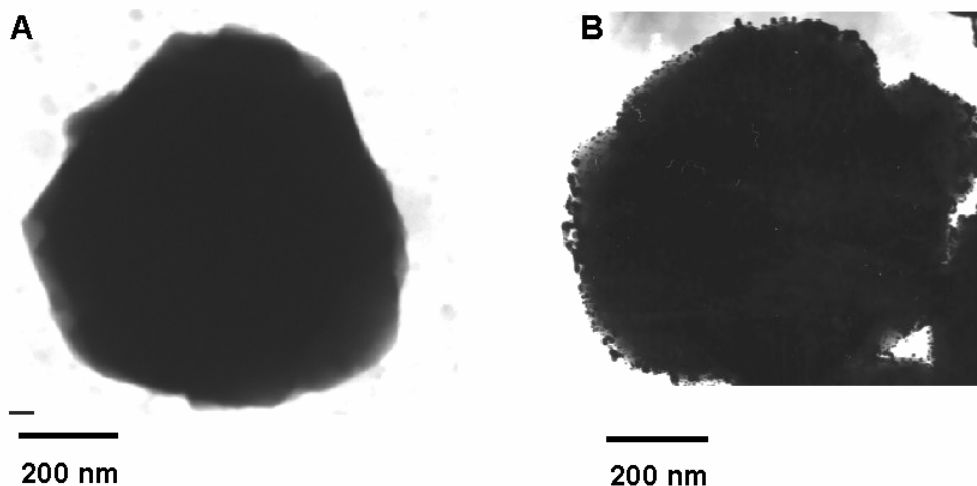


**Figure 4.9:** Representative TEM images of before (A) and after (B) binding of gold nanoparticles to amine-functionalized zeolite particles on a carbon-coated TEM grid.

This indicates clearly that the gold nanoparticles are bound to the zeolite at fairly high concentration. As mentioned previously and confirmed by FTIR analysis (Fig.4.8B), the gold nanoparticles bind to the zeolite template via the primary amine groups. The structure of the gold nano-zeolite particles is illustrated in Fig.4.7.

*4.5.6 X-ray diffraction (XRD)*

Fig.4.10 shows XRD patterns recorded from the as-prepared amine-functionalized zeolite powder (curve 1) and the amine functionalized zeolite powder after complexation with gold nanoparticles (curve 2). Further to binding of gold nanoparticles to the underlying zeolite template, no changes whatsoever are seen in the peak positions and peak intensities of the Bragg reflections arising from the zeolite clearly indicating that the crystallinity of the zeolite is maintained after binding of gold nanoparticles. This is an important result given that encapsulation of hetero polyanions in channels of Si-MCM 41 has been reported to lead to loss in crystallinity of the mesoporous template [37]. The XRD result thus suggests that the gold nanoparticles are bound to the surface of the zeolite particles and are not trapped within the pores of the

zeolite. This is understandable since the size of the gold nanoparticles in this study is ca. 4 nm while the zeolite pore diameter is estimated to be 1.2 nm.
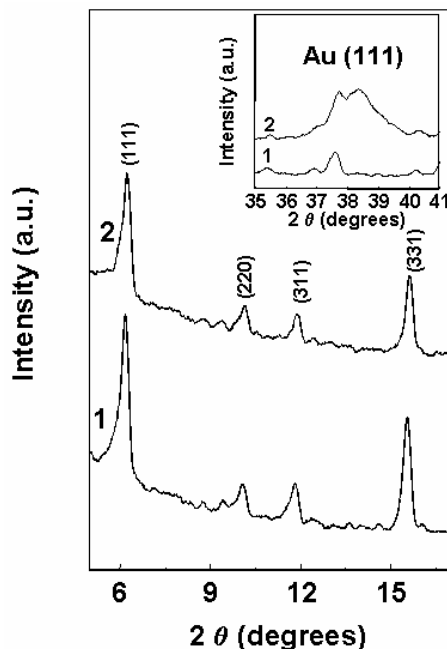


**Figure 4.10:** XRD patterns recorded from films of amine-functionalized zeolite (curve 1) and amine-functionalized zeolite after complexation with gold nanoparticles (curve 2) on Si(111) substrates. The inset shows XRD patterns recorded from films of amine-functionalized zeolite (curve 1) amine-functionalized zeolite after complexation with gold nanoparticles (curve 2) in the gold (111) Bragg reflection region.

The inset of Fig.4.10 is an expanded region of the patterns shown in the main part of the figure. The (111) Bragg reflection from gold nanoparticles bound to the zeolite template (curve 2) can clearly be seen, this peak being absent in the as-prepared amine-functionalized zeolite powder (curve 1). This provides additional confirmation of the binding of gold nanoparticles to the zeolite.

**4.6 Preparation of Pepsin-zeolite-gold nanoparticle bioconjugate**

10 mg of the zeolite-Au powder was dispersed in 2 mL KCl-HCl buffer (0.02 M, pH 2). To this solution, 200 μl of a stock solution consisting of 10 mg/mL of pepsin in KCl-HCl buffer (0.02 M, pH 2) was added under vigorous stirring. After 1 h of

stirring the zeolite-Au-pepsin bioconjugate material were separated by centrifugation (Fig.4.11). The powder thus obtained was rinsed several times with KCl-HCl buffer (0.02 M, pH 2) solution and re-suspended in buffer solution (pH 2) and stored at 4 °C for further experiments.

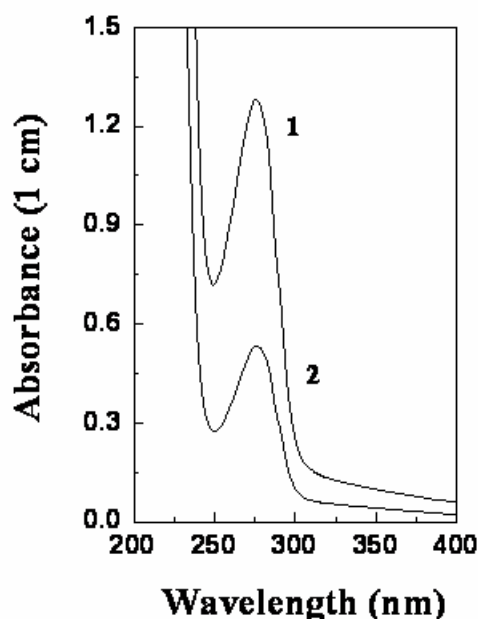*4.6.1 Enzyme quantitative analysis in the bioconjugate*



**Figure 4. 11:** UV-vis spectra of pepsin solution in buffer (pH 2, curve 1) and supernatant of the zeolite-Au-pepsin bioconjugate solution separate after centrifugation (curve 2).

Fig.4.11 shows the UV-vis spectra of initial concentration (1 mg/mL) of free pepsin in buffer (curve 1) and the supernatant after centrifugation of bioconjugates (curve 2). The concentration of the enzyme in the bioconjugate was determined from a calibration curve of the absorbance of different concentrations of pepsin in KCl-HCl buffer (0.02 M, pH 2). From the decrease in the intensity of the enzyme in the supernatant, the amount of the enzyme bound to the zeolite-Au composite material was found to be 0.6 mg/10 mg of zeolite-Au [24]. As compared to our earlier work, the

amount of enzyme binding to PU-AU was 1.1 % by weight of template. However, the amount to enzyme binding to zeolite-Au is considerably higher (6 wt %).

*4.6.2 Scanning Electron Microscopy (SEM) and Energy dispersive analysis of X-rays (EDAX)*

Fig.4.12A and B show representative SEM images of drop-cast films of the zeolite-Au 'core-shell' material and the zeolite-Au-pepsin bioconjugate material on Si(111) substrate respectively. The surface texture of the zeolite particles capped with gold nanoparticles was quite smooth (Fig. 4.12A). The SEM instrument was clearly unable to resolve the gold nanoparticles bound to the surface of the zeolite core. After conjugation of the Au–zeolite material with pepsin, thin sheets of presumably aggregated enzyme can be seen together with smooth Au–zeolite spheres (Fig. 4.12B, shown by arrows).
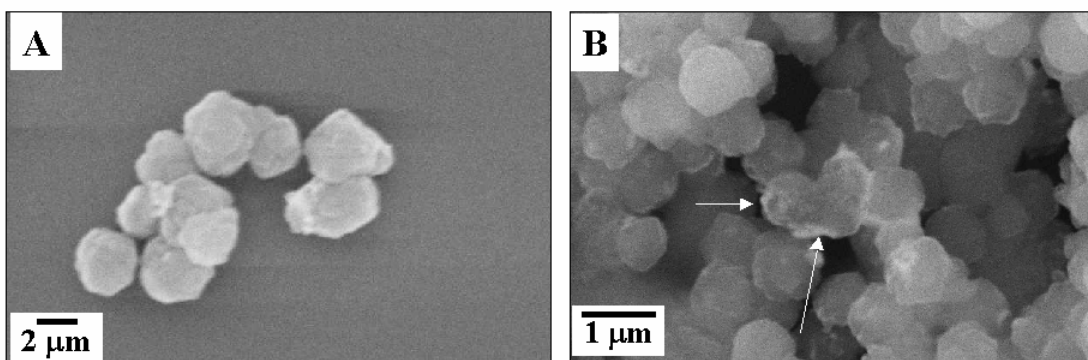


**Figure 4.12:** SEM images of zeolite-Au 'core-shell' composite material before (A) and after (B) binding of the enzyme pepsin

Spot profile EDAX analysis of the sheets (shown by arrow in Fig.4.12B) confirmed that they were composed of only the enzyme (through a strong sulfur signal from cysteine residues of pepsin). These sheets thus correspond to aggregated pepsin molecules, with such protein aggregation having been observed by Caruso *et al.* [25] in multilayer films of polymer–anti-IgG composites. The sulfur signal was absent in the Au–zeolite ''core-shell' particles, as expected.

**4.7 Biocatalytic activity measurements**

The biocatalytic activity of the pepsin bound to the Au-zeolite composite material and was compared with the free enzyme in solution as described in Section 4.4. In order to determine the confidence limits of the biocatalytic activity measurements for the pepsin-zeolite-Au bioconjugate material, separate measurements of the biocatalytic activity (IU/μg) were made as described above for 6 different zeolite-Au pepsin bioconjugate solutions. Biocatalytic activity of the bioconjugates was found to be 14.1 IU/μg and that of free enzyme in solution was 13.7 IU/μg. Indeed, there is a marginal enhancement in the biocatalytic activity in the bioconjugate material that is outside experimental uncertainty.

*4.7.1 Reusability of the bioconjugate*

**Table 2**

Biocatalytic activities of the pepsin-zeolite and pepsin-Au-zeolite bioconjugate materials during successive reuses.

| No of cycles | Biocatalytic activity of pepsin immobilized on amine functionalized zeolite (IU/μg)[#] | Biocatalytic activity of pepsin immobilized on gold nanoparticles bound to zeolite (IU/μg)[#] |
|---|---|---|
| 1 | 10.3 | 14.6 |
| 2 | 6.5 | 12.9 |
| 3 | 4.1 | 12.0 |
| 4 | 2.5 | 10.7 |
| 5 | 0 | 9.3 |
| 6 | 0 | 8.2 |
| 7 | 0 | 4.7 |

# One unit of enzyme will produce a change in absorbance at 280 nm of 0.001 per minute at pH 2 and 37 $^0$C measured as acid soluble products using casein as the substrate.

In order to understand the role of the gold nanoparticles bound to zeolite in the binding pepsin, the enzyme was also bound directly to amine functionalized zeolite. From UV-vis spectroscopy the amount of enzyme bound to amine functionalized zeolite was estimated to be 0.4 mg/10 mg of zeolite possibly through weak interactions such as hydrogen bonding and electrostatic interactions. Table 2 lists the biocatalytic activities calculated from reaction of the zeolite-Au-pepsin and zeolite-pepsin bioconjugate materials over seven sequential reuse cycles. In the first reaction, the biocatalytic activity in the zeolite-pepsin material is ca. 70 % of that observed in the zeolite-Au-pepsin system. Thereafter, the biocatalytic activity of the zeolite- pepsin material falls off rapidly losing complete activity by the 5$^{th}$ cycle of reaction. On the other hand, the zeolite-Au-pepsin system exhibits only a 36 % loss in biocatalytic activity by the 5$^{th}$ reuse cycle and even after 7 cycles of reaction retains ca. 32 % of the original biocatalytic activity. These results clearly show the remarkable reuse characteristics of the zeolite-Au-pepsin bioconjugate material and represent a major advance in our studies on development of gold nanoparticle based enzyme immobilization protocols. While the exact reasons for the better reuse characteristics of the zeolite-Au-pepsin system are not clear at the moment, we believe the pepsin molecules are bound much more strongly to the gold nanoparticles than to the zeolite particles. This would reduce significantly leaching out of the enzyme during the successive reaction cycles and thus, lead to improved retention of biocatalytic activity.

### *4.7.2 pH dependent biocatalytic activity*

Fig.4.13A shows plots of the biocatalytic activity of free pepsin molecules in solution (triangles) and pepsin bound to the zeolite-Au template (circles) for reactions carried out as a function of solution pH in the range 2 to 12. Three separate measurements at each pH were performed to check the reproducibility of the data. It is seen that optimum biocatalytic activity in both the cases is at pH 2, with a marginal loss in biocatalytic activity at pH 5. At pH 6.5, however, free enzyme molecules in solution retain only 2% of the biocatalytic activity recorded at pH 2, while the pepsin molecules immobilized on the zeolite-Au template retain as much as 52% of the catalytic activity recorded at pH 2. Even at pH 8 and 10, pepsin in the bioconjugate material shows

significant catalytic activity. This highlights the important role of the gold nanoparticles in enhancing and stabilizing the catalytic activity of pepsin in the immobilized state.
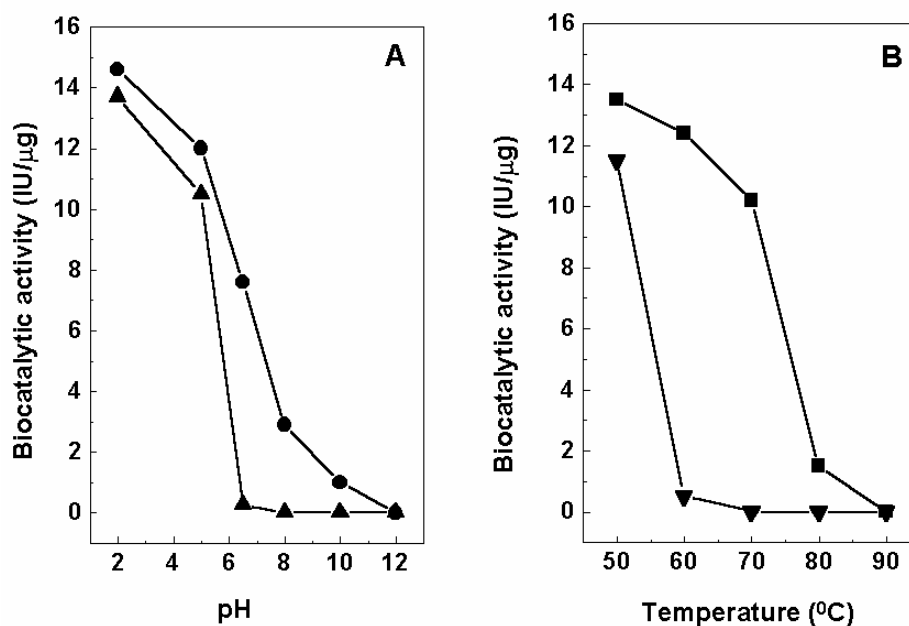


**Figure 4.13:** pH-dependent biocatalytic activity of free pepsin in solution (triangles) and pepsin in the Au-zeolite bioconjugate material (circles). (B) Temperature-dependent biocatalytic activity of free pepsin in solution (triangles) and pepsin in the Au-zeolite bioconjugate material (squares). The solid lines in all cases are aids to the eye and have no physical significance.

*4.7.3 Temperature dependent biocatalytic activity*

Fig.4.13B shows plots of the variation in biocatalytic activity of free pepsin molecules in solution (triangles) and pepsin immobilized on the zeolite-Au template (squares) as a function of temperature of reaction. Three separate measurements at each temperature were performed to check the reproducibility of the data. At higher temperatures, dramatic differences in the biocatalytic activity of the enzyme in the two cases are observed. At 60 $^{o}$C, free enzyme has lost almost all of its biocatalytic activity (only 4 % of the biocatalytic activity at 50 $^{o}$C), while pepsin immobilized on the zeolite-Au template retained 92% of the optimum biocatalytic activity (50 $^{o}$C measurement). This remarkable trend continues at higher temperatures as well with

retention of 75% of optimum biocatalytic activity for the immobilized enzyme at 70 $^o$C. The increase in the thermal stability of the enzyme in the bioconjugates is from the conformational integrity of the enzyme structures after binding the gold nanoparticles through the amine groups and cysteine residues present in the enzymes. Such increase in the thermal stability is also observed by pepsin immobilization on the surface of alumina nanoparticles [28]. Moreover, the thermal stability of the enzymes is observed after the covalent immobilization of enzymes to the different solid supports [38]. These results show that the gold nanoparticle bound to the amine functionalized zeolite particles not only efficiently immobilize pepsin in its native state but that they also stabilize the enzyme molecules under harsh conditions of pH and temperature.

## 4.8 Summary

In this chapter, we have demonstrated the assembly of gold nanoparticles on the surface of polyurethane and amine functionalized zeolite microspheres. The binding of gold nanoparticles to the PU microspheres occurs through the interaction of the urethane nitrogens with the gold particles while in zeolite particles it occurs through the free amine groups of the APTS on the surface of zeolite. The gold nanoparticles on the surface of theses microspheres are used to immobilize enzymes such as pepsin. Bioconjugation of the gold nanoparticles-PU/zeolite spheres with pepsin leads to a new class of biocatalyst that combines the utility of immobilization in terms of reuse with easy access of substrates to the enzyme normally reserved for enzymes present directly in solution. The bioconjugates material exhibited outstanding reuse capability and temperature/pH stability.

**References:**

1)  Niemeyer, C. M.; Mirkin, C. A. *Nanobiotechnology, Concepts, Applications and Perspectives*, Wiley-VCH Verlag GmbH & Co. KGaA **2004**.

2)  Niemeyer, C. M. *Angew. Chem. Int. Ed.* **2001**, *40*, 4128-4158.

3)  Rembaum, A.; Dreyer, W. J. *Science* **1980**, *208*, 364-368.

4)  (a) Hainfield, J. F. *Science* **1987**, *236*, 450-453. (b) Safer, D. E.; Hainfield, J.; Wall, J. S.; Reardon, J. E. *Science* **1982**, *218*, 290-291.

5)    (a) Storhoff, J. J.; Lazarides, A. A.; Mucic, R. C.; Mirkin, C. A.; Letsinger, R. L.; Schatz, G. C. *J. Am. Chem. Soc.* **2000**, *122*, 4640-4650. (b) Elghanian, R.; Storhoff, J. J.; Mucic, R. C.; Letsinger, R. L.; Mirkin, C. A. *Science* **1997**, *277*, 1078-1081.

6)    Sastry, M.; Lala, N.; Patil, V.; Chavan, S. P.; Chittiboyina, A. G. *Langmuir* **1998**, *14*, 4138-4142.

7)     Hirsch, L. R.; Jackson, J. B.; Lee, A.; Halas, N. J.; West, J. L. *Anal. Chem.* **2003**, *75*, 2377-2381.

8)    Hirsch, L. R.; Stafford, R. J.; Bankson, J. A.; Sershen, S. R.; Rivera, B.; Price, R. E.; Hazale, J. D.; Halas, N. J. *Proc. Natl. Acad. Sci. USA* **2003**, *100*, 13549-13554.

9)    Stonehuerner, J. G., Zhao, J., O'Daly, J. P., Crumbliss, A. L., and Henkens, R. W. *Biosens. Bioelectron.* **1992**, *7*, 421-428.

10)   Zhao, J., O'Daly, J. P., Henkens, R. W., Stonehuerner, J., and Crumbliss, A. L. *Biosens. Bioelectron.* **1996**, *11*, 493-502.

11)   Crumbliss, A. L., Perine, S. C., Stonehuerner, J., Tubergen, K. R., Zhao, J., O'Daly, J. P. *Biotechnol. Bioeng.* **1992**, *40*, 483-490.

12)   Gole, A.; Dash, C.; Ramakrishnan, V.; Sainkar, S. R.; Mandle, A. B.; Rao, M.; Sastry, M. *Langmuir* **2001**, *17*, 1674-1679.

13)   Gole, A.; Dash, C.; Soman, C.; Sainkar, S. R.; Rao, M.; Sastry, M. *Bioconjugate Chem.* **2001**, *12*, 684-690.

14)   Gole, A.; Vyas, S.; Phadtare, S.; Lachke, A.; Sastry, M. *Colloids and Surfaces B* **2002**, *25*, 129-138.

15)   (a) Phadtare, S.; Kumar, A.; Vinod, V. P.; Dash, C.; Palaskar, D. V.; Rao, M.; Shukla, P. G.; Sivaram, S.; Sastry, M. *Chem. Mater.* **2003**, *15*, 1944-1949. (b) Phadtare, S.; Vyas, S.; Palaskar, D. V.; Lachke, A.; Shukla, P. G.; Sivaram, S.; Sastry, M. *Biotechnol. Prog.* **2004**, DOI 10.1021/bp0499000.

16)   (a) Mukhopadhyay, K.; Phadtare, S.; Vinod, V. P.; Kumar, A.; Rao, M.; Chaudhari, R. V.; Sastry, M. *Langmuir* **2003**, *19*, 3858-3863. (b) Phadtare, S.; Vinod, V. P.; Muhkopadhyay, K.; Kumar, A.; Rao, M.; Chaudhari, R. V.; Sastry, M. *Biotechnol. Bioeng.* **2004**, *85*, 629-637.

17) Schmitt, A.; Fernandez-Barbero, A.; Cabrerizo-Vilchez, M.; Hidalgo-Alvarez, R. *Prog. Colloid Polym. Sci.* **1997**, *104*, 144-147.

18) Elgersma, A. V.; Zsom, R. L. J.; Norde, W.; Lyklema, J. *J. Colloid Interface Sci.* **1990**, *138*, 145-156.

19) (a) Ramanathan, S.; Shukla, P. G.; Sivaram, S. *Pure Appl. Chem.* **1998**, *70*, 1295-1299. (b) Shukla, P. G.; Sivaram, S. US patent 5859,075 CA **1999**, 129: 276913.

20) Patil, V.; Malvankar, R. B.; Sastry, M. *Langmuir* **1999**, *15*, 8197-8206.

21) El-Sayed, M. *Acc. Chem. Res.* **2001**, *34*, 257-264.

22) (a) Blatchford, C. G.; Campbell, J. R.; Creighton, J. A. *Surf. Sci.* **1982**, *120*, 435-455. (b) Galletto, P.; Brevet, P. F.; Girault, H. H.; Antoine, R.; Broyer, M. *J. Phys. Chem. B* **1999**, *103*, 8706-8710.

23) (a) Leff, D. V.; Brandt, L.; Heath, J. R. *Langmuir* **1996**, *12*, 4723-4730. (b) Brown, L. O.; Hutchison, J. E. *J. Am. Chem. Soc.* **1999**, *121*, 882-883. (c) Sastry, M.; Kumar, A.; Mukherjee, P. *Colloids and Surfaces A* **2001**, *181*, 255-259. (d) Kumar, A.; Mukherjee, P.; Guha, A.; Adyantaya, S. D.; Mandle, A. B.; Kumar, R.; Sastry, M. *Langmuir* **2000**, *16*, 9775-9783. (e) Selvakannan, PR.; Mandal, S.; Pasricha, R.; Adyanthaya, S. D.; Sastry, M. *Chem. Commun.* **2002**, 1334-1335. (f) Joshi, H.; Shirude, P. S.; Bansal, V.; Ganesh, K. N.; Sastry, M. *J. Phys. Chem. B* **2004**, *108*, 11535-11540.

24) (a) Stoscheck, C. M. *Meth. Enzymol.* **1990**, 182, 50-68. (b) Nick Pace, C.; Vajdos, F.; Fee, L.; Grimsley, G.; Gray, T. *Protein Science* **1995**, *4*, 2411-2423.

25) Caruso, F.; Furlong, D. N.; Ariga, K.; Ichinose, I.; Kunitake, T. *Langmuir* **1998**, *14*, 4559-4565.

26) Gole, A.; Dash, C.; Rao, M.; Sastry, M. *Chem. Commun.* **2000**, 297-298.

27) Gole, A.; Vyas, S.; Sainkar, S. R.; Lachke, A.; Sastry, M *Langmuir* **2001**, *17*, 5964-5970.

28) Li, J.; Wang, J.; Gavalas, V. G.; Atwood, D. A.; Bachas, L. G. *Nano. Lett.* 2003, *38*, 55-59.

29) van Blaaderen, A.; Vrji, A. *J. Colloids Interface Science* **1993**, *156*, 1-18.

30) Yiu, H. H. P.; Wright, P. A.; Botting, N. P. *J. Mol. Cata. B: Enzymatic* **2001**, *15*, 81-92.

31) Lei, C.; Shin, Y.; Liu, J.; Ackerman, E. J. *J. Am. Chem. Soc.* **2002**, *124*, 11242-11243.

32) Mitchell, D. T.; Lee, S. B.; Trofin, L.; Li, N.; Nevanen, T. K.; Soderlund, H.; Martin, C. R. *J. Am. Chem. Soc.* **2002**, *124*, 11864-11865.

33) Westcott, S. L.; Oldenburg, S, J.; Lee, T. R.; Halas, N. J. *Chem. Phys. Lett.* **1999**, *300*, 651-655.

34) Chen, M. M. Y.; Katz, A. *Langmuir* **2002**, *18*, 8566-8572.

35) Prouzet, E.; Pinnavaia, T. J. *Angew. Chem. Int. Ed.* **1997**, *36*, 516-518.

36) Bardosova, M.; Tredgold, R. H.; Ali-Adib, Z. *Langmuir* **1995**, *11*, 1273-1276.

37) Kaleta, W.; Nowinska, K. *Chem. Commun.* **2001**, 535-536.

38)  (a) Arica, M. Y.; Hasirici, V.; Alaeddinoglu, N. G. *Biomaterials* **1995**, *16*, 761-768. (b) Akgol, S.; Yalcinkaya, Y.; Bayramoglu, G.; Denizil, A.; Arica, M. Y. *Process Biochem.* **2002**, *38*, 675-683. (c) Takahashi, H.; Li, B.; Sasaki, T.; Miyazaki, C.; Kajino, T.; Inagaki, S. *Chem. Mater.* **2000**, *12*, 3301-3308.

# Chapter V

# Free-standing gold nanoparticle polymeric membrane: Scaffolds for enzyme and whole cell immobilization

Gold nanoparticles embedded in a polymeric membrane provide a biocompatible surface for the immobilization of enzymes. The presence of gold nanoparticles in the membrane enables facile modification of the surface properties of the membrane and this has been used to bind enzymes to the membrane leading to the formation of a new biocatalyst. The new biocatalyst is easily separated from the reaction medium, exhibits excellent reuse characteristics over ten successive cycles as well as temporal, pH and temperature stability. The gold nanoparticle polymeric membrane is easily functionalized by amino acids, alkanethiols, alkylamines etc. The Octadecylamine bound to gold nanoparticle polymeric membrane renders hydrophobicity and thereafter may be used for the immobilization of whole cells. Immobilized *Candida bombicola* cells were used to catalyze the biotransformation of arachidonic acid to sophorolipids and thereafter, acid hydrolysis to 20-hydroxyecosatetraenoic acid (20-HETE). The whole cells bound to gold nanoparticle polymeric membranes are easily separated from the reaction mixture and exhibit excellent reusability.

## 5.1 Introduction

Nanomaterials in the form of membranes are used as scaffolds for the binding of various biomolecules [1]. These functionalized membranes have potential applications in separation of compounds, selective catalysis, artificial organs, etc. [2]. New methods have been developed for the synthesis of various nanomaterials, which includes membrane-based synthesis [3]. This method involves the synthesis of desired materials within the pores of a nanoporous membrane. Since the membrane contains cylindrical pores of uniform diameter, monodisperse nanocylinders of the desired material whose dimensions can be carefully controlled are obtained. The pores of polypropylene hollow fiber microfiltration membrane (PPHFMM) are modified by two polypeptides with short and long hydrophobic side chains. Thereafter, enzymes were immobilized on these membranes by adsorption [4a]. Butterfeild *et al.* have shown the site-specific immobilization of enzymes subtilisin and organophosphorous hydrolase (OPH) that orients the active site away form the polymeric membrane surface resulting in a higher enzyme activity and stability when compared with the free enzyme in solution [4b].

The response of different types of cells on materials is important for applications in tissue engineering and regenerative medicine. Materials and fabrication technologies are critically important for tissue engineering in designing temporary, artificial extracellular matrices (scaffolds), which support three dimensional tissue formation. Tissue engineering has been defined as an interdisciplinary field that applies the principles of engineering and life sciences towards the development of biological substitutes that restore, maintain or improve tissue functions [5]. Tissue engineering involves the creation of multicellular tissues from individual cells.  It is recognized that the behavior of the adhesion, proliferation and differentiation on materials depends largely on surface characteristics such as wetability, chemistry, charge, rigidity and roughness. In many cases, cells are sensitive to surface topography and a wide variety of cell properties can be affected [6a]. The surface properties of biodegradable polymer on the interactions of the cells are one of the most important parameters when tissue engineered scaffolds are designed [6b]. Scaffolds play a crucial role in guiding cells to

grow, synthesize extracellular matrix and other biological molecules, and facilitate the formation of functional tissues and organs [7a]. Chemically functionalized surfaces prepared by self-assembly of alkanethiolate monolayers on gold surfaces were used for the growth of bovine aortic endothelial cells (BAEC) [7b]. Moreover, multiple chemical functionalities are also desirable for the growth of cells. The gold nanoparticle polymeric membranes discussed in this chapter are easily functionalized by one of more functional groups [8] and have potential applications for the growth of cells.

In a previous chapter, we had discussed the assembly of gold nanoparticles on polymer and zeolite microspheres and thereafter the use of gold nanoparticles for enzyme immobilization. In this chapter, we will discuss the synthesis of a free-standing gold nanoparticle embedded polymeric membrane at the interface between chloroform containing bis(2-(4-aminophenoxy)ethyl)ether (DAEE) and aqueous chloroauric acid solution and thereafter the use of the gold nanoparticle polymeric membrane in the immobilization of the enzyme pepsin [9]. The gold nanoparticles in the polymeric membrane are functionalized by octadecylamine (ODA) and thereafter the hydrophobic membrane is used for the immobilization of whole cells [10].

## 5.2 Preparation of gold nanoparticle embedded polymeric membrane

In this laboratory free-standing gold nanoparticle polymeric membrane was prepared at the liquid-liquid interface by a procedure given by Sastry and co-workers [11]. According to this procedure, 100 mL of $10^{-2}$ M concentrated aqueous solution of chloroauric acid (HAuCl$_4$) was mixed with 100 mL of $10^{-2}$ M bis(2-(4-aminophenoxy)ethyl)ether (DAEE) in chloroform for 4 h. A purple colored membrane was observed to form at the interface in the biphasic mixture within 1 h of reaction (Fig.5.1). This membrane was separated and repeatedly washed with chloroform and deionized water prior to enzyme immobilization.

### 5.2.1 UV-visible spectroscopy

Fig.5.2A shows the UV-vis spectrum of gold nanoparticle polymeric membrane transferred onto a quartz substrate. A strong absorption band centered at 540 nm is

observed. This absorption band arises due to excitation of surface plasmons in gold nanoparticles and is responsible for their vivid pink-purple color [12].
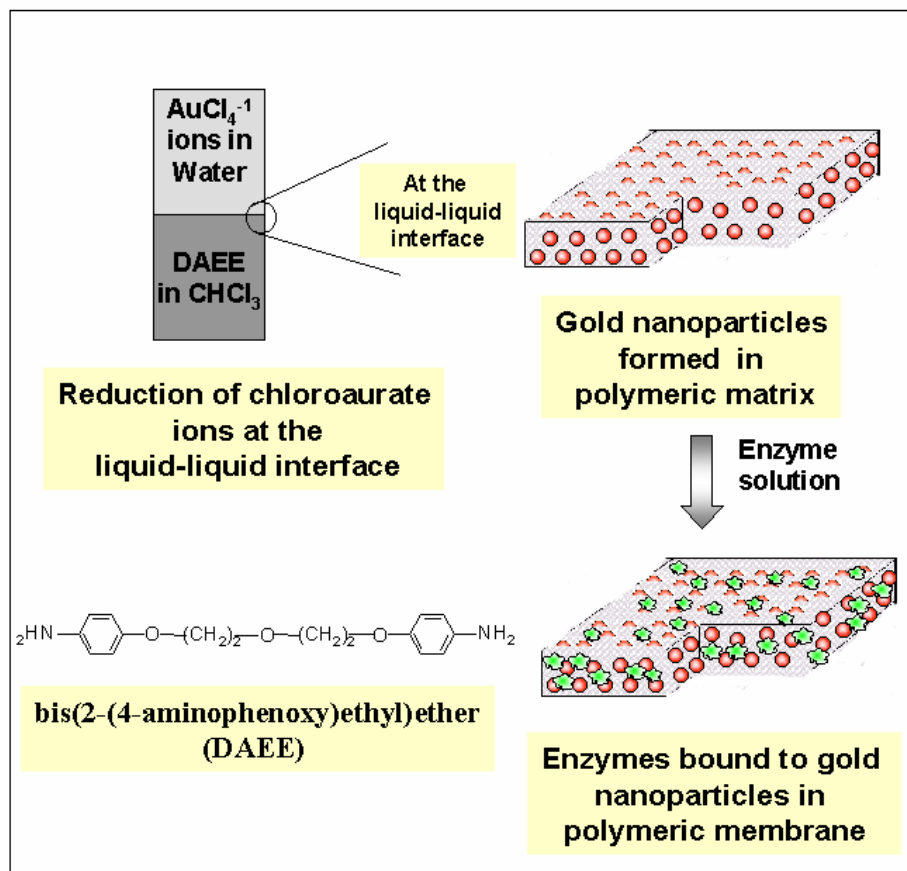


**Figure 5.1:** Schematic (not to scale) showing the synthesis of gold nanoparticle polymeric membrane at the liquid-liquid interface and thereafter their use for enzyme immobilization.

The amine groups of DAEE molecules at the interface are protonated (pH of HAuCl$_4$ solution ~ 3.2) leading to electrostatic complexation with AuCl$_4^-$ ions. The electrostatic complexation with gold ions is a crucial step in the formation of the gold nanoparticle polymeric membrane. This was confirmed by a control experiment where a similar interfacial reaction was carried out with the aqueous HAuCl$_4$ solution maintained at pH 9. At this pH, the amine groups in DAEE would not be protonated and no membrane formation was observed even after 12 h of reaction at the liquid-liquid interface. Reduction of chloroaurate ions takes place at the interface and the

oxidized DAEE molecules cap the spontaneously formed gold nanoparticles preventing their further aggregation. The inset of Fig.5.2A shows the UV-visible spectra recorded from the AuCl$_4$ ions in the aqueous solution during the formation of gold nanoparticle polymeric membrane at the liquid-liquid interface for different times of reaction (t = 0, 15, 45, 60, 120, 180 and 240 min). The peak position at 214 nm corresponds to light absorption by aqueous AuCl$_4$ ions [13]. It is observed that there is a steady decrease in the peak intensity at 214 nm with time indicating that the chloroaurate ions are consumed in the formation of gold nanoparticles at the liquid-liquid interface.
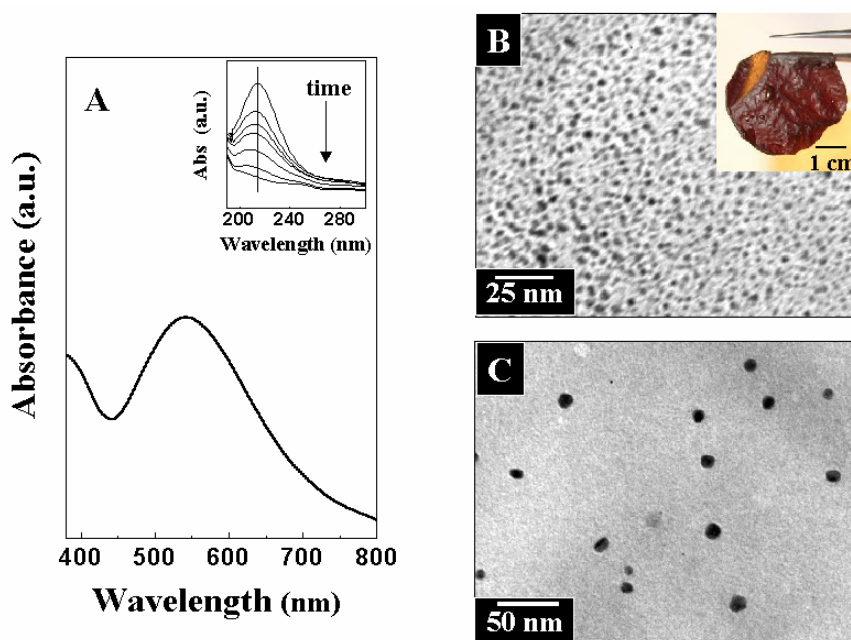


**Figure 5.2:** (A) UV-vis spectrum recorded from the gold nanoparticle polymeric membrane on a quartz substrate. Inset shows the UV-vis spectra recorded from the aqueous solution of chloroaurate ions during the formation of gold nanoparticle polymeric membrane at the liquid-liquid interface at different time of reaction. The curves correspond to t = 0, 15, 45, 60, 120, 180 and 240 min the arrow of time indicated in the figure. (B) TEM micrographs of as-prepared gold nanoparticle polymeric membrane and after (C) leaching of gold nanoparticles from polymeric membrane. Inset of (B) shows photograph of the air-dried, free-standing gold nanoparticle polymeric membrane.

These membranes could be synthesized in a wide range of sizes and thickness by simple variation in the reaction time and DAEE: AuCl$_4$ molar ratio [11]. The gold

nanoparticle polymeric membrane used in this study had a thickness of ca. 0.5 mm after drying. The gold nanoparticle polymeric membrane is not easily dissolved in most of the organic solvents such as toluene, chloroform etc. and does not swell significantly when immersed in either non-polar organic solvents or water. The gold nanoparticle polymeric membranes are extremely stable towards microbial degradation and hence, provide an excellent biocompatible surface for the immobilization of enzymes.

*5.2.2 Estimation of gold nanoparticles in the polymeric membrane*

An estimation of the gold nanoparticle fraction in the polymeric membrane was done by leaching out the gold nanoparticles from the membrane using a saturated $I_2$ solution in KI for 12 h under mild stirring conditions. The dissolved gold solution was analyzed by atomic absorption spectroscopy (AAS) in the following manner. 10 mg of the gold nanoparticle polymeric membrane was dissolved in 20 mL of saturated $I_2$ solution in KI and the volume was made up to 100 mL using deionized water. The solution was analyzed by a Varian Spectra AA 220 atomic absorption spectrometer (AAS) and was compared with a gold standard to estimate the weight percent of gold nanoparticles in the membrane. The mass loading of the gold nanoparticles in the gold nanoparticle polymeric membrane was estimated from AAS analysis to be ca. 35% by weight.

*5.2.3 Transmission electron microscopy (TEM)*

Fig5.2B shows TEM micrographs of the membrane. It can be clearly seen that the gold nanoparticles (dark features) are uniformly dispersed in the polymeric membrane with little evidence for aggregation of the gold particles. The gold nanoparticles are fairly spherical and range in size from 4 to 10 nm. As mentioned previously, the chloroaurate ions form electrostatic complexes with the protonated amine groups of DAEE molecules and then are reduced. After reducing the chloroaurate ions, the oxidized DAEE molecules form a polymer and cap the spontaneously formed gold nanoparticles preventing their further aggregation. This occurs in a highly localized manner at the liquid-liquid interface leading to membrane formation at the interface. DAEE molecules possess two terminal aniline segments, which are known to be good reducing agents (Fig.5.1). Oxidation of DAEE most

probably proceeds through formation of a polymeric network derived from DAEE at the liquid-liquid interface. The gold atoms formed by the reduction of $AuCl_4^-$ ions diffuse along the polymeric network, aggregate into larger gold nanoparticles as seen in the Fig.5.2B thereby yielding a polymeric network with inclusions of gold nanoparticles at the liquid-liquid interface (see Fig.5.1 for the structure of the gold nanoparticle polymeric membrane).

Fig.5.2C shows a TEM micrograph of a gold nanoparticle polymeric membrane after leaching out the gold nanoparticles by iodine treatment as described in Section 5.2.2. The dark spots seen in Figs.5.2B corresponding to the gold nanoparticles are not seen in the bare polymeric membrane. The infrequent dark regions in Fig.5.2C correspond to entrapped iodine as a consequence of immersion in KI solution for gold nanoparticle removal. This was confirmed from electron diffraction measurements of the dark spots.
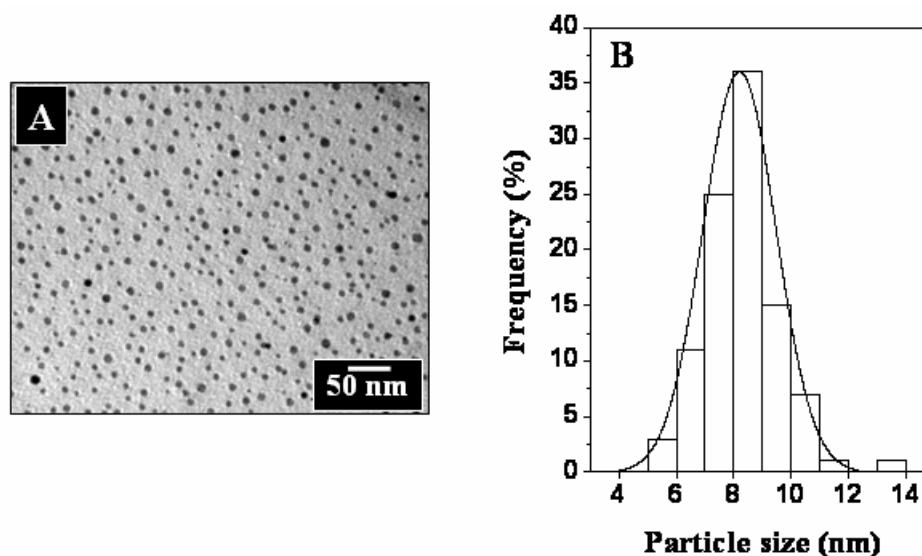


**Figure 5.3:** (A) TEM micrograph of gold nanoparticles leached from the polymeric membrane. (B) Particle size distribution of the gold nanoparticles leached from the polymeric membrane.

Gold nanoparticles in the polymeric membrane were leached by dissolving the polymeric membrane in dilute hydrochloric acid for 30 min to form water soluble polyaniline hydrochloride. Fig.5.3A shows the TEM micrograph of gold nanoparticles

separated from the polymeric membrane. The particle size distribution histogram for the accompanying TEM micrograph is shown in Fig.5.3B. The mean size of the particles was measured to be 8.2 nm with a standard deviation of 1.3 nm.

*5.2.4 X-ray diffraction (XRD) and Energy dispersive analysis of X-rays (EDAX)*

Fig.5.4 shows the powder XRD pattern of the gold nanoparticle polymeric membrane. The sharp Bragg reflections seen in the figure underline the fact that the gold particles present in the membrane are crystalline. The Bragg reflections in the gold nanoparticle polymeric membrane could be indexed on the basis of the fcc structure of gold and are identified in Fig.5.4 [14]. It is interesting to note that the ratios of the (311) reflection with other reflections is greater that that observed in powder diffractions patterns for gold [14] indicating that there is preferred growth of the gold nanocrystals along the (311) direction within the membrane.
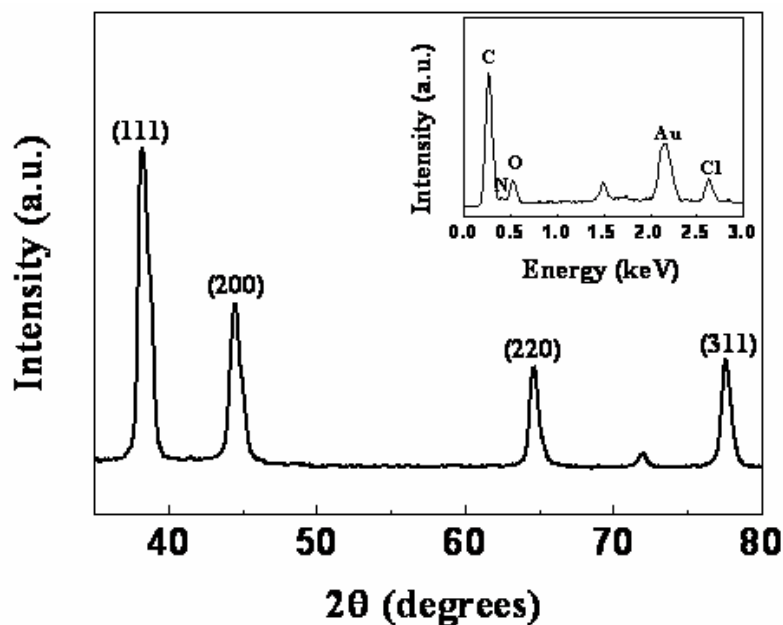


**Figure 5.4:** XRD pattern recorded from gold nanoparticle polymeric membrane. Inset shows the spot profile EDAX recorded form the gold nanoparticle polymeric membrane.

The inset of Fig.5.4 shows the EDAX spectrum recorded from one of the gold nanoparticles bound to the polymeric membrane. In addition to the expected prominent

Au signal, a weak chlorine signal is also observed which is attributed to the presence of unreduced gold ions (AuCl$_4^-$) bound to the surface of the gold nanoparticles in membrane. As mentioned earlier, the first step in the formation of the gold nanoparticle polymeric membrane is electrostatic complexation of AuCl$_4^-$ ions with protonated amine groups of DAEE molecules at the liquid-liquid interface and incomplete reduction of the chloroaurate ions would explain their presence in the membrane.

## 5.3 Preparation of Pepsin-gold nanoparticle polymeric membrane bioconjugate

10 mg of the gold nanoparticle polymeric membrane was placed in 4.5 mL KCl-HCl buffer (0.02 M, pH 2). To this solution, 500 μl of a stock solution consisting of 5 mg/mL of pepsin in KCl-HCl buffer (0.02 M, pH 2) was added under mild stirring conditions. After 1 h of stirring (Fig.5.1), the free-standing gold nanoparticle polymeric membrane was separated. The bioconjugate obtained was rinsed several times with KCl-HCl buffer (0.02 M, pH 2) solution, re-suspended in buffer (pH 2) solution, and stored at 4 °C prior to further experiments.

### 5.3.1 Enzyme quantitative analysis in the gold nanoparticle polymeric membrane

Enzyme quantitative analysis in the bioconjugates was done by UV-vis spectroscopy. The loss in absorbance at 280 nm in the supernatant (arising from π-π* transitions in tryptophan and tyrosine residues in proteins) [15] was used to quantify the amount of pepsin bound to the gold nanoparticle polymeric membrane for biocatalytic activity (in IU/μg) determination.

### 5.3.1 (A) Determination of equilibrium time for the complete binding of enzyme to gold nanoparticle polymeric membrane

UV-vis spectroscopy measurements were carried out to determine the equilibration time for complete binding of the enzyme to the gold nanoparticle polymeric membrane and the polymeric membrane after leaching out of the gold nanoparticles. 10 mg of the two membranes were immersed in the 5 mL KCl-HCl buffer (0.02 M, pH 2) solution containing enzyme of concentration 0.5 mg/mL. 1 mL of the supernatant was analyzed by UV-vis absorption spectroscopy for different time of immersion of the membrane in the enzyme solution. After each measurement, the

analyte was added back to the original enzyme solution to simulate the reaction conditions precisely.
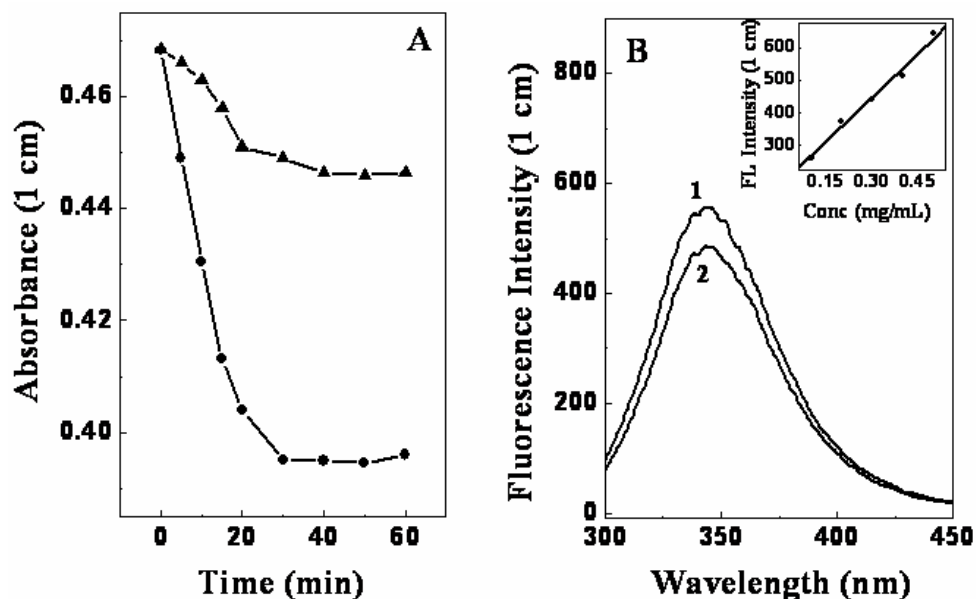


**Figure 5.5:** (A) Absorbance at 280 nm of the supernatant of the pepsin solution after immersion of the gold nanoparticle polymeric membrane (circles) and bare polymeric membrane (triangles) for different time. (B) Fluorescence spectra of initial pepsin in KCl-HCl buffer (0.5 mg/mL) at pH 2 (curve 1) and supernatant after separation of pepsin-gold nanoparticle polymeric membrane (curve 2). The inset shows the fluorescence intensity at different concentrations of pepsin in solution at pH 2.

Fig.5.5A shows that there is an initial rapid binding of the enzyme with 70 % of the total enzyme immobilized on gold nanoparticle polymeric membrane (circles) whereas only 48 % of the total enzyme is immobilized on the bare polymeric membrane (triangles) within the first 15 min of immersion. Hence, it is clear that the gold nanoparticles in the membrane play an important role in binding of the enzyme to the polymeric membrane. It is seen that the equilibrium time required for saturation of the enzyme on the gold nanoparticle polymeric membrane surface is 35 min. In all further experiments, the gold nanoparticle polymeric membranes were immersed in enzyme solution for 1 h to ensure complete binding of the enzyme to the support. From UV-vis spectroscopy measurements, the amount of pepsin bound to 10 mg of the gold nanoparticle polymeric membrane was found to be 0.26 mg, the immobilization of the enzyme on the gold nanoparticles occurring via amine groups and cysteine residues in

the proteins which are known to bind strongly with gold colloids [16]. It is possible that pepsin binds directly to the polymeric backbone. This contribution was estimated by first leaching out the gold fraction of the gold nanoparticle membrane by iodine treatment and then immersing the polymer membrane in pepsin under conditions identical to that employed for the as-prepared gold nanoparticle polymeric membrane. From UV-vis spectroscopy analysis, it was determined that 10 mg of the bare polymeric membrane bound ca. 0.08 mg of pepsin, possibly through non-specific electrostatic and hydrogen bonding interactions.

*5.3.1 (B) Fluorescence spectroscopy*

The presence of small amount of the gold nanoparticles in the supernatant could lead to an error in enzyme loading determination from UV-vis spectroscopy measurements. In order to overcome this problem, fluorescence spectroscopy was also used to quantify the amount of enzyme in the pepsin-gold nanoparticle polymeric membrane material. Fluorescence measurements were carried out on the initial concentration of the pepsin in solution at pH 2 and supernatant of pepsin in solution after separation of pepsin-gold nanoparticle polymeric membrane. The enzyme solutions were excited at 280 nm and the emission band was monitored in the range 300 to 500 nm. The loss in fluorescence intensity (arising from $\pi$-$\pi^*$ transitions in tryptophan and tyrosine residues in proteins) was used to quantify the amount of pepsin bound to the gold nanoparticle polymeric membrane [17]. From the calibration curve of the fluorescence intensity for different concentrations of the pepsin in solution, the amount of the enzyme in the bioconjugate was known and used in determination of the specific activity of the pepsin-gold nanoparticle polymeric membrane biocatalyst. Fig.5.5B shows the fluorescence emission spectra of the as-prepared pepsin solution (0.5 mg/mL) at pH 2 (curve 1) and the supernatant after separation of the gold nanoparticle polymeric membrane bioconjugate material (curve 2). The concentration of enzyme in the bioconjugate was determined from the calibration curve (fluorescence intensity of different concentrations of pepsin in solution at pH 2) shown in the inset of Fig.5.5B. From the decrease in intensity of the fluorescence emission band of the enzyme in the supernatant, the amount of enzyme bound to 10 mg of the nanogold

membrane was found to be 0.3 mg, which is in reasonable agreement with the UV-vis spectroscopic estimate. From fluorescence spectroscopy measurements, direct binding of pepsin to the bare polymeric membrane was estimated to be 0.1 mg, again in agreement with UV-vis spectroscopic estimates.

## 5.4 Biocatalytic activity measurements

The biocatalytic activity of free pepsin in solution and of pepsin-gold nanoparticle polymeric biocatalyst in KCl-HCl buffer (pH 2) was determined by reaction with 0.6 % casein at 37 $^{o}$C for 60 min as described in earlier chapter Section 4.4. Since the amount of pepsin bound to the bioconjugate could be estimated quite accurately from independent UV-vis and fluorescence spectroscopy measurements, it is possible to compare the specific biocatalytic activity of the enzyme in the bioconjugate material and similar amount of free enzyme in solution under identical assay conditions. The biocatalytic activity of the free pepsin in solution was determined to be 13.6 IU/µg (Units per microgram) and that of the enzyme in the gold nanoparticle polymeric membrane was 13.5 IU/µg. An analysis of the biocatalytic activity of the pepsin-gold nanoparticle polymeric membrane bioconjugate material in five separate reactions yielded a standard deviation of ca.10 % and therefore, the biocatalytic activity of the enzyme immobilized on the gold nanoparticle polymeric membrane bioconjugate material relative to free enzyme in solution is expected to be experimentally significant.

### *5.4.1 Reusability of the bioconjugate*

In order to understand the role of the gold nanoparticles in the binding pepsin, the enzyme was also bound directly to the polymeric membrane after leaching out of the gold nanoparticles. A small percentage of pepsin was bound to the polymeric component of the gold nanoparticle polymeric membrane through non-specific interactions and it would be important to understand the contribution of this non-specifically bound pepsin component to the overall biocatalytic behavior of the bioconjugate material. Three separate measurements were performed to check the reproducibility of the data. Fig.5.6 shows the results of 10 successive cycles of reuse of the pepsin-gold nanoparticle polymeric membrane (squares) and pepsin-polymeric membrane (triangles). In the first reaction, the biocatalytic activity in the pepsin-

polymeric material is 9.8 IU/µg, ca. 72 % of that observed in the pepsin-gold nanoparticle polymeric membrane. Thereafter, the biocatalytic activity of the pepsin-polymeric material falls off rapidly losing complete activity by the 6th cycle of reaction. On the other hand, the pepsin-gold nanoparticle polymeric membrane system shows ca. 79 % of biocatalytic activity after the 3rd reuse cycle and retains 57 % of the initial biocatalytic activity after the 8th cycle of reaction. These results clearly underline the remarkable reuse characteristics of the pepsin-gold nanoparticle polymeric membrane bioconjugate material and represent a major advance in our studies on development of gold nanoparticle based enzyme immobilization protocols.
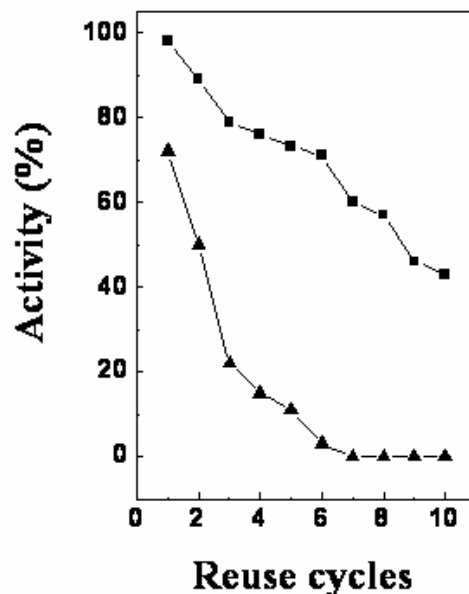


**Figure 5.6:** Biocatalytic activity of pepsin bound to gold nanoparticle polymeric membrane (squares) and pepsin bound to the bare polymeric membrane (triangles) over 10 successive reuse cycles. The solid lines are aids to the eye and have no physical significance.

This excellent retention of biocatalytic activity of pepsin-gold nanoparticle polymeric membrane bioconjugate during reuse is to be contrasted with the almost complete loss in activity of the same enzyme immobilized in our earlier work in thermally evaporated fatty amine films after just 3 cycles of reuse [18]. Clearly the

blockage of diffusion pathways of substrate molecules implicated in the earlier study for loss in activity with recycling is not operative in the bioconjugation strategy presented in this work. This is a salient feature of the work with immense commercial implications. However, the monotonic and perceptible loss in biocatalytic activity of the pepsin-gold nanoparticle polymeric membrane biocatalyst with reuse needs elaboration. It is possible that the gold nanoparticles detach from membrane during successive reaction cycles. Another possibility is the leaching out of pepsin from the bioconjugate material in successive reactions due to weak binding with the underlying gold nanoparticle polymeric membrane.

In order to distinguish between the two mechanisms, atomic absorption spectroscopy (AAS) measurements were performed on the supernatant obtained after centrifugation of the reaction medium during each of the reaction cycles. Gold could not be detected by AAS [detection sensitivity ~ parts per million (ppm)] in any of the reaction cycles clearly showing that the nanoparticles are strongly bound to the underlying polymeric membrane. This results points to loss of enzyme from the gold nanoparticle polymeric membrane surface during reaction. UV-vis spectroscopy measurements were carried out on the supernatant from 10 mg of the pepsin-nanogold membrane bioconjugate material immersed in 5 mL of KCl-HCl buffer (pH 2). 1 mL of the supernatant was analyzed in intervals of 1 h, which is characteristic of the reaction times in the reuse measurements. After each measurement, the analyte was added back to the original solution to simulate the reaction conditions precisely. It was observed that after 5 h of immersion, roughly 30 % of the total pepsin bound to the gold nanoparticle polymeric membrane was released into solution (estimated from the absorbance at 280 nm). This percentage loss of enzyme correlates well with degree of loss of biocatalytic activity during the first five-reuse cycle (Fig.5.6, squares). We believe the initial loss of pepsin corresponds to loss of weakly bound enzyme from the bioconjugate, this being the weakly bound pepsin component bound non-specifically to the polymeric membrane and not the gold nanoparticles.

Furthermore, immobilized enzymes have a limited lifespan and thus, deactivation is not always avoidable. Since a significant amount of leaching of pepsin

was not observed after 5 h of immersion of pepsin-gold nanoparticle polymeric membrane in KCl-HCl buffer (pH 2), the decrease in activity of the immobilized biocatalyst is attributed to deactivation of the enzyme bound to the gold nanoparticle polymeric membrane. Such a decrease in activity is observed for the enzyme cholesterol oxidase covalently immobilized on the surface of polyacrylonitrile hollow fibres which retains ca. 41 % of the initial biocatalytic activity after 10 reuse cycles [19a]. The enzyme pummelo limonoid glucosyltransferase also showed a decrease in biocatalytic activity when covalently immobilized on different solid supports after significant reuse [19b].

In order to remove the weakly bound enzyme from the bioconjugate material, the pepsin-gold nanoparticle polymeric membrane was immersed in 5 mL 10 mM NaCl salt solution for 1 h and thereafter was tested for biocatalytic activity variation over 5 successive reuse cycles. Care was taken to wash the pepsin-gold nanoparticle polymeric membrane with copious amount of deionised water before each reuse. The pepsin-gold nanoparticle polymeric membrane showed 12.7 IU/μg for the first reuse and 10.1 IU/μg biocatalytic activity for the 3$^{rd}$ cycle of reaction. Moreover, the biocatalyst retains ca. 50 % of the initial biocatalytic activity during the 5$^{th}$ cycle of reaction. The small loss in biocatalytic activity in the first few cycles relative to the pepsin-gold nanoparticle polymeric bioconjugate with weakly bound pepsin clearly indicates that the weakly bound enzyme has been successfully leached out. A similar leaching of the enzyme was observed for the enzyme fungal protease bound through weak interactions to amine-functionalized zeolites [20]. However, the decrease in activity of the immobilized biocatalyst during the successive reuse cycles is attributed to deactivation of the enzyme bound to the gold nanoparticle polymeric membrane.

## 5.4.2 pH dependent biocatalytic activity

The pH dependent variation in the biocatalytic activity of the pepsin-gold nanoparticle polymeric membrane and free enzyme was studied at four different pH values (pH 2, KCl-HCl buffer; pH 4, 6, citrate acetate buffer and pH 8 KCl-NaOH buffer) by pre-incubating for 1 h at 28 $^o$C. All the reactions were carried out after pre-incubation for 1 h at the different pH and measuring the biocatalytic activity at pH 2, 37

°C as described in Section 4.4. Reproducibility of the data was tested in three separate measurements carried out under identical conditions.

## Table 1

pH profile of biocatalytic activity of free pepsin in solution and pepsin-gold nanoparticle polymeric membrane biocomposite using casein as the substrate at 37 °C.

| pH | Biocatalytic activity of free pepsin in solution (IU/µg) [#] | Biocatalytic activity of pepsin immobilized on gold nanoparticle polymeric membrane (IU/µg)[#] |
|---|---|---|
| 2 | 13.6 | 13.5 |
| 4 | 11.0 | 11.2 |
| 6 | 3.8 | 10.0 |
| 8 | 0 | 0.2 |

## Table 2

Temperature profile of biocatalytic activity of free pepsin in solution and pepsin-gold nanoparticle polymeric membrane biocomposite using casein as the substrate at pH 2.

| Temperature (°C) | Biocatalytic activity of free pepsin in solution (IU/µg) [#] | Biocatalytic activity of pepsin immobilized on gold nanoparticle polymeric membrane (IU/µg)[#] |
|---|---|---|
| 40 | 13.6 | 13.5 |
| 50 | 9.9 | 10 |
| 60 | 5.7 | 9.2 |
| 70 | 0 | 5.6 |

[#] One unit of enzyme will produce a change in absorbance at 280 nm of 0.001 per minute at pH 2 and 37 °C measured as acid soluble products using casein as the substrate.

Table 1 shows the biocatalytic activity of free pepsin in solution and pepsin bound to the gold nanoparticle polymeric membrane as a function of solution pH in the range 2 to 8. It is seen that optimum biocatalytic activity in both the cases is at pH 2, with a marginal loss in biocatalytic activity at pH 4. At pH 6, however the free enzyme in solution retain only 27 % of the biocatalytic activity recorded at pH 2, while the pepsin immobilized on the gold nanoparticle polymeric membrane retains as much as 73 % of the catalytic activity recorded at pH 2. Even at pH 8, pepsin in the bioconjugate material shows significant catalytic activity.

*5.4.3 Temperature dependent biocatalytic activity*

The temperature stability of the pepsin-gold nanoparticle polymeric biocatalyst was checked by pre-incubating the bioconjugate for 1 h at different temperatures in the range 40-70 °C and was compared with an identical amount of free enzyme in the KCl-HCl buffer (pH 2) under similar conditions. All the reactions were carried out after pre-incubation for 1 h at the different temperatures and measuring the biocatalytic activity at pH 2 and 37 °C as described in Section 4.4. Three separate measurements were done to check the reproducibility of the assay. Table 2 lists the variation in biocatalytic activity of free pepsin in solution and pepsin immobilized on the gold nanoparticle polymeric membrane as a function of temperature. At higher temperatures, dramatic differences in the biocatalytic activity of the enzyme in the two cases are observed. At 60 °C the enzyme in the pepsin-gold nanoparticle polymeric membrane shows 67 % of the initial biocatalytic activity, while the free enzyme in solution retains only 41 % biocatalytic activity. At 70 °C, the difference is much more marked with the pepsin-gold nanoparticle polymeric membrane retaining 40 % of initial biocatalytic activity while the free enzyme in solution is unstable. The increase in the thermal stability of the enzyme in the pepsin- gold nanoparticle polymeric bioconjugate material may arise from the conformational integrity of the enzyme structures after binding to the gold nanoparticles through the amine and cysteine residues present in the enzymes. The covalent linkage between the gold nanoparticles in the polymeric membrane and pepsin would therefore lead to reduced conformational freedom with respect to change in environmental parameters such as temperature and pH. Such enhancement in stability

of immobilized enzymes as a function of temperature and pH has been observed for pepsin bound to alumina nanoparticles [21] and for other enzymes immobilized on different supports [22].

*5.4.4 Time dependent stability of bioconjugate*

The temporal stability of the pepsin bound to gold nanoparticle polymeric membrane (10 mg in weight) was checked as a function of time of aging for seven days at 4 $^o$C in KCl-HCl buffer (0.02 M, pH 2) and was compared with an identical amount of free enzyme in solution maintained under similar conditions.

**Table 3**

Biocatalytic activity of free pepsin in solution and pepsin-gold nanoparticle polymeric membrane biocomposite as a function of aging at 4 $^o$C in KCl-HCl buffer (pH 2) using casein as the substrate.

| No. of days | Biocatalytic activity of pepsin in solution (IU/µg)[#] | Biocatalytic activity of pepsin immobilized on gold nanoparticle polymeric membrane (IU/µg)[#] |
|---|---|---|
| 1 | 13.7 | 13.7 |
| 3 | 5.5 | 13.0 |
| 5 | 3.0 | 12.5 |
| 7 | 0 | 12.4 |

[#] One unit of enzyme will produce a change in absorbance at 280 nm of 0.001 per minute at pH 2 and 37 $^o$C measured as acid soluble products using casein as the substrate.

Table 3 shows the biocatalytic activity of the free enzyme in solution and pepsin-gold nanoparticle polymeric membrane as a function of time of aging at 4 $^o$C. It is observed that there is no loss in the biocatalytic activity of the pepsin-gold nanoparticle polymeric membranes even after three days of storage and only a marginal decrease in activity is seen after seven days. On the other hand, the free enzyme in

solution shows a steady loss in biocatalytic activity. After three days 60 % of the initial biocatalytic activity of free enzyme in solution was lost and only 20 % of the initial biocatalytic activity is retained after five days of storage. Improved stability of the enzyme pepsin was also observed when covalently attached to porous zirconia [23]. It is clear that the gold nanoparticle polymeric membrane provides an excellent support for enzymes that enhances biocatalyst stability against microbial degradation and thus, provides a highly biocompatible environment for the immobilized enzymes.

## 5.5 Preparation of ocatadecylamine (ODA) bound gold nanoparticle polymeric membrane
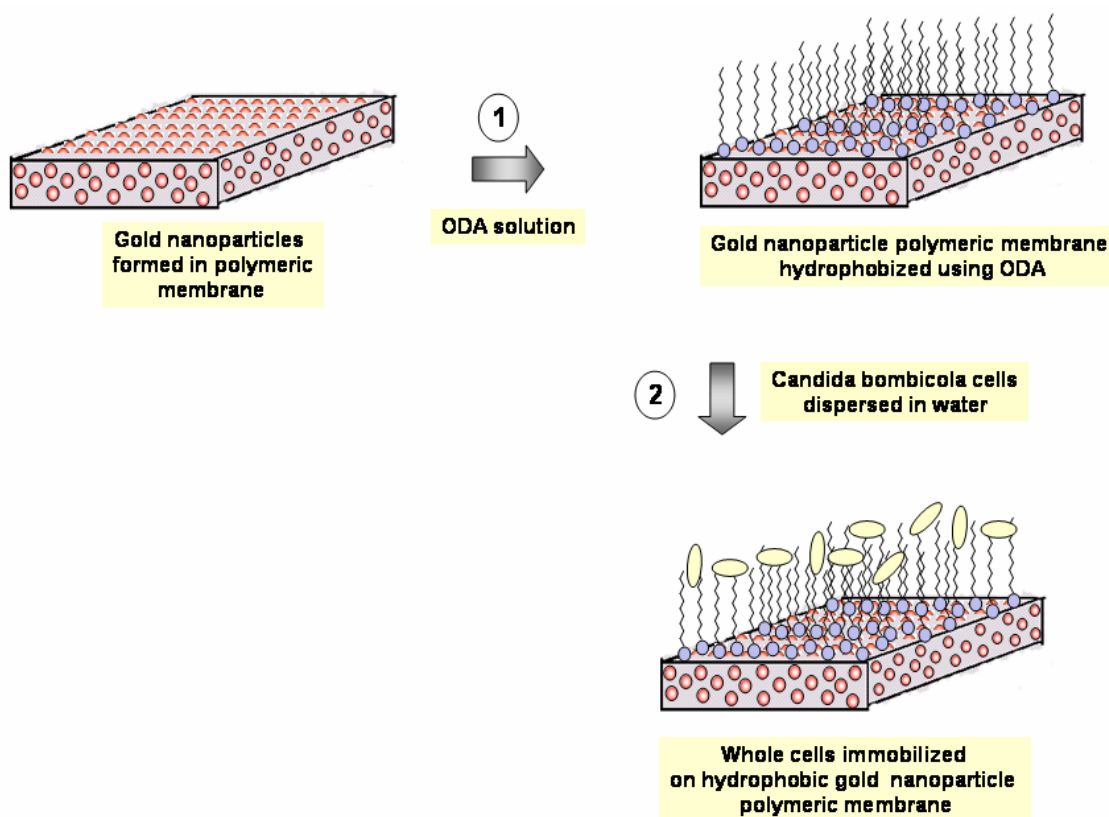


**Figure 5.7**: Schematic (not to scale) showing the immobilization of *Candida bombicola* whole cells on ODA bound gold nanoparticle polymeric membrane.

In this laboratory, we have been interested in assembly of specific cells on surfaces from the point of view of using the cells as sources of enzymes for

biotransformations and synthesis of new materials. We have shown that *Yarrowia lipolitica* [24] yeast cells can be immobilized on patterned hydrophobic regions of thermally evaporated fatty lipid films. These yeast cells are known to bind the hydrocarbon chains of the lipids through the hydrophobic interactions between the cells walls of the yeasts and lipids. As part of our search for newer and more versatile materials with tailorable surfaces for cell immobilization, we describe herein the synthesis of a free-standing gold nanoparticle polymeric membrane whose surface may readily be modified to render it compatible for a variety of applications. The surface chemical properties of the gold nanoparticles embedded in the polymeric membrane are easily modified using different molecules such as amino acids [8] alkanethiols, alkylamines, etc [10].

10 mg of the gold nanoparticle polymeric membrane of 0.5 mm thickness was immersed in $10^{-2}$ M ODA solution prepared in ethyl alcohol for 12 h leads to the complexation of ODA molecules with gold nanoparticles [25]. To remove the uncoordinated ODA molecules the gold nanoparticle polymeric membrane was washed with copious amount of ethyl alcohol and thereafter with chloroform and dried in air prior to further use.

## 5.5.1 Fourier transform infrared spectroscopy (FTIR)

Fig.5.8 shows the FTIR spectra recorded from the gold nanoparticle polymeric membrane before (curve 1) and after (curve 2) binding with ODA molecules by immersion of the membrane in an ethanol solution of $10^{-2}$ M ODA for 12 h. The uncoordinated ODA molecules in the gold nanoparticle polymeric membrane were washed with copious amount of ethyl alcohol and thereafter with chloroform. ODA readily dissolves in ethyl alcohol and chloroform, however ODA molecules bound strongly to the gold nanoparticles through amine groups and are not removed by washing with the solvents such as ethyl alcohol and chloroform. Two prominent features labeled *a* (2850 cm$^{-1}$) and *b* (2920 cm$^{-1}$) are due to the methylene antisymmetric and symmetric vibrations from the hydrocarbon chains of octadecylamine molecules bound to the gold nanoparticle polymeric membrane (curve 2).
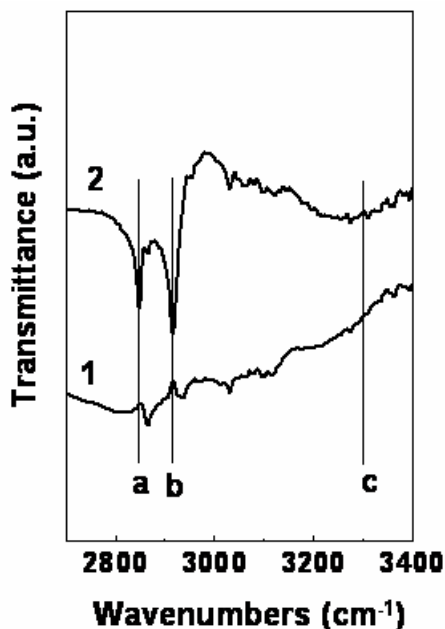
**Figure 5.8**: FTIR spectra recorded from the gold nanoparticle polymeric membrane before (curve 1) and after (curve 2) binding with ODA.

These bands are clearly missing in the as-prepared gold nanoparticle polymeric membrane (curve 1). The frequency of these resonances indicates that the ODA molecules on the gold particle surface are in a closed-packed state. The absence of an N-H stretch vibration band at ca. 3300 cm$^{-1}$ in the ODA-functionalized gold nanoparticle polymeric membrane (curve 2, feature c) indicates that ODA binds to the gold nanoparticles through the amine groups [25].

**5.6 Immobilization of *Candida bombicola* cells on octadecylamine (ODA) bound gold nanoparticle polymeric membrane**

*5.6.1 Growth of Candida bombicola cells*

*Candida bombicola* cells ATCC 22214 were pre-cultivated in 50 mL medium at 30 $^{o}$C consisting of (g l$^{-1}$): glucose, 100; yeast extract, 1; $(NH_4)_2SO_4$, 1; $MgSO_4 \cdot 7H_2O$, 0.3; $Na_2HPO_4$, 2; $NaH_2PO_4$, 7; pH 5.5 and shaken at 160 rpm [26,27]. Cells from the late growth phase (24 h) were inoculated into 1 lit. flasks containing 400 mL culture medium.

*5.6.2 Immobilization of Candida bombicola cells on ODA bound gold nanoparticle polymeric membrane*

20 mg each of hydrophobic gold nanoparticle polymeric membrane (ODA bound) were immersed in an aqueous dispersion of the cells (~ $10^8$ cells/mL) for 4 h (the optimum time of immersion was estimated from our earlier experiments) [28]. The amount of cells immobilized on the hydrophobic gold nanoparticle polymeric membrane was estimated from the initial and the final cell count after immobilization. To determine the confidence limits of this experiment, separate measurements were done for 3 different hydrophobic gold nanoparticle polymeric membranes. The amount of cells immobilized on 20 mg of hydrophobic gold nanoparticle polymeric membrane was estimated from the initial (~ $10^8$ cells/mL) and the final cell counts after immobilization to be approximately 0.3 mg. The cells immobilized on surface of hydrophobic gold nanoparticle polymeric membrane were washed 3 times by copious amount of deionized water prior to reuse. In addition to the as-prepared gold nanoparticle polymeric membrane, the yeast cells were also immobilized onto the polymeric membrane from which the gold nanoparticles were leached out by iodine treatment.

*5.6.3 Scanning electron microscopy (SEM)*

The immobilization of the *Candida bombicola* cells on as-prepared and hydrophobized gold nanoparticle polymeric membranes was studied by scanning electron microscopy (SEM). Fig.5.9 A and B shows representative low and high magnification SEM images of the gold nanoparticle polymeric membrane transferred from the liquid-liquid interface onto Si(111) substrates. It is seen that surface of the gold nanoparticle polymeric membranes is not smooth on a micron length scale. A highly uniform mesh-like structure is seen in the gold nanoparticle polymeric membrane. The hydophobized gold nanoparticle polymeric membrane was immersed in an aqueous suspension of *Candida bombicola* cells for 4 h and washed thoroughly prior to imaging by SEM. Fig.5.9C and D show SEM images recorded after immobilization of the *Candida bombicola* cells onto the hydrophobic gold nanoparticle polymeric membrane.
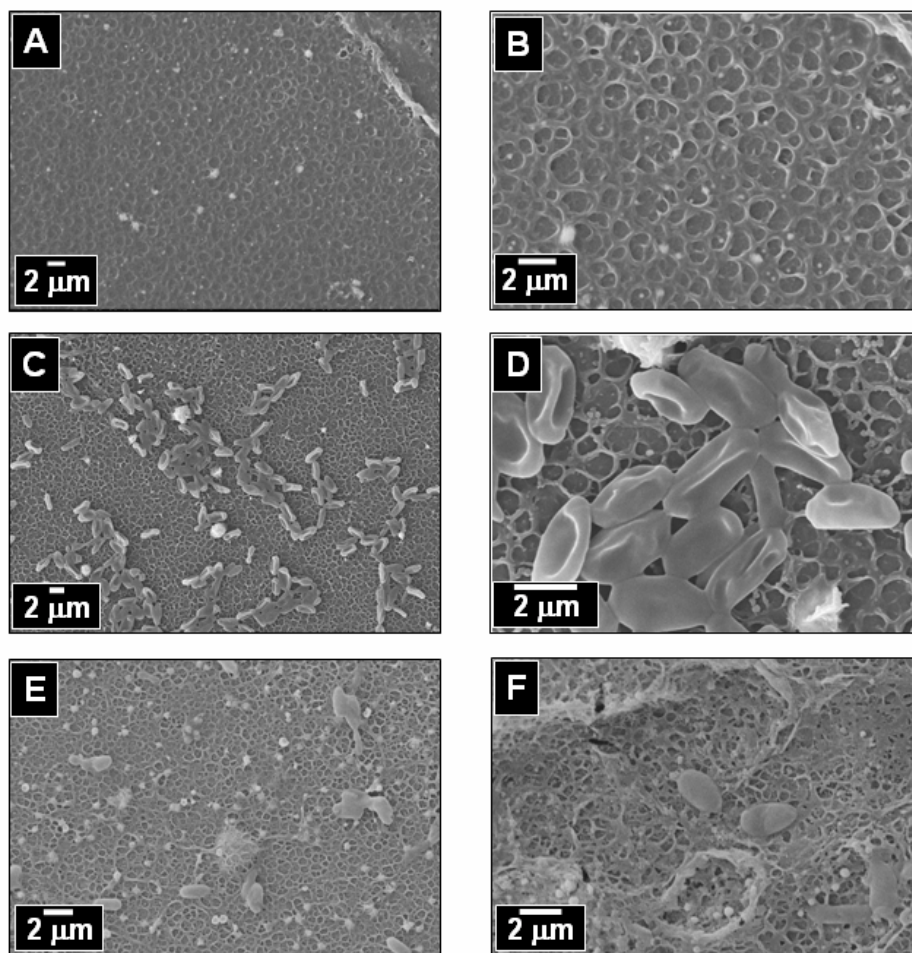
**Figure 5.9:** (A) & (B) SEM images of the as-prepared gold nanoparticle polymeric membrane transferred onto Si(111) substrate. (C) & (D) SEM images of the hydrophobized (ODA bound) gold nanoparticle polymeric membrane after immersion in *Candida bombicola* cell. (E) & (F) SEM images of the as-prepared gold nanoparticle polymeric membrane (without binding of ODA) immersed in *Candida bombicola* cell dispersed in deionized water.

These SEM images clearly show that the yeast cells are immobilized uniformly over the surface of the hydrophobic gold nanoparticle polymeric membrane. The process of attachment of the cells to the hydrophobic gold nanoparticle polymeric membranes is illustrated in Fig.5.7. That hydrophobization of the gold nanoparticle polymeric membrane is important for cell immobilization is shown in the SEM images recorded from the as-prepared membrane after immersion in dispersion of *Candida bombicola* cells (Fig.5.9E and F). These SEM images show that under these conditions, a negligibly small percentage of the yeast cells are bound to the surface of the

membrane. It is well known that these yeast cells bind to hydrophobic regions of a surface [24] and thus, the use of octadecylamine-modified gold nanoparticle polymeric membranes provides an optimum and versatile surface for immobilization of the *Candida bombicola* cells.

In order to understand better the interaction between the polymer membrane and the *Candida bombicola* cells, the membrane from which gold nanoparticles were leached out by iodine treatment was also immersed in the aqueous dispersion of *Candida bombicola* cells. Care was taken to wash the polymeric membrane with copious amount of chloroform to remove iodine and thereafter with deionized water to remove excess KI prior to use.
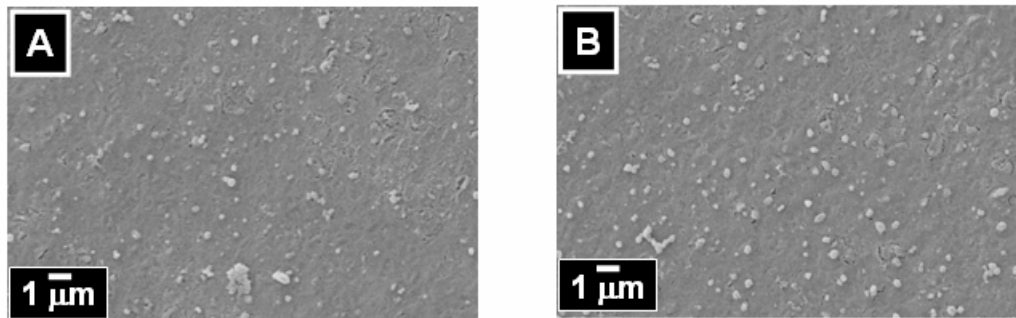


**Figure 5.10**: (A) & (B) SEM images of the gold nanoparticle polymeric membrane after leaching out the gold nanoparticles and thereafter, immersion in the *Candida bombicola* cell culture medium.

Fig.5.10A and B show SEM images obtained after immersion of the polymeric membrane minus gold nanoparticles in the *Candida bombicola* cell solution for 4 h. It is seen that hardly any of the yeast cells attached to the polymeric surface. This experiment clearly underlines the important role played by hydrophobic gold nanoparticles embedded in the polymeric membrane in the immobilization of the yeast cells.

**5.7 Synthesis of 20-hydroxyeicosatetraenoic (20-HETE)**

*Candida bombicola* cells possess cytochrome P450 enzyme in their cell walls that is capable of catalyzing the hydroxylation of arachidonic acid [29a]. In cytochrome P450 dependent arachidonic acid monooxygenase reactions the catalytic activity

turnover of this enzyme was nicotinamide adenine dinucleotide phosphate (NADPH) dependent [29b]. Since the yeast cells are used the cofactors such as NADPH are not required and are readily supplied by the cells along with the primary enzyme. This is a major advantage in using the whole cells rather than using enzyme. *Candida bombicola* cells are known to produce extracellular biosurfactants known as sophorolipids. The lactonic and acids forms of sophorolipids are known to form during the reaction.
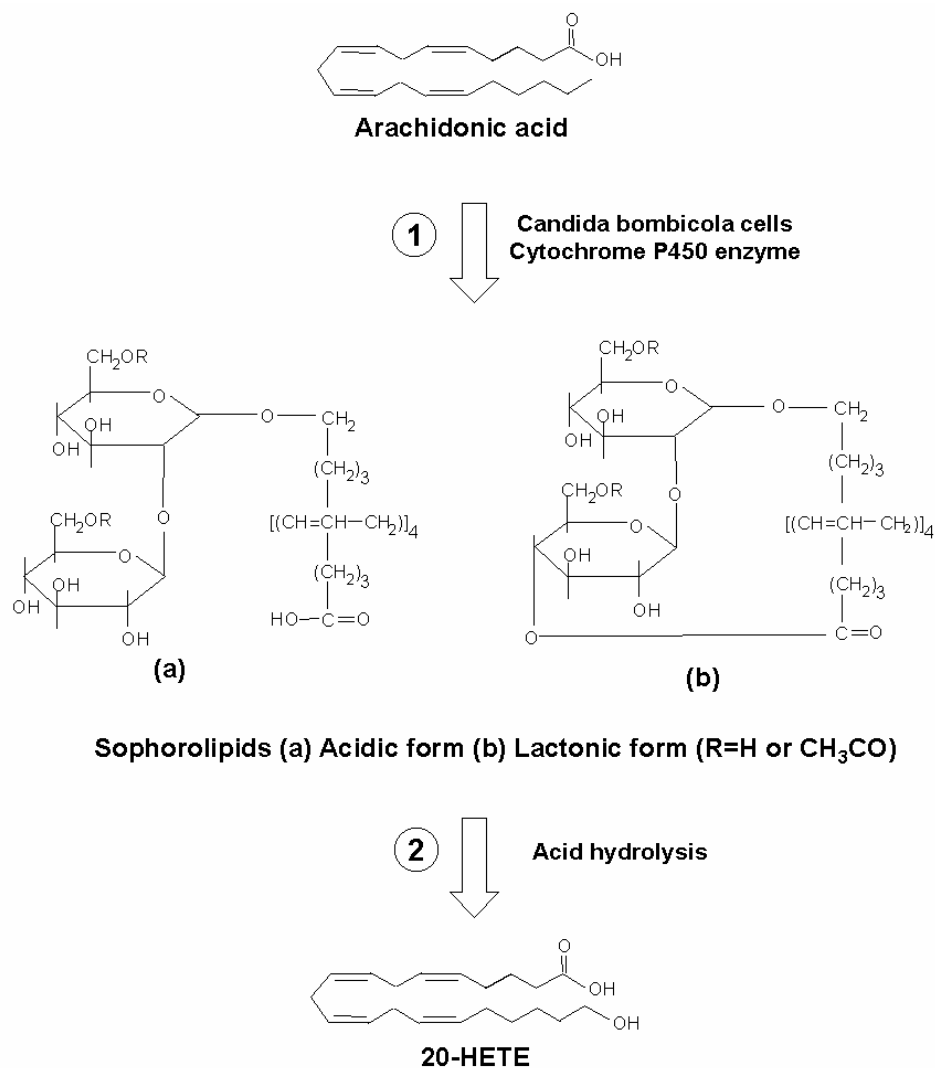


**Figure 5.11:** Reaction scheme showing the conversion of arachidonic acid to 20-HETE by using *Candida bombicola* yeast cells.

The structures of the sophorolipds are shown in Fig.5.11, step 1. Thereafter, acid hydrolysis of these sophorolipids yields 19-HETE and 20-HETE (Fig. 5.11, step 2).

*5.7.1 Synthesis of sophorolipids*

The yeast cells immobilized on the 20 mg of hydrophobic polymeric gold nanoparticle membrane were immersed in a reaction medium containing 5 mL of 10 % sterile glucose and 30 mg of arachidonic acid in 200 µL of alcohol and incubated for 96 h at 30 $^o$C under slow shaking. Sophorolipids are produced as a mixture of acidic and lactonic forms (Fig5.11, step 1). Hu *et al.* have reported earlier that lactonic form represents the largest fraction of the products in sophorolipids obtained from the *Candida bombicola* cells [30]. After the reaction, the supernatant was decanted and used for extraction of sophorolipids in ethyl acetate [27]. The sophorolipids were separated by thin-layer chromatography (TLC) on standard Kiesel-gel 60 plates and were detected by mass spectroscopy. Fig.5.12A and B show the mass spectra of the sophorolipids formed from arachidonic acid.
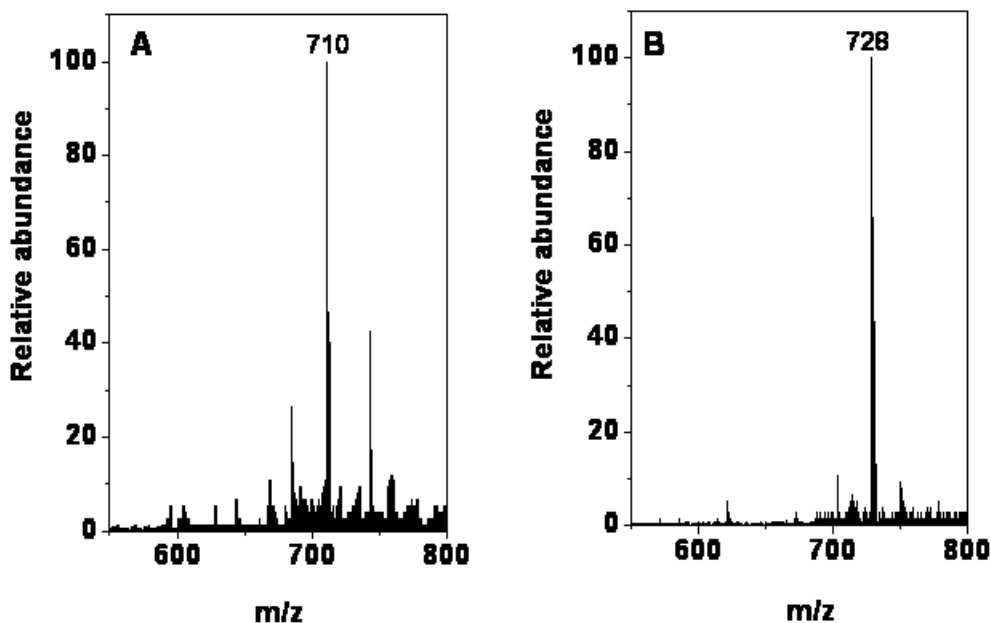


**Figure 5.12:** Mass spectrum of the sophorolipids produced from the arachidonic acid. The sophorolipids are Lactonic (A) and Acidic (B) forms of diacetate as detected by mass spectroscopy.

Significant ions occurred at *m/z* [710] (Fig.5.12A) and *m/z* [728] (Fig.5.12B), and the structures were determined to be lactonic and the acidic forms of the diacetate respectively (Fig.5.11). The hydroxy forms of the sophorolipids (lactonic and acidic)

are known to synthesized during these reactions (Fig.5.11) [30]. The immobilized yeast cells transformed 80 w/v % of arachidonic acid to sophorolipid compared with the same amount of free cells in solution. Due to difficulty in separation of the mixtures of acidic and lactonic forms of sophorolipids, these compounds are not quantitatively estimated.

*5.7.2 Acid hydrolysis of sophorolipids*

Acid hydrolysis of the sophorolipids (Fig.5.11, step 2) was done under $N_2$ atmosphere with 1 M HCl for 12 h at 25 $^{\circ}$C liberated the fatty acids, which were extracted with an equal volume of chloroform. Hydroxylated fatty acids were purified on 500 mg Aminopropyl Sep-Pak Cartridges (Waters). Samples in 0.5 mL chloroform were applied to cartridges pre-equilibrated with 5 mL n-hexane. Neutral lipids were eluted with 25 mL chloroform/2-propanol (2:1, v/v), mono-hydroxylated fatty acids with 25 mL 2% (v/v) acetic acid in diethyl ether and phospholipids with 25 mL methanol. The hydroxy fatty acid fraction was rotary evaporated and the residue taken up in a small volume of chloroform. Hydroxy fatty acids were purified by TLC on standard Kiesel-gel 60 plates and developed with petroleum ether (b.p. 60-80 $^{\circ}$C) diethyl ether/ acetic acid (50:50:1, by volume).

Iodine vapors were used to visualize fatty acids and the corresponding bands were immediately eluted with methanol/chloroform (2:1 v/v) and derivatized to their methyl ester silyl ethers. The acid hydrolysis of these sophorolipids yields 19-HETE and 20-HETE (Fig.5.11, step 2). The 20-HETE formed was detected by GC-MS as the hydroxylated fatty acids released from the sophorolipids and was compared with standard 20-HETE. The hydroxyl group in the 20-HETE compounds was detected by preparation of methyl ester silyl ether of 20-HETE. The acid hydrolyzed products were reacted with diazomethane solution and thereafter with the bis silyl trimethyl fluroacetamide (BSTFA) to give methyl ester silyl ether of 20-HETE.
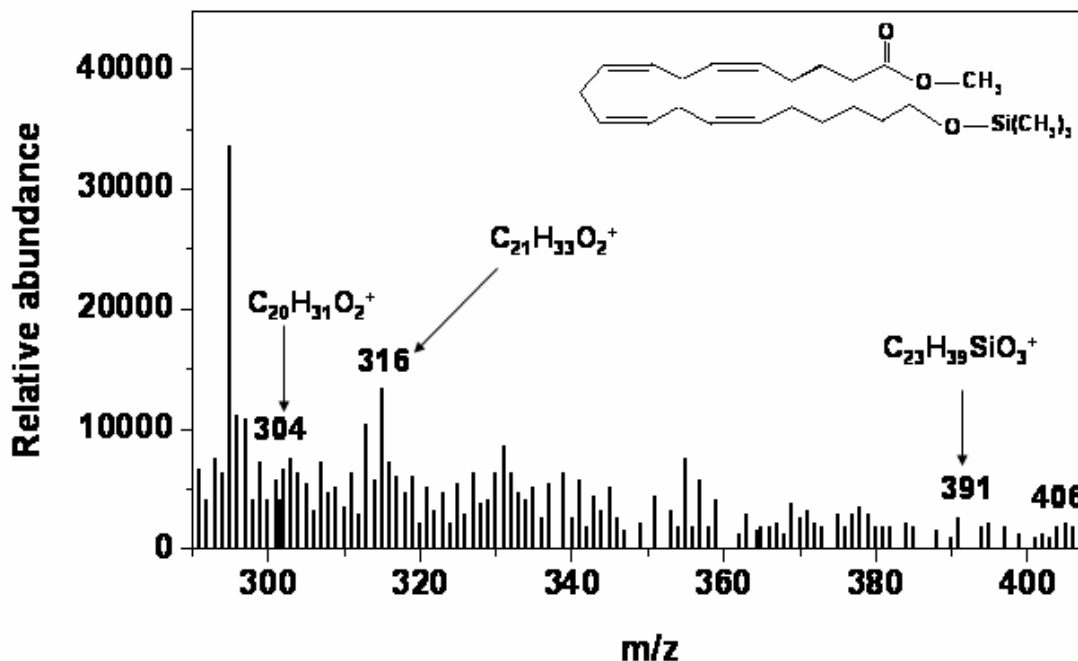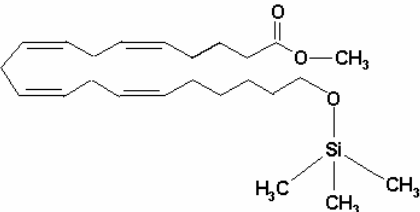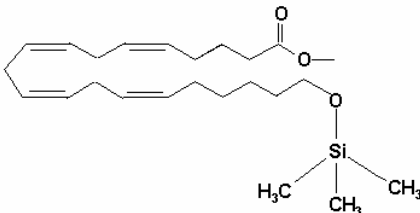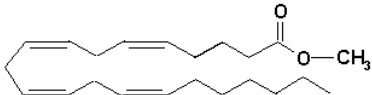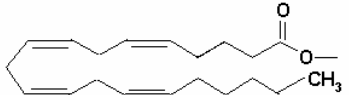
**Figure 5.13:** Partial electron impact mass spectrum of 20-HETE as detected by GC-MS. The inset shows the structure of the methyl ester silyl ether of 20-HETE.

Fig.5.13 shows the partial mass spectrum of methyl ester silyl ether of 20-hydroxy-5Z,8Z,11Z,14Z-eicosatetraenoic acid 20-HETE as detected by GC-MS. Significant ions occurred at *m/z* [406 $M^+$], 391 [$M^+$ - 15], 316 [$M^+$ - 90], 304 [($M^+$ +1) – 103]. The structures for the significant ions observed in Fig.5.13 are given in Table 4. Selective ion monitoring also showed a prominent signal at m/z 103 $(CH_3)_3$-Si-$O^+$-$CH_2$ [27]. The mass spectrum thus clearly indicates that the hydroxyl group is at the C20 position and that the compound was 20-HETE. Confirmation of the identity of 20-HETE was obtained by the observed co-elution of 20-HETE standard by GC-MS with the isolated material.

**Table 4**

The structures of the significant ions occurred of methyl ester silyl ether

of 20-HETE

| Structure | m/z |
|---|---|
|  | 406 |
|  | 391 |
|  | 316 |
|  | 304 |

The binding of the cells to the ODA bound gold nanoparticle polymeric membranes is sufficiently strong to permit reuse of the bioconjugate. Consequently, the immobilized cells on the hydrophobic gold nanoparticle polymeric membrane were reused in five successive reaction cycles with marginal loss in biocatalytic activity. The yeast cells bound to the hydrophobic gold nanoparticle polymeric membrane transformed 70 w/v % and 60 w/v % of arachidonic acid to sophorolipid in the third and fifth reactions cycles respectively.
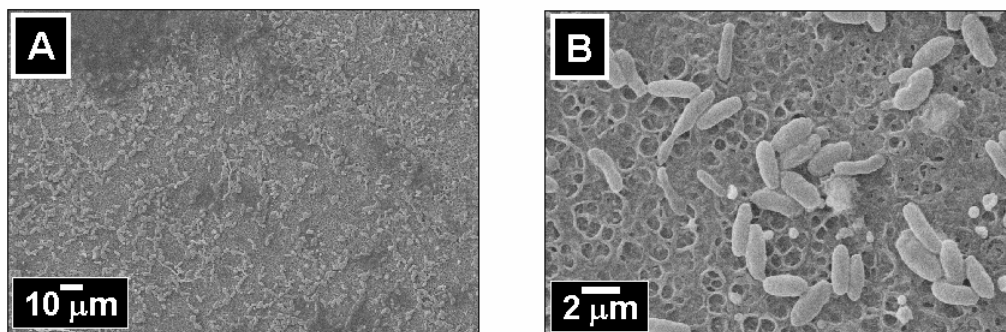
**Figure 5.14:** Low (A) and high (B) magnification SEM images of Candida bombicola whole cells immobilized on hydrophobized gold nanoparticle polymeric membrane after five cycle of reaction.

Fig.5.14A and B show SEM images of different regions of the gold nanoparticle polymeric membrane-*Candida bombicola* bioconjugate material after five cycles of reaction (incubating in the reaction medium for 30 $^{o}$C for 96 h). Thus, the yeast cells are strongly bound to the hydrophobic gold nanoparticle polymeric membrane permitting excellent reuse of the bioconjugate marterial.

**5.8 Summary**

In this chapter, we have described the synthesis of a free-standing gold nanoparticle polymeric membrane by the spontaneous reduction of aqueous chloroaurate ions by the diamine molecule (DAEE) in chloroform at a liquid-liquid interface. The membrane consists of gold nanoparticles embedded in a polymeric background (matrix) and is robust and malleable. The presence of gold nanoparticles in the membrane enables facile modification of the properties of the membrane and this has been used to bind to the enzyme pepsin to the membrane leading to the formation of an interesting new biocatalyst. The new biocatalyst is easily separated from the reaction medium, exhibits excellent reuse characteristics over ten successive cycles, temporal, harsh pH and temperature stability. The octadecylamine (ODA) bound to the gold nanoparticle polymeric membrane renders the membrane hydrophobic character and thereafter is used for the immobilization of *Candida bombicola* cells. Cytochrome P450 present in the immobilized *Candida bombicola* cells was used to catalyze the

biotransformation of arachidonic acid to sophorolipids and thereafter, acid hydrolysis yields 20-HETE.

**References:**

1) Nanobiotechnology, Concepts, Applications and Perspectives. Ed. Niemeyer, C. M.; Mirkin, C. A. Wiley-VCH Verlag GmbH & Co. KGaA 2004.

2) Jirage, K. B.; Hulteen, J. C.; Martin, C. R. *Science* **1997**, *278*, 655-658.

3) Martin, C. R. *Chem. Mater.* **1996**, *8*, 1739-1746.

4) (a) Deng, H.; Xu, Z.; Liu, Z.; Wu, J.; Ye, P. *Enzyme Microbial Technology* **2004**, *35*, 437-443. (b) Butterfeild, A. D.; Colvin, J.; Liu, J.; Wang, J.; Bachas, L.; Bhattacharrya, D. *Analytica Chimica Acta* **2002**, *470*, 29-36.

5) Langer, R.; Vacanti, J. P. *Science* **1993**, *260*, 920-926.

6) (a) Singhvi, R.; Kumar, A.; Lopez, G. P.; Stephanopoulos, G. N.; Wang, D. I.; Whitesides, G. M.; Ingber, D. E. *Science* **1994**, *264*, 696-698. (b) Yang, J.; Bei, J.; Wang, S. *Biomaterials* **2002**, *23*, 2607-2614.

7) (a) Zhang, R.; Ma, P. X. *J. Biomed. Mater. Res.* **2000**, *52*, 430-438. (b) Tidwell, C. D.; Ertel, S. I.; Ratber, B. D. *Langmuir* **1997**, *13*, 3404-3413.

8) (a) Rautaray, D.; Kumar, S.; Wadgaonkar, P. P.; Sastry, M. *Chem. Mater.* **2004**, *16*, 988-993. (b) Rautaray, D.; Kumar, S.; Wadgaonkar, P. P.; Sastry, M. US patent filed (NCL 28-2003), **2003**.

9) (a) Phadtare, S., Vinod, V. P., Wadgaonkar, P. P., Rao, M., Sastry, M. *Langmuir* **2004**, *20*, 3717-3723. (b) Phadtare, S.; Sastry, M. US patent filed (NCL 40-2004) **2004**.

10) Phadtare, S.; Shah, S.; Prabhune, A.; Wadgaonkar, P. P.; Sastry, M. *Biotechnol. Prog.* **2004**, DOI 10.1021/bp049792h.

11) (a) Selvakannan, PR. Senthil Kumar, P.; More, A. S.; Shingte, R. D.; Wadgaonkar, P. P.; Sastry, M. *Adv. Mater.* **2004** *16*, 966-971. (b) Selvakannan, PR. Senthil Kumar, P.; More, A. S.; Shingte, R. D.; Wadgaonkar, P. P.; Sastry, M. US patent filed (NF 387/03) **2003**.

12) (a) Patil, V.; Malvankar, R. B.; Sastry, M. *Langmuir* **1999**, *15*, 8197-8206. (b) Alvarez, M. M.; Khoury, J. T.; Schaaff, T. G.; Shafigullin, M. N.; Vezmar, I.;

Whetten, R. L.; *J. Phys. Chem. B* **1997**, *101*, 3706-3712. (c) Sastry, M.; Kumar, A.; Mukherjee, P. *Colloids and Surfaces A* **2001**, *181*, 255-259. (d) Selvakannan, PR.; Mandal, S.; Pasricha, R.; Adyanthaya, S. D.; Sastry M. *Chem. Commun.* **2002**, 1334-1335.

13) Henglein, A. *Langmuir* **1999**, *15*, 6738-6744.

14) The XRD patterns were indexed reference to the gold structure from *ASTM* chart (card no. 4-0784).

15) (a) Stoscheck, C.M. *Meth. Enzymol.* **1990**, *182*, 50-68. (b) Nick Pace, C.; Vajdos, F.; Fee, L.; Grimsley, Gray, T. *Protein Science* **1995**, *4*, 2411-2423.

16) (a) Patolsky, F.; Gabriel, T.; Willner, I. *J. Electroanalytical Chem.* **1999**, *479*, 69-73. (b) Niemeyer, C. M.; Ceyhan, B. *Angew. Chem. Int. Ed.* **2001**, *40*, 3685-3688. (c) Gole, A.; Dash, C.; Ramakrishnan, V.; Sainkar, S. R.; Mandle, A. B.; Rao, M.; Sastry, M. *Langmuir* **2001**, *17*, 1674-1679. (d) Gole, A.; Dash, C.; Soman, C.; Sainkar, S. R.; Rao, M.; Sastry, M. *Bioconjugate Chem.* **2001**, *12*, 684-690. (e) Gole, A.; Vyas, S.; Phadtare, S.; Lachke, A.; Sastry, M. *Colloids and Surfaces B* **2002**, *25*, 129-138. (f) Zhao, J.; O'Daly, J. P.; Henkens, R. W.; Stonehuerner, J.; Crumblis, A. L. *Biosens. Bioelectron.* **1996**, *11*, 493-502. (g) Keating, C. D.; Kovaleski, K. M.; Natan, M. J. *J. Phys. Chem. B* **1998**, *102*, 9404-9413.

17) Eftink, M. R.; Ghiron, C. A. *Anal. Biochem.* **1981**, *114*, 199-227.

18) Gole, A.; Dash, C.; Rao, M.; Sastry, M. *Chem. Commun.* **2000**, 297-298.

19) (a) Lin, C.; Yang, M. *Biotechnol. Prog.* **2003**, *19*, 361-369. (b) Karim M. R.; Hashinaga, F. *Process Biochemistry* **2002**, *38*, 809-814.

20) Phadtare, S.; Vinod, V. P.; Mukhopadhyay, K.; Kumar, A.; Rao, M.; Chaudhari, R. V.; Sastry, M. *Biotechnol. Bioeng.* **2004**, *85*, 629-637.

21) Li, J.; Wang, J.; Gavalas, V. G.; Atwood, D. A.; Bachas, L. G. *Nano. Lett.* **2003**, *3*, 55-58.

22) (a) Arica, M. Y.; Hasirci, V.; Alaeddinoglu, N. G. *Biomaterials* **1995**, *16*, 761-768. (b) Akgol, S.; Yalcinkaya, Y.; Bayramoglu, G.; Denizli, A.; Arica, M. Y. *Process Biochem.* **2002**, *38*, 675-683. (c) Takahashi, H.; Li, B.; Sasaki, T.; Miyazaki, C.; Kajino, T.; Inagaki, S. *Chem. Mater.* **2000**, *12*, 3301-3308.

23) Huckel, M.; Wirth, H.; Hearn, M. T. W. *J. Biochem. Biophys. Meth.* **1996**, *31*, 165-169.

24) Gole, A.; Dixit, V.; Lala, N.; Sainkar, S. R.; Pant, A.; Sastry, M. *Colloids and Surface B* **2002**, *25*, 363-368.

25) Kumar, A.; Mandal, S.; Selvakannan, PR.; Pasricha, R.; Mandale, A. B.; Sastry, M. *Langmuir* **2003**, *19*, 6277-6282.

26) Hommel, R. K.; Stegner, S.; Huse, K.; Kleber, H. *Appl. Microbiol. Biotechnol.* **1994**, *40*, 724-728.

27) Prabhune, A.; Fox, S. R.; Ratledge, C. *Biotechnol. Lett.* **2002**, *24*, 1041-1044.

28) Phadtare, S.; Parekh, P.; Shah, S.; Tambe, A.; Joshi, R.; Sainkar, S. R.; Prabhune, A.; Sastry, M. *Biotechnol. Prog.* **2003**, *19*, 1659-1663.

29) (a) Capdevila, J. H.; Falck, J. R.; Harris, R. C. *J. Lipid Res.* **2000**, *41*, 163-181. (b) Bolcato, C. A.; Frye, R. F.; Zemaitis, M. A.; Poloyac, S. M. *J. Chromatogr. B* **2003**, *794*, 363-372.

30) Hu, Y.; Ju, L. *J. Biotechnol.* **2001**, *87*, 263-272.

# Chapter VI

# Patterned thermally evaporated fatty lipid films for whole cell immobilization as enzyme sources in biotransformations

In this chapter, patterned thermally evaporated octadecylamine (ODA) lipid films are used for the immobilization of *Candida bombicola* cells. The attachment of the cells to the ODA film surface occurs possibly through nonspecific interactions such as hydrophobic interactions between the cell walls and the ODA molecules. The enzyme cytochrome P450 present in the immobilized yeast cell membrane was used to catalyze the biotransformation of the arachidonic acid to sophorolipids and thereafter, acid hydrolysis to 20-hydroxyecosatetraenoic acid (20-HETE). The biocomposite films could be easily separated from the reaction mixture and exhibit excellent reusability.

## 6.1 Introduction

Cell-cell and cell-extracellular matrix (ECM) adhesion is a complex and highly regulated process which plays a crucial role in most fundamental cellular functions including motility, proliferation, differentiation and apoptosis [1]. It is not yet known how the adhesion and signaling of cells is coordinated by integrin clustering, integrin-integrin separation distances and integrin pattern geometries in cell membranes, nor how many integrins are necessarily involved in the formation of stable adhesion [2]. The monolayer systems are targeted for a variety of applications, including cell adhesion and patterning [3]. The surfaces with which cells interacts are important for maintaining cellular viability and localization. The features of these surfaces can act as signals that influence cellular behavior. Generally self-assembled monolayers (SAMs) are well characterized surfaces that have been used for the patterning and cell attachment [4,5]. The patterning of the attachment of cells in cultures are done by various techniques such as microcontact printing (μ-CP) [6a,b], micropatterned supported lipid membranes [6c], elastomeric membranes [7], laser ablation [8], etc. Recently, Ree *et al.* have demonstrated the preparation of patterned fluid phospholipid bilayers by photochemical degradation of lipids using short wavelength ultraviolet radiations [9]. These methods help in generating models of cell and tissue surfaces to investigate basic principles to control cell adhesion and cell growth.

In particular, supported lipid bilayer membranes have been subjected to great attention because of their extraordinary ability to preserve many biological properties of cellular membranes [10]. Sustained interest in these supported membranes is due to their relevance in designing synthetic biocompatible surfaces [11]. Lateral fluidity of supported membranes is an important feature that distinguishes them from other surfaces. In earlier studies in this laboratory, patterned protein films were prepared by encapsulation in arrays of the lipids using octadecylamine (ODA) and arachidic acid (AA) deposited on different substrates using masks [12]. Thereafter, various enzymes such as pepsin, fungal protease, cytochrome c, etc. were encapsulated in the different elements of the array by sequential immersion of the array elements in the different protein solutions. Moreover, *Yarrowia lipolytica* yeast cells were also immobilized on patterned thermally evaporated ODA lipid films [13]. The immobilization of the yeast

cells occurs only on hydrophobic surfaces presented by the lipid film elements in the patterned structure, the attachment of the cells to the lipid film occurring possibly through hydrophobic interactions between the hydrocarbon chains of the fatty amine film and the cell wall of the yeasts.

In a previous chapter, we had discussed the immobilization of *Candida bombicola* yeast cells immobilized on ODA functionalized gold nanoparticle polymeric membrane and thereafter, application in biotransformation of arachidonic acid to sophorolipids and thereafter, acid hydrolysis gives 20-hydroxyecosatetraenoic acid (20-HETE). In this chapter, we will discuss the immobilization of *Candida bombicola* yeast cells on patterned thermally evaporated octadecylamine lipid films as enzyme source for the biotransformation of arachidonic acid [14].

## 6.2 Immobilization of *Candida bombicola* yeast cells on thermally evaporated octadecylamine (ODA) lipid films

### 6.2.1 Growth of Candida bombicola cells

*Candida bombicola* cells ATCC 22214 were grown as described in earlier Section 5.6.1.

### 6.2.2 Preparation of patterned thermally evaporated octadecylamine (ODA) lipid films

250 Å thick films of ODA were thermally evaporated on gold coated quartz crystal as discussed in Section 2.1. A 40 μm x 40 μm mesh size transmission electron microscope (TEM) grid was used as a mask in the deposition of patterned ODA films on Si(111) substrate.

### 6.2.3 Immobilization of Candida bombicola cells on patterned thermally evaporated ODA lipid films

The immobilization of yeast cells on the ODA surface was followed by QCM by immersion of the 250 Å thick ODA film on gold-coated AT cut quartz crystals for different time intervals in an aqueous dispersion of the cells ($\sim 10^8$ cells/mL) and measuring the frequency change of the crystals *ex-situ* after thorough washing and drying of the crystals.
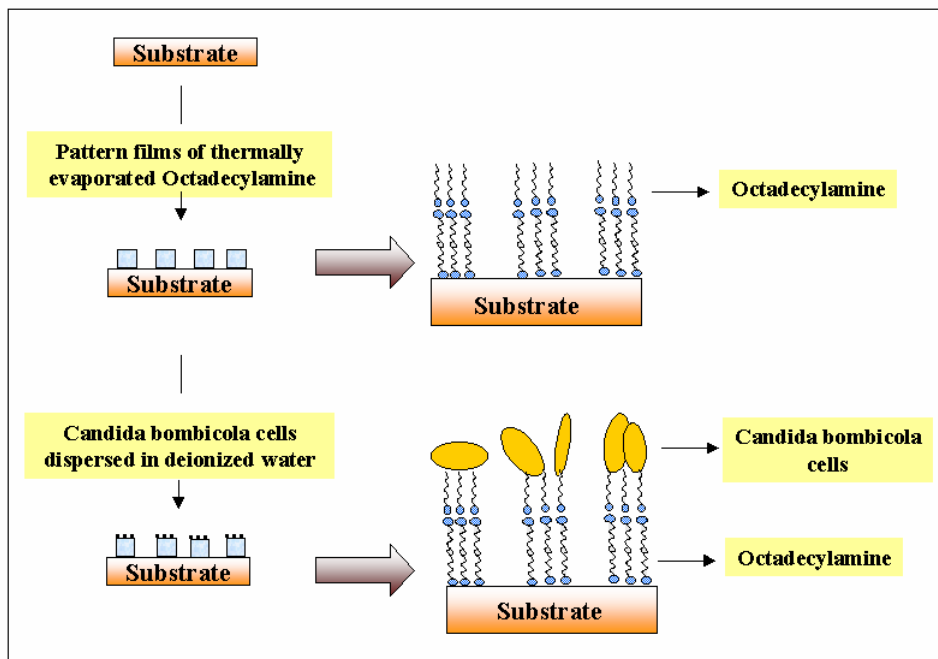
**Figure 6.1:** Schematic representation (not to scale) showing the immobilization of *Candida bombicola* whole cells on patterned thermally evaporated octadecylamine (ODA) lipid films.
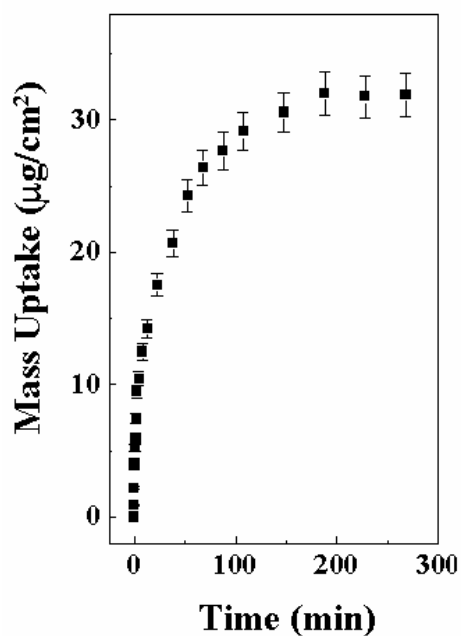


**Figure 6.2:** QCM mass uptake data recorded during immobilization of *Candida bombicola* cells onto a 250 Å thick ODA films. The error bars are based on an analysis of three separate QCM measurements.

The frequency counter used was an Edwards FTM5 instrument operating at a frequency stability and resolution of $\pm$ 1 Hz. For a 6 MHz crystal used in the study, translates into a mass resolution of 12 ng/cm$^2$. The frequency change was converted to mass loading using the Sauerbrey formula [15]. Fig.6.2 shows the QCM kinetics of cell immobilization onto 250 Å thick thermally evaporated ODA films. Since the mass of the individual cells is not known, we have used the frequency change merely indicator of the attachment of the cells on the hydrophobic ODA surface. It is observed from the figure that there is a rapid attachment of the cells with 90 % of the cells being immobilized within the first 100 minutes of immersion. The cell density on the ODA film surface eventually reaches saturation after ca. 4 h of immersion in the yeast cell suspension. In all the experiments, this optimum time of immersion (4 h) in the *Candida bombicola* cells solution was used to obtain films of the immobilized cells (see Fig6.1).

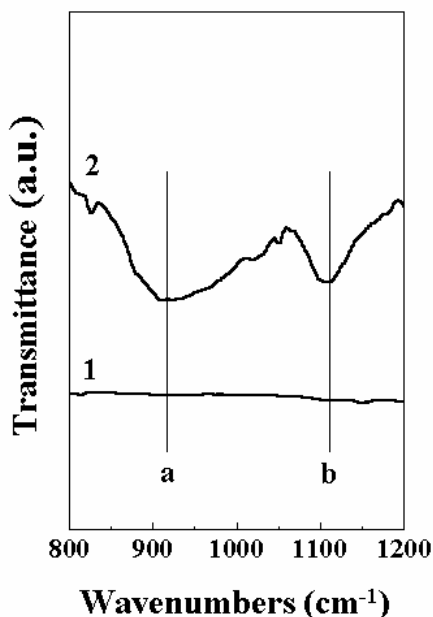*6.2.4 Fourier transform infrared spectroscopy (FTIR)*



**Figure 6.3:** FTIR spectra recorded from an as-deposited 250 Å thick ODA film (curve 1) and ODA film after complete immobilization of the *Candida bombicola* cells (curve 2) on Si(111) substrates.

Fig.6.3 shows the FTIR spectra recorded from a 250 Å thick as-deposited ODA film (curve 1) and the ODA film after immersion in *Candida bombicola* cells solution for 4 h (curve 2). Two prominent features labeled *a* (917 cm$^{-1}$) and *b* (1110 cm$^{-1}$) in the figure can be seen for the cells immobilized on ODA lipid films (curve 2) which are clearly absent in the as-deposited ODA film (curve 1). These two absorption bands *a* and *b* are characteristic of excitation of deoxyribose-phosphate vibration modes and vibrations in the deoxyribose groups in the DNA molecules of the yeast cells respectively [16].

*6.2.5 Scanning electron microscopy (SEM) and energy dispersive analysis of X-rays (EDAX)*
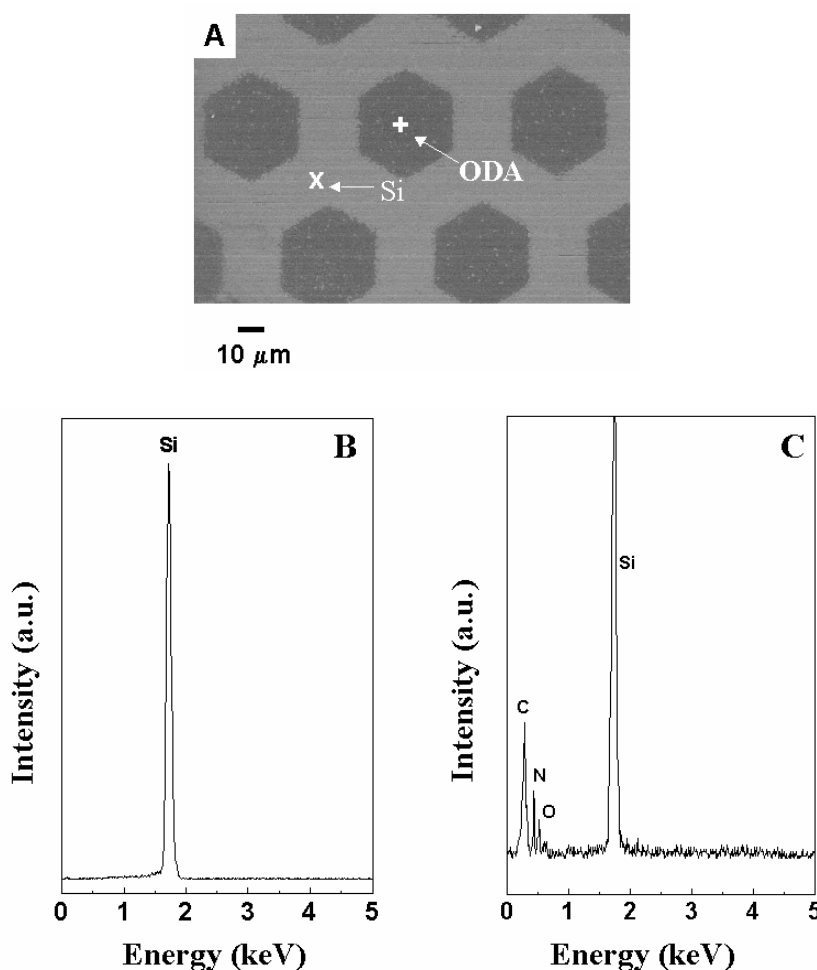


**Figure 6.4:** (A) SEM images recorded from patterned thermally evaporated ODA thin film. (C) and (D) shows EDAX spot profile analysis on masked (marked as x in Fig.6.4A) and exposed surface of patterned ODA lipid films (marked as + in Fig.6.4A).

Fig.6.4 shows an SEM image of the as-deposited ODA film on a Si(111) substrate using a TEM grid as a mask. It is seen that well-defined individual hexagonal elements of the ODA film have been deposited on the substrate. Fig.6.4C and D show energy dispersive analysis of x-rays (EDAX) spot profile analysis on masked (marked as x in Fig.6.4A) and exposed substrate (marked as + in Fig.6.4A) of the patterned surfaces of ODA lipid films. Fig. 6.4C shows nitrogen signal from the exposed surface, hence confirms the deposition of the ODA, however nitrogen signals were absent from the masked region, this confirms that ODA is not deposited in this region. Thereafter, this film was immersed in an aqueous suspension of *Candida bombicola* cells for 4 h and washed thoroughly prior to imaging by SEM.

Fig.6.5A and B show the low and high magnification SEM image recorded after immobilization of the *Candida bombicola* cells onto the hexagonal ODA patterns. It is clearly seen from SEM image that the yeast cells are immobilized extremely faithfully on the ODA elements with negligible binding of the cells to the exposed silicon surface.



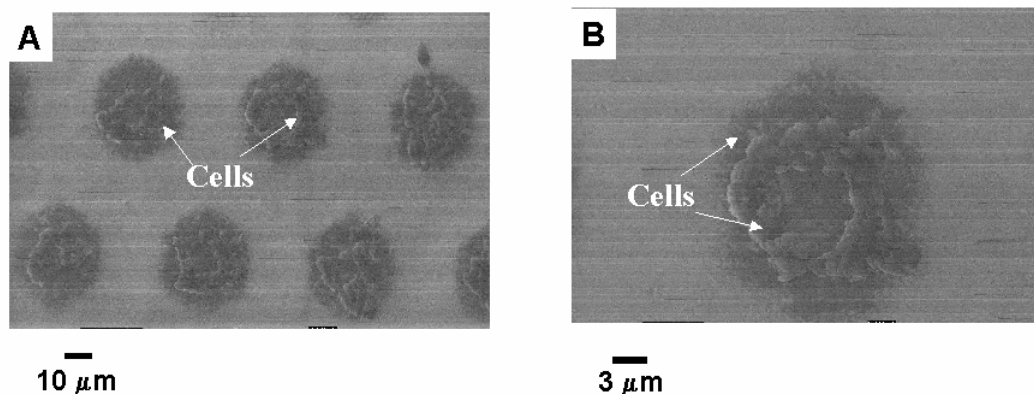**Figure 6.5:** (A) and (B) Low and high magnification of SEM images after immobilization of *Candida bombicola* cells onto the ODA film surface.

It is well known that cells bind to hydrophobic regions of a surface [13] and thus, the use of patterned thermally evaporated fatty lipid films provides an excellent means of spatial organization of cells on any solid support. The process of attachment

of the *Candida bombicola* cells to the patterned hydrophobic ODA film regions is illustrated in Fig.6.1.

## 6.3 Synthesis of 20-hydroxyeicosatetraenoic acid (20-HETE)

As seen in earlier Section 5.7, *Candida bombicola cells* possess cytochrome P450 enzyme present in their cell membranes that catalyze the biotransformations of arachidonic acid in presence of glucose to form sophorolipids (see Fig. 5.11 for reaction scheme) [17a]. In cytochrome P450 dependent arachidonic acid monooxygenase reactions the catalytic activity turnover of this enzyme was nicotinamide adenine dinucleotide phosphate (NADPH) dependent [17b]. Since the yeast cells are used the cofactors such as NADPH are not required and are readily supplied by the cells along with the primary enzyme. This is a major advantage in using the whole cells rather than using enzyme.
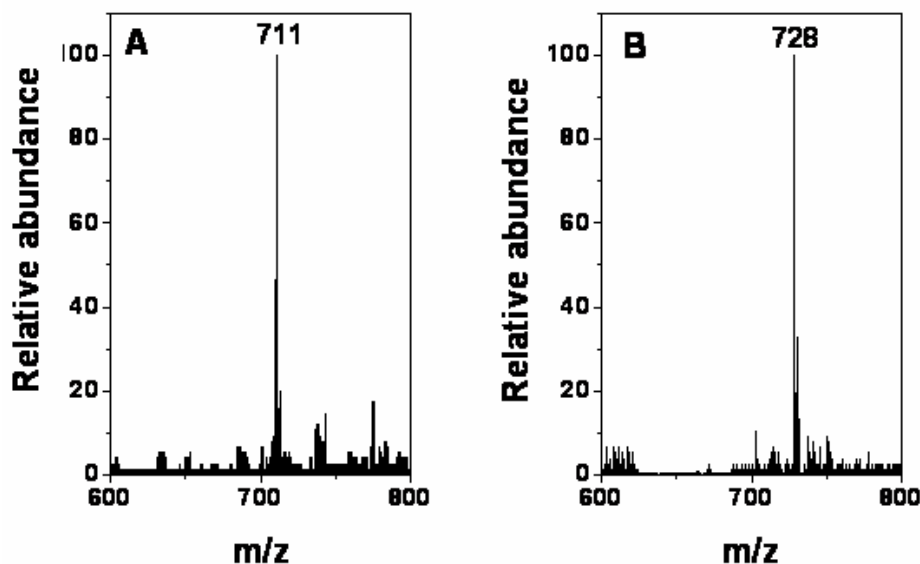
*6.3.1 Synthesis of sophorolipids*



**Figure 6.6:** Mass spectrum of the sophorolipids produced from the aracidonic acid. The sophorolipids are identified as lactonic (A) and acidic (B) forms of diacetate.

The yeast cells immobilized on the 250 Å thick ODA films were immersed in the reaction medium containing 5 mL 10% sterile glucose and 30 mg arachidonic acid and were incubated for 96 h at 30 °C under slow shaking. After the reaction, the supernatant was decanted and used for extracting sophorolipid [17c]. Earlier Hu *et al.* have reported that lactonic form represents the largest fraction of the products in sophorolipids obtained from *Candida bombicola* yeast cells [18]. After the reaction the supernatant was decanted and used for extraction of sophorolipids in ethyl acetate [17c]. Fig.6.6 shows the mass spectra of sophorolipids obtained from arachidonic acid during the biotransformation reaction by immobilized *Candida bombicola* cell. The sophorolipids were separated by thin-layer chromatography (TLC) on standard Kiesel-gel 60 plates. Significant ions occurred at m/z [710] and [728] which are lactonic and acidic forms of diacetate respectively (Fig.5.11, step 1). The immobilized yeast cells transformed 70 w/v % of the arachidonic acid to sophorolipid. However, in earlier chapter we had seen that the *Candida bombicola* cells immobilized on hydrophobized gold nanoparticle polymeric membrane transformed 80 w/v % arachidonic acid. Since the lactonic and acidic forms of diacetate are difficult to separate from the products, their quantitative analysis is not done. The hydroxyl forms of the sophorolipids are known to form during the reaction, however were not observed during the reaction. The similar behavior is also observed for *Candida bombicola* cells immobilized on hydrophobized gold nanoparticle embedded polymeric membrane [19].

### 6.3.2 Acid hydrolysis of sophorolipids and isolation of 20-HETE

As mentioned briefly in the introduction, our interest in *Candida bombicola* cells centers on the ability of the cells to catalyze the transformation of arachidonic acid to 20-HETE (Fig.5.11, Chapter 5) and therefore, it is of paramount importance to establish the viability of the immobilized cells in performing this biochemical function. The sophorolipids formed during the biotransformations of arachidonic acid were subjected to acid hydrolysis as described in Section 5.7.2 to form 19-HETE and 20-HETE compounds. The hydroyecosatetraenoic acids were reacted with diazomethane solution and thereafter with the bis silyl trimethyl fluroacetamide (BSTFA) to give methyl ester silyl ether of hydroyecosatetraenoic acid.
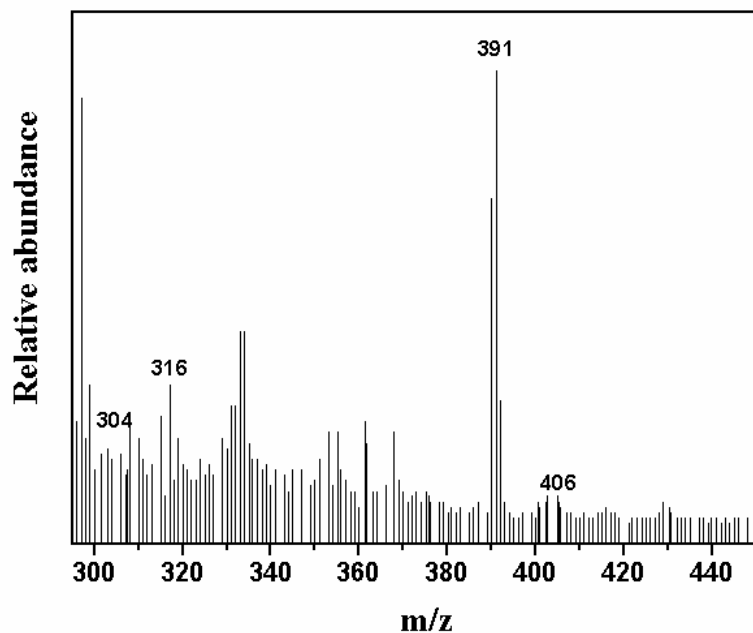
**Figure 6.7:** Partial electron impact mass spectrum of 20-HETE as detected by GC-MS. The compounds were extracted from sophorolipids synthesized using the *Candida bombicola* cells immobilized on the hydrophobized ODA lipid films and was identified as the methyl ester silyl ether of 20-HETE.

Fig.6.7 shows the partial mass spectrum of methyl ester silyl ether of 20-hydroyecosatetraenoic acid as detected by GC-MS. Significant ions occurred at *m/z* [406 $M^+$], 391 [$M^+$ - 15], 316 [$M^+$ - 90], 304 [($M^+$ +1) – 103] (see Table 4, Chapter 5 for the structures). Selective ion monitoring also showed a prominent signal at m/z 103 [$(CH_3)_3$-Si-$O^+$-$CH_2$] [17c]. The mass spectrum thus clearly indicates that the hydroxyl group is at the C20 position and that the compound was 20-HETE. Confirmation of the identity of 20-HETE was obtained by the observed co-elution of 20-HETE standard by GC-MS with the isolated material. It is observed that, *Candida apicola* yeast cells are known to produce 19-HETE and 20-HETE [17b]. However, in our case *Candida bombicola yeast* cells are known to form only 20-HETE.
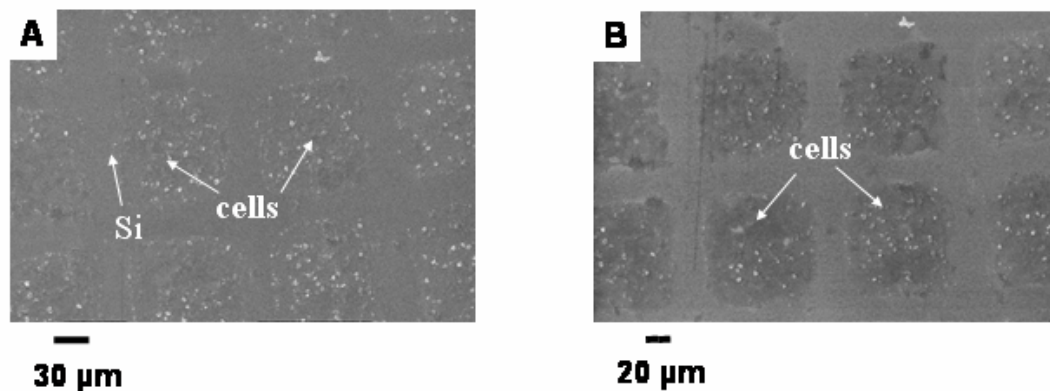
**Figure 6.8:** Low (A) and high (B) magnification SEM images of *Candida bombicola* whole cells immobilized on thermally evaporated octadecylamime lipid films after one cycle of reaction.

Fig. 6.8 (A) and (B) show SEM images of different regions of the *Candida bombicola* cells bound to ODA lipid films after one cycles of reaction (incubating in the reaction medium for 30 $^{\circ}$C for 96 h). Thus, the yeast cells are strongly bound to the hydrophobic ODA lipid film permitting excellent reuse. The films of the immobilized cells could be reused after reaction and through washing with only a marginal loss in biocatalytic activity ca. 10 % after 5 cycles, indicating that the cells are strongly bound to the ODA lipid films.

**6.4 Summary**

In this chapter, we have demonstrated the immobilization of *Candida bombicola* yeast cells on patterned thermally evaporated ODA films. The assembly of yeast cells to ODA films occurs possibly through hydrophobic interactions between cell walls and ODA molecules. The immobilized yeast cells were biologically active, and cytochrome P450 enzyme present in the *Candida bombicola* cell membranes could be used to biotransformtion of arachidonic acid to sophorolipids and thereafter, acid hydrolysis gives 20-HETE. The biocomposite films are easily separated from the reaction medium and were reused.

**References:**

1) Chen, C. S.; Mrksich, M.; Huang, S.; Whitesides, G. M.; Ingber, D. E. *Science* **1997**, *276*, 1425-1428.

2) Lasky, L. A. *Nature* **1997**, *390*, 15-17.

3) Swalen, J. D.; Allara, D. I.; Andrade, J. D.; Chandross, E. A.; Garoff, S.; Israelachvil, J.; McCarthy, T. J.; Murray, R.; Pease, R. F.; Rabolt, J. R.; Wynne, K. J.; Yu, H. *Langmuir* **1987**, *3*, 932-950.

4) (a) Bain, C. D.; Troughton, E. B.; Tao, Y.-T, Evall, J.; Whitesides, G. M.; Nuzzo, R. G. *J. Am. Chem. Soc.* **1989**, *111*, 321-335. (b) Yousaf, M. N.; Houseman, B. T.; Mrksich, M. *Proc. Natl. Acad. Sci. USA* **2001**, *98*, 5992-5996.

5) (a) Stenger, D. A.; Georger, J. H.; Dulcey, C. S.; Hickman, J. J.; Rudolph, A. S.; Nielsen, T. B.; McCort, S. M.; Calvert, J. M. *J. Am. Chem. Soc.* **1992**, *114*, 8435-8442. (b) Lopez, G. P.; Albers, M. W.; Schreiber, S. L.; Carroll, R.; Peralta, E.; Whitesides, G. M. *J. Am. Chem. Soc.* **1993**, *115*, 5877-5878.

6) (a) Singhvi, R.; Kumar, A.; Lopez, G. P.; Stephanopoulos, G. N.; Wang, D. I. C.; Whitesides, G. M.; Ingber, D. E. *Science* **1994**, *264*, 696-671. (b) St. John, P. M.; Davis, R.; Cady, N.; Czajka, J.; Batt, C. A.; Craighead. *Anal. Chem.* **1998**, *70*, 1108-1111. (c) Groves, J. T.; Mahal, L. K.; Bertozzi, C. R. *Langmuir* **2001**, *17*, 5129-5133.

7) Ostuni, E.; Kane, R.; Chen, C. S.; Ingber, D. E.; Whitesides, G. M. *Langmuir* **2000**, *16*, 7811-7819.

8) Thissen, H.; Hayes, J. P.; Kingshott, P.; Johnson, G.; Harvey, E. C.; Griesser, H. J. *Smart Mater. Struct.* **2002**, *11*, 792-799.

9) Yee, C. K.; Amweg, M. L.; Parikh, A. N. *J. Am. Chem. Soc.* **2004**, *126*, 13962-13972.

10) Sackmann, E. *Science* **1996**, *271*, 43-48.

11) Sackman, E.; Tanaka, M. *Trends Biotechnol.* **2000**, *18*, 58-64.

12) Gole, A.; Sastry, M. *Biotechnol. Bioeng.* **2001**, *74*, 172-178

13) Gole, A.; Dixit, V.; Lala, N.; Sainkar, S. R.; Pant, A.; Sastry, M. *Colloids and Surfaces B* **2002**, *25*, 363-368.

14) Phadtare, S.; Parekh, P.; Shah, S.; Tambe, A.; Joshi, R.; Sainkar, S. R.; Prabhune, A.; Sastry, M. *Biotechnol. Prog.* **2003**, *19*, 1659-1663.

15) Sauerbrey, G. *Z.Phys. (Munich)* **1959**, *155*, 206-222. (b) Buttry, D. A.; Ward, M. D. *Chem. Rev.* **1992**, *92*, 1355-1379. (c) Wang, J.; Frostman, L. M.; Ward, M. D. *J. Phys. Chem.* **1992**, *96*, 5224-5228.

16) Taillandier, E.; Liquier, J. *Meth. Enzymol.* **1992**, *211*, 307-335.

17) (a) Capdevila, J. H.; Falck, J. R.; Harris, R. C. *J. Lipid Res.* **2000**, *41*, 163-181. (b) Bolcato, C. A.; Frye, R. F.; Zemaitis, M. A.; Poloyac, S. M. *J. Chromatogr. B* **2003**, *794*, 363-372. (c) Prabhune, A.; Fox, S. R.; Ratledge, C. *Biotechnol. Lett.* **2002**, *24*, 1041-1044.

18) Hu, Y.; Ju, L. *J. Biotechnol.* **2001**, *87*, 263-272.

19) Phadtare, S.; Shah, S.; Prabhune, A.; Wadgaonkar, P. P.; Sastry, M. *Biotechnol. Prog.* **2004**, DOI 10.1021/bp049792h.

# Chapter VII


## Conclusions

---

This chapter contains concluderary remark on the salient features of the work described in the thesis and future potential developments in the area.

---

**7.1 Summary of the work**

Biomolecules may easily denature or loose their biocatalytic activity after adsorbing on solid surfaces. This may be the primary reason for the design of a completely new class of materials, which can provide a biocompatible environment that can readily conserve the native structure of biomolecules. This thesis describes the use of stacks of lipid bilayers and surface of gold nanoparticles as a biocompatible surface for the immobilization of enzymes and whole cells. The formation of penicillin G acylase (PGA), invertase and fungal protease lipid biocomposites has been described. The diffusion of the enzymes primarily depends on the electrostatic interactions and secondary interactions such as hydrogen bonding, hydrophobic interactions are also responsible for the entrapment within the lipid bilayers. The important issue of mass transport problem within the stearic acid lipid films was studied by pre-ordering the lipid films by entrapment of lead ions. The $Pb^{2+}$ ions lamellar ordered structure of the lipid films enhances diffusivity of the protein in the lipid matrix compared to the as-deposited unordered lipid films. The immobilized biocatalysts show enhanced temporal, temperature and pH stability indicating the protective nature offered by the lipid matrix towards harsh environmental conditions. Gold nanoparticles are also used as a biocompatible surface for the immobilization of enzymes. Enzyme binds to the gold nanoparticles through the amine groups and cysteine residues present in it. These bioconjugates showed excellent biocatalytic activity, however a major drawback was that their reusability was extremely poor. To overcome this problem, gold nanoparticles were bound to the massive polyurethane and zeolite microspheres and thereafter, were used for the binding of enzyme pepsin. These bioconjugates were easily separated form the reaction mixture and showed excellent reuse characteristics.

This thesis also discuses the gold nanoparticle embedded polymeric membrane as scaffolds for immobilization of enzymes and whole cells. The presence of gold nanoparticles in the membrane enables facile modification of the properties of the membrane and this has been used for the immobilization of enzyme pepsin. This new biocatalyst exhibits excellent reuse characteristics over 10 successive cycles and temporal stability. Membrane enzymes such as cytochrome P450 are difficult to extract

and are unstable outside the cell membrane. Hence it was of paramount interest to used yeast cells for the hydroxylation of arachidonic acid to form sophorolipids. Since the yeast cells are used the cofactors such as nicotinamide adenine dinucleotide phosphate (NADPH) is not required and is readily supplied by the cells along with the primary enzyme. This is a major advantage in using the whole cells rather than using enzyme. The octadecylamine bound to the gold nanoparticle polymeric membrane provides hydrophobic and biocompatible environment for the immobilization of *Candida bombicola* cells. The *Candida bombicola* yeast cells immobilized on the hydrophobic gold membranes and are used for the synthesis of sophorolipids and thereafter, acid hydrolysis gives 20-hydroxyecosatetraenoic acid (20-HETE).

## 7.2 Scope for future work

Thermally evaporated lipid films are a versatile method for the generation of patterned protein films by encapsulation of different proteins in arrays of the lipids and shows promise for single-chip multianalyte immunoassay/multiplex, high-throughput biosensor and catalysis applications. Immobilizing various proteins on a single chip can easily perform multi-step biocatalytic reactions requiring many enzymes, wherein each enzyme would specifically react with its substrate giving desired final product. This protocol is general and can be extended towards the immobilization of poly nucleic acids, hormones and biological cells. The facility of patterning can be extended towards the patterned immobilization of DNA, and can be used for screening genomic libraries. Patterning of thermally evaporated lipid films can be used to fabricate arrays of different specific ligands for cell surface receptors which will address fundamental questions critical for understanding and controlling the adhesion, proliferation and differentiation of cells. Gold nanoparticle polymeric membranes can act as scaffolds for growth of different cells in tissue engineering. These membranes can be used for the growth of different minerals and thus suggests potential biomedical applications as biocompatible implants, grafting in bone surgery, etc.

# LIST OF PUBLICATIONS

1) *"Glucose induced in-situ reduction of chloroaurate ions entrapped in a fatty amine: formation of gold nanoparticles-lipid composite"*
Gole, A., Kumar, A., Phadtare, S., Mandale, A. B., Sastry, M. Phys. Chem. Comm. 19 (2001) 1-4.

2) *"Studies on the formation of bioconjugate of Endoglucanase with colloidal gold"*
Gole, A., Vyas, S., Phadtare, S., Lachke, A., Sastry, M. Colloids and Surfaces B: Biointerface 25 (2002) 129-138.

3) *"Penicillin G Acylase-fatty lipid biocomposite films show excellent catalytic activity and long term stability/reusability"*
Phadtare, S., Parekh, P., Gole, A., Patil, M., Pundle, A., Prabhune, A., Sastry, M. Biotechnol. Prog. 18 (2002) 483-488.

4) *"Improved performance of preordered fungal protease-stearic acid biocomposite: Enhanced catalytic activity, reusability, and temporal stability"*
Phadtare, S., Dash, C., Gole, A., Vinod, V. P., Rao, M., Sastry, M. Biotechnol. Prog. 18 (2002) 700-705.

5) *"Synthesis of stable gold hydrosol by the reduction of chloroaurate ions by the amino acid, aspartic acid"*
Mandal, S., Selvakannan, PR., Phadtare, S., Pasricha, R., Sastry, M. Proc. Indian Acad. Sci. (Chem. Sci.) 114 (2002) 513-520.

6) *"Assembling gold nanoparticles in solution using phosphorothiolate DNA as structural interconnects"*
Kumar, A.; Phadtare, S.; Pasricha, R.; Guga, P.; Ganesh, K. N.; Sastry, M. Current Science 84 (2003) 101-104.

7) *"Capping of gold nanoparticles by the amino acid lysine renders them water dispersible"*
Selvakannan, PR.; Mandal, S.; Phadtare, S.; Pasricha, R.; Sastry, M. Langmuir 19 (2003) 3545-3549.

8) *"Gold nanoparticles assembled on amine functionalized Na-Y zeolite: A biocompatible surface for enzyme immobilization"*
Mukhopadhyay, K.; Phadtare, S.; Vinod, V. P.; Kumar, A.; Rao, M.; Chaudhari, R. V.; Sastry, M. Langmuir 19 (2003) 3858-3863

9) *"Direct assembly of gold nanoparticles "Shells" on polyurethane microspheres "Cores" and their application as enzyme immobilization template"*
Phadtare, S.; Kumar, A.; Vinod, V. P.; Dash, C.; Palaskar, D. V.; Rao, M.; Shukla, P. G.; Sivaram, S.; Sastry, M. Chem. Mater. 15 (2003) 1944-1949.

10) *"Fractal gold nanostructures produced by the spontaneous reduction of chloroaurate ions in thermally evaporated hexadecylaniline thin films"*
Mandal, S.; Phadtare, S.; Selvakannan, P R.; Pasricha, R.; Sastry, M. <u>Nanotechnology</u> 14 (2003) 878-881.

11) *"Candida bombicola Cells Immobilized on Patterned Lipid Films as Enzyme Sources for the Transformation of Arachidonic Acid to 20-HETE"*
Phadtare, S.; Parekh, P.; Shah, S.; Tambe, A.; Joshi, R.; Sainkar, S. R.; Prabhune, A.; Sastry, M. <u>Biotechnol. Prog.</u> 19 (2003) 1659-1663.

12) *"Time-dependent complexation of cysteine-capped gold nanoparticles with octadecylamine Langmuir monolayers at the air-water interface"*
Mayya, K. M.; Gole, A.; Jain, N.; Phadtare, S.; Langevin, D.; Sastry, M. <u>Langmuir</u> 19 (2003) 9147-9154.

13) *"Studies on interactions between similarly charged polyelectrolytes: fatty lipid system"*
Gole, A.; Phadtare, S.; Langevin, D.; Sastry, M. <u>Langmuir</u> 19 (2003) 9321-9327.

14) *"Water-soluble protected tryptophan-protected gold nanoparticles prepared by the spontaneous reduction of the aqueous chloroaurate ions by the amino acid"*
Selvakannan, PR.; Mandal, S.; Phadtare, S.; Gole, A.; Pasricha, R.; Adyantaya, S.; Sastry, M. <u>J. Colloids and Interface Science</u> 269 (2004) 97-102.

15) *"Invertase-Lipid biocomposite films: Preparation, Characterization, and enzymatic activity"*
Phadtare, S., D'Britto, V., Pundle, A., Prabhune, A., Sastry, M. <u>Biotechnol. Prog.</u> 20 (2004) 156-161.

16) *"Immobilization and Biocatalytic activity of fungal protease on gold nanoparticles loaded zeolite microspheres"*
Phadtare, S.; Vinod, V. P.; Mukhopadhyay, K.; Kumar, A.; Rao, M.; Chaudhari, R. V.; Sastry, M. <u>Biotechnol. Bioeng.</u> 85 (2004) 629-637.

17) *"Free-standing nanogold membranes as scaffolds for enzyme immobilization"*
Phadtare, S.; Vinod, V. P.; Wadgaonkar, P. P.; Rao, M.; Sastry, M. <u>Langmuir</u> 20 (2004) 3717-3723.

18) *"Enhancing the reusability of endoglucanase-gold nanoparticles bioconjugate by tethering to polyurethane microspheres"*
Phadtare, S.; Vyas, V. P.; Palaskar, D. V.; Lachke, A.; Shukla, P. G.; Sivaram, S.; Sastry, M. <u>Biotechnol. Prog.</u> (2004) DOI 10.1021/bp0499000.

19) *"Interfacing biology with nanoparticles"*
Mandal, S.; Phadtare, S.; Sastry, M. <u>Current Appl. Physics</u> (2004) Inpress.

20) *"Immobilization of Candida bombicola Cells on Free Standing organic gold nanoparticle membrane and their use as enzyme source in biotransformation"*, Phadtare, S.; Shah, S.; Wadgaonkar, P. P.; Prabhune, A.; Sastry, M. Biotechnol. Prog. (2004) DOI 10.1021/bp049792h.

## PATENTS FILED

1) *"A hybrid organic- inorganic composite films"*
Gole, A.; Kumar, A.; Phadtare, S.; Sastry, M.  US Patent and Indian Patent filed (2001).

2) *"Method for the manufacture of hybrid organic-inorganic composite film"*
Gole, A.; Kumar, A.; Phadtare, S.; Sastry, M. US Patent and Indian Patent filed (2001).

3) *"A process for the immobilization of enzymes"*
Phadtare, S.; Sastry, M. US Patent and Indian Patent filed (2004).